# Results of laboratory experiments

Results Phase 1A & B;

1A: Sediment analysis & erosion of remoulded beds under currents

1B: Erosion of placed-bed and deposited-beds under currents.



MUSA

ON THE INTERACTION BETWEEN MUD AND SAND

June, 2022; Results of laboratory experiments Phase 1A and 1B:

1A: Sediment analysis & erosion of remoulded beds under currents

1B: Erosion of placed-bed and deposited-beds under currents.


TKI MUSA project

**Author(s)**

Márcio Boechat Albernaz, MSc

Leo C. van Rijn, Em. Prof

Doke C. Schoonhoven, MSc

Luitze M. Perk, MSc

# Results of laboratory experiments Phase 1A and 1B

TKI MUSA project

| Client | MUSA consortium |
|---|---|
| Contact | Luitze Perk |
| Reference | |
| Keywords | Sand, mud, laboratory experiments, erosion under currents, remoulded beds, placed beds, deposited beds, sand-mud mixtures |

| Document control | |
|---|---|
| Version | Final |
| Date | 28-06-2022 |
| Project nr. | 11204950-001 |
| Document ID | |
| Pages | 130 |
| Status | Final |

| Doc. version | Author | Reviewer | Approver | Publish |
|---|---|---|---|---|
| Final | Márcio Boechat Albernaz, MSc<br>Leo C. van Rijn, Em Prof<br>Doke C. Schoonhoven, MSc<br>Luitze M. Perk, MSc | B. Grasmeijer | | |
| | | | | |

MUSA

# About the MUSA project

Estuaries and tidal basins form the transition zones between land and sea. They contain important habitats for flora and fauna and are extensively used by people, like for navigation. For ecological and navigational purposes, it is important to understand and predict the evolution of channels and shoals, including sedimentation rates and the composition of the bed sediments. The bed material of large estuaries and tidal basins largely consists of mixtures of mud and sand, with predominantly sandy channels and mainly muddy intertidal areas. The interaction between sand and mud, in combination with currents and waves, leads to complex dynamics in these areas, with migrating channels and shoals.

Much is known about the behaviour of the individual sediment fractions, but the knowledge and understanding of sand-mud interaction remains limited, as do the available tools and models to accurately predict the bed evolution and sediment transport rates in sand-mud areas. Existing models, like the ones by Van Ledden (2003), Soulsby & Clarke (2005) or Van Rijn (2007) have only limitedly been verified with observations due to a lack of good quality observational data. Also, none of the available approaches cover the complete spectrum of sand-mud interaction, which includes settling, erosion processes induced by the combination of waves and currents, and the bed shear stress. Therefore, in practice sand and mud fractions are often treated separately. This decoupled approach limits the predictive capacity of numerical models, and therefore the impact of human intervention such as deepening of channels and port construction on maintenance dredging volumes and other morphological changes.

In the MUSA-research project, a consortium of contractors, consultants and research organizations join forces to increase the understanding of sand-mud dynamics by means of fieldwork campaigns and laboratory experiments, and to implement this knowledge in engineering tools and advanced models for the prediction of mud and sand transport and associated morphology in tidal conditions with both currents and waves.

Report Phase 1A-B

28 June 2022

MUSA

# Summary

The main goal of MUSA is to improve the engineering tools predicting the amount of erosion and deposition of sand-mud mixtures. Basic parameters involved are:

- sediment composition of the bed;
- bulk density of the top layer of the bed;
- critical bed-shear stress for erosion;
- erosion rate of the bed surface;
- settling velocity in low and high concentration flows.

Most of these parameters are strongly interrelated, but proper relationships are not well known. Herein we present the results derived from Phase 1A and 1B of the MUSA-project. Phase 1A focused on the collection, analyses and primary description of sediment samples and their associated erosion rates obtained from physical experiments with remoulded (disturbed) samples. Phase 1B focused on deposited beds, placed beds (beds in full originating from the field) and exploring the effects of varying bed roughness.

The goal of this report is to provide (1) the description of activities during sampling, (2) to present the sediment characteristics in terms of grain size distribution, wet and dry bulk densities, and organic matter content, and (3) their consolidation characteristics and finally (4) the associated critical shear stress and erosion rates. The latter is divided in remoulded beds (Phase 1A, see Section 3.4) and deposited beds and placed beds (Phase 1B, see Section 4.3).

Within the study, more than 100 sediment samples were collected at Noordpolderzijl (Wadden Sea - NL), Western Scheldt (NL), Scheldt River (BE), Plymouth Estuary (UK) and Bengal Bay. The samples were analysed mainly at the laboratory of WaterProof Marine Consultancy & Services BV. (WaterProof). Firstly, the sediment samples were characterized with respect to the percentage of sand in each sample and the wet and dry densities. The sediment samples covered a wide range of sand-mud percentages which was a crucial prerequisite for the project. The percentage of fines (< 63 $\mu$m) ranged between approximately 5% and 95%. The analyses also included the mineralogical composition, the grain size distribution, organic material content, wet and dry density, consolidation rates and critical shear stress for surface erosion and mass erosion and the associated erosion rates.

The dry-wet densities and the silt-clay ratios presented a wide range of values together with the organic matter content. This wide range of sediment composition contributes to a broader and stronger validation of our results and analyses. Regarding the consolidation experiments, the tested samples were in line with previous research, and allowed for the assessment of erosion characteristics in a wide spectrum of consolidation, and therefore density, values as we expect to observe in natural systems.

The erosion experiments were performed with the EROMES instrument and flow-flume for 3 to 4 different densities of each sample (mud-sand mixture). It was found that the critical shear stresses increased for higher densities and for higher percentages of silt and clay (i.e. mud), with stronger response for higher clay percentages due to its cohesive properties. For lower bulk densities, e.g. <400 kg/m³, and higher sand contents (low cohesion properties) no clear correlation was observed with respect to the critical shear stress. These finding agree with the theoretical background and previous research based on the fact that the cohesion properties of mud, especially clay, and higher bulk densities require more energy to be eroded in comparison with sandy and low-density sediments.

The presence of the rough elements (i.e. shells and pebbles) generally led to lower critical flow velocities ($u_{crit}$) due to additional turbulence created around the elements. In most cases, the erosion initiated around the individual pebbles or shells or at the craters after their displacement. The pebbles and shells were displaced at flow velocities of about 0.5 to 0.6 m/s. The beds with a high percentage of coverage were armoured against erosion as long as the elements remained stable (i.e. flow < 0.5 m/s) and were not dislodged. In terms of bed-shear stress values, the effect of rougher elements was negligibly small or slightly increased the critical bed shear stress for erosion. This is because the bed shear stress is also

MUSA

influenced by the roughness ($k_s$). Therefore, the reduction in the critical flow velocity is somehow compensated by the increase in roughness.

There is a clear effect of bed type (remoulded, deposited or field) on the critical depth-averaged flow velocity and the associated critical bed-shear stress for surface erosion. The deposited beds including the fluffy layer eroded under lower critical shear stress than the reference remoulded samples, while the field beds required higher values to erode. The critical bed-shear stress of the fluffy top layer of a deposited bed is relatively low (0.15 to 0.2 $N/m^2$). The critical bed-shear stress of firmer sublayer just below the fluffy top (depth > 3 mm) is higher (0.75 $N/m^2$) but still lower than that of the remoulded bed. The critical bed-shear stress for erosion of the thin top layer of fields beds with loose particles and flocs is also lower (0.4 to 0.5 $N/m^2$). However, once this top layer is removed, the erosion of the firm sublayer requires a relatively high critical bed-shear stress, which is found to be higher (15% to 50%) than that of a remoulded bed. The variation in erodibility of the field bed samples probably stems from the level of consolidation and the effects of biota.

Report Phase 1A-B

28 June 2022

MUSA

# Contents

# 2 Introduction to the lab and field measurements

## 2.1 Background

The main goal of MUSA is to improve the engineering tools predicting the amount of erosion and deposition of sand-mud mixtures. Basic parameters involved are:

- sediment composition of the bed;
- bulk density of the top layer of the bed;
- critical bed-shear stress for erosion;
- erosion rate of the bed surface;
- settling velocity in low and high concentration flows.

Most of these parameters are strongly interrelated, but proper relationships are not well known.

Based on a literature analysis performed at the start of the MUSA project, relevant knowledge gaps have been identified (Van Rijn et al., 2020 – Report 1204950_TKI-MUSA_01A_FINAL). Based on these knowledge gaps research questions have been defined.

## 2.2 Research questions

The main research questions of this MUSA project are grouped in 3 main subjects; (1) erosion, (2) deposition and (3) sediment density and are described below:

Main research questions related to erosion:

1. What is the effect of varying percentages of clay, silt and sand and degree of consolidation on the erodibility?
2. What is the role of bed irregularities (gravel, shells) on the erodibility?
3. How are the critical stresses and erosion rates of the sand and mud fractions related to bulk sediment properties (bed density) and basic hydrodynamic parameters?
4. What is the effect of the easily erodible upper fluffy layer (as found in field conditions)?

Main research questions related to deposition:

5. What is the influence of the settling velocity and sediment concentration distribution on the deposition flux close to the bed, and how can this be related to hydrodynamic forcing and sediment properties?
6. What is the role of sand on mud floc size, shape, density, and the resulting settling rates?
7. How to obtain an accurate settling velocity distribution using settling tube and video-camera results? And, related to this, what is the effect of sample transfer to the laboratory on floc size and settling velocity?

Main research questions related to sediment density:

8. What is the best method to measure the density of the upper 50 cm of the bed, with a focus on the transition layer between water and seabed?
9. What is the dry bed density of the upper 50 cm of mud-sand beds in tidal conditions and how does this relate to other sediment properties (e.g. composition, compaction, mud/clay content and minerology)?
10. What is a simple method for extraction and analysis of samples in shallow and in deep water?

Research questions 1, 3 and 9 are addressed in this report.

## 2.3 Approach

To answer the above research questions an extensive Measurement Plan has been prepared (Perk and Van Rijn, 2020 – 1204950_TKI-MUSA_01A_FINAL). The proposed experiments and field measurements are divided in 2 main phases; (1) Laboratory experiments and (2) Field measurements. Each phase comprises a number of sub-phases in which focus is given on a certain type of experiments and measurements. The experiments foreseen for Phase 1 and Phase 2 are listed below.

Report Phase 1A-B

28 June 2022

**Phase 1: Laboratory experiments**

- 1A: Erosion of remoulded bed samples of mud and sand under currents
- 1B: Erosion of placed-bed and deposited-bed samples of mud-sand in currents.
- 1C: Erosion of remoulded bed samples of mud and sand in waves
- 1D: Erosion of placed-bed samples of mud and sand in combined currents and waves
- 1E: Settling velocity and floc size in laboratory (HR Wallingford)
- 1F: Spare: experiments to fill in knowledge gaps identified during the project

**Phase 2: Field measurements**

- 2A: Settling velocities and floc size in tidal channel with mud-sand bed (Holwerd); spring 2022
- 2B: Erosion of mud-sand beds in tidal channels (Field measurements spring 2022)
- 2C: Erosion of mud-sand beds in tidal channels (Field measurements autumn 2022)

The Phase 1A series of laboratory experiments focusing on sediment characterization and erosion of remoulded bed samples of mud and sand in currents are presented in this report. A more detailed analysis and synthesis will be included during the follow-up phases of the project.

This report is a living document and is continuously updated each time more results from the experiments performed under the various phases become available and will be finalized at the end of the MUSA-Project.

## 2.4    Outline

This report describes the method and results of the experiments and field measurements which are performed within Phase 1A and 1B of the MUSA project.

Chapter 3 presents the Phase 1A experiments that describes the sediment sampling (Chapter 3.2), the methodology of laboratory analyses and physical experiments (Chapter 3.3), presents the results (Chapter 3.4) and conclusions are drawn in Chapter 3.5.

Chapter 4 addresses the Phase 1B experiments encompassing the laboratory methodology on Chapter 4.2, results on chapter 4.3 and conclusions on Chapter 4.4.

# 3 Method and results of Phase 1A experiments

## 3.1 Introduction

Phase 1A aims to contribute to research questions 1, 3 and 9 as introduced in Chapter 2:

1. What is the effect of varying percentages of clay, silt and sand and degree of consolidation on the erodibility?
3. How are the critical stresses and erosion rates of the sand and mud fractions related to bulk sediment properties (bed density) and basic hydrodynamic parameters?
9. What is the dry bed density of the upper 40-50 cm of mud-sand beds in tidal conditions and how does this relate to other sediment properties?

For that, more than 100 sediment samples were collected at the following sites:

- Noordpolderzijl (Wadden Sea, Netherlands);
- Western Scheldt Estuary (Netherlands);
- Scheldt River (Belgium);
- Plymouth Estuary (UK);
- Bengal Bay (proximity of Ganges-Brahmaputra delta).

Firstly, the sediment samples were characterized with respect to the percentage of sand and mud in each sample and the wet and dry densities. The sediment samples covered a wide range of sand-mud percentages which was a crucial prerequisite for the project. The percentage of fines (< 63 $\mu$m) ranged between 3 and 95%.

Based on this a selection was made of fewer representative samples which were analysed in more detail. The percentage of fines (< 63 $\mu$m) ranged between 3% and 95%. The analyses performed on the selected samples included the mineralogical composition, the grain size distribution (using three methods: Laser Diffraction, Hydrometer and Sedigraph), organic material content, wet and dry density, consolidation rates and critical shear stress for surface erosion and mass erosion (by performing flume tests and EROMES tests) and the associated erosion rates.

In this chapter the collection of sediment is described in Section 3.2. In Section 3.3 the methodology used for the Phase 1A laboratory experiments is described. The results of the analysis are described under Section 3.4. This will be further detailed during the follow-up phases of the project, including a synthesis on all experiments. Section 3.5 describes the main conclusions and recommendations of this Phase 1A.

## 3.2 Collection of Sediment

Sediment samples were collected from the locations specified in tables below.

We make a distinction between 2 types of sites (Table 3.1):

- Sites close together where a wide range in sandy/silty/clayey samples can be taken at relatively close distance from each other;
- Sites in different places where predominantly silty/clayey sediment is available and where differences in mineralogy can be expected considering the 3 main groups of clay minerals (Illite, Chlorite kaolinites, micas, and smectites).

In September 2020 samples were collected from Noordpolderzijl (NL) and the Western Scheldt estuary (NL). Later, in 2021, we received new samples from Plymouth Estuary (UK – HR Wallingford), samples from Bengal Bay (vicinity of the Ganges-Brahmaputra delta - Jan de Nul) and samples from the Scheldt River (Belgium near Oosterweel – DEME).

MUSA

*Table 3-1: Sites where samples were taken (until March 2021)*

| Sites where sediment samples have been taken: | | |
|---|---|---|
| Country | Location | Samples |
| NL | Noordpolderzijl (NPZ) | samples taken at 4 locations in the entrance to the port of Noordpolderzijl where transition between 95% sand and 95% mud takes place along 3 km long, 1 m deep channel |
| NL | Western Scheldt Estuary | Samples taken from 13 locations along the north and south intertidal banks where both sandy and silty locations are available |
| UK | Plymouth Estuary | Samples taken from 5 locations along Plymouth estuary (courtesy from HR Wallingford) |
| BE | Scheldt River | Samples taken from the bank of Scheldt river near Oosterweel (courtesy from DEME) |
| - | Bengal Bay (BB) | Samples taken from the Bengal Bay near Ganges-Brahma Putra delta (courtesy from Jan de Nul) |

The sites were chosen as starting point because they show a wide range of sand-silt-clay compositions and different sediment sources with different mineralogy. In addition, the choice of sites allows for comparison with previous research, for example that of Van Rijn (2020) at Noordpolderzijl and the bi-yearly MONEOS monitoring of Rijkswaterstaat at the Western Scheldt (NL).

At Noordpolderzijl (NL), small and large (>10L) sediment samples were collected at 4 locations on 27 August 2020. In the Western Scheldt samples were collected between 3 and 9 September 2020. The sampling date, and locations for the large samples are presented in Table 3-2.

The sampling strategy consisted of three types of samples:

- Small surface samples of 71 mL, called hereafter as jar-samples, that allow for fast analyses and in-situ evaluation of sand-mud percentages;
- Small sub-surface samples (71 mL) for assessing how the sediment characteristics vary along the first 0.5 m of the sediment bed;
- Larger sample of 10-20L, referred to hereafter as barrel-sample, for detailed sediment analyses and for the execution of consolidation and erosion tests.

The samples were manually collected with a spade or spoon (Figure 3-2), and the in-situ wet bulk density was determined by dividing the sample weight by its volume. The samples were stored in cool conditions and away from direct sunlight to avoid changes in the organic matter content before being used in the laboratory at WaterProof.

In total over 60 small surface samples and about 50 small sub-surface samples were collected. Besides, 25 larger samples (> 10L) were collected. In this report we focus on the larger barrel-samples, (base samples) with which many experiments have been executed. Nonetheless all samples are included where relevant, for example in the bulk density analyses. The location, main sediment characteristics (densities, %fines< 63 $\mu$m, %sand> 63 $\mu$m) and vertical reference level of all samples is provided in:
MUSA database spreadsheet (11204950_TKI-MUSA_02B_Database_phase1A.xlsx).
Table 3-2 provides the sample locations, dates, site names, sample numbers and coordinates.

Report Phase 1A-B

28 June 2022

*Table 3-2: Sampling date, and locations from where the selected barrel samples were collected*

| Location | Sampling date | Site | Sample nr | RWS nr | Lat | Lon |
|---|---|---|---|---|---|---|
| Wadden Sea | 27-8-2020 | Noordpolderzijl | H2 | - | 6°34'56.66"W | 53°26'0.486"N |
| Wadden Sea | 27-8-2020 | Noordpolderzijl | B5 | - | 6°34'54.28"W | 53°26'7.141"N |
| Wadden Sea | 27-8-2020 | Noordpolderzijl | B8 | - | 6°34'51.6"W | 53°26'16.8"N |
| Wadden Sea | 27-8-2020 | Noordpolderzijl | B9 | - | 6°34'48"W | 53°26'27.6"N |
| Western Scheldt | 3-9-2020 | Hulst | HU1 | 411 | 3°57'36.549"W | 51°22'25.341"N |
| Western Scheldt | 3-9-2020 | Baalhoek | BH1 | 551 | 4°3'3.6"W | 51°21'57.6"N |
| Western Scheldt | 3-9-2020 | Saefetinghe | SA1 | 591 | 4°12'49.157"W | 51°22'6.721"N |
| Western Scheldt | 3-9-2020 | Paal Harbour | PA1 | - | 4°6'39.6"W | 51°21'7.2"N |
| Western Scheldt | 4-9-2020 | Baarland | BA1 | - | 3°52'22.8"W | 51°23'49.2"N |
| Western Scheldt | 4-9-2020 | Zweemersdam | ZW1 | - | 3°51'25.2"W | 51°23'27.6"N |
| Western Scheldt | 4-9-2020 | Zweemersdam | ZW2 | - | 3°51'25.2"W | 51°23'27.6"N |
| Western Scheldt | 7-9-2020 | Terneuzen | TE | | 3°51'56.842"W | 51°20'19.963"N |
| Western Scheldt | 7-9-2020 | Paulina Polder | PPW | 781 | 3°42'41.978"W | 51°21'28.445"N |
| Western Scheldt | 7-9-2020 | Griete Harbour | GR1 | - | 3°53'6"W | 51°20'53.88"N |
| Western Scheldt | 7-9-2020 | Griete Harbour | GR1.5 | - | 3°53'6"W | 51°20'55.32"N |
| Western Scheldt | 9-9-2020 | Bath | BATH3 | 123 | 4°11'55.837"W | 51°24'8.51"N |
| Western Scheldt | 9-9-2020 | Bath-Appelzak | AZ1 | 111 | 4°14'23.712"W | 51°23'10.768"N |
| Western Scheldt | 9-9-2020 | Waarde-west | WAW1 | 401 | 4°5'17.053"W | 51°24'22.056"N |
| Western Scheldt | 2021 | Bath-pump | BA-PU | | 4° 13' 8.07"W | 51°23'55.42"N |
| Western Scheldt | 2021 | Bath-Appelzak | BA-APP | | 4°14'33.66"W | 51°23'0.72"N |
| Western Scheldt | 2021 | Oosterweel | SO3 | | 4°22'18.92"W | 51°14'11.78"N |
| Plymouth Estuary | 2021 | Plymouth | PLUK1 | | 4°6'11.4"W | 50°22'24.3"N |
| Plymouth Estuary | 2021 | Plymouth | PLUK4 | | 4°6'11.3"EW | 50°22'24.8"N |
| Bengal Bay | 2021 | Bengal Bay | BB3 | | NA | NA |
| Bengal Bay | 2021 | Bengal Bay | BB2 | | NA | NA |

A brief overview of the individual sampling locations is presented below.

### 3.2.1 Noordpolderzijl (NPZ)

The sampling locations at the harbour of Noordpolderzijl (NPZ), located at the Dutch part of the Wadden Sea, are depicted in Figure 3-1 and Figure 3-2. A shallow tidal channel of about 10 meters width connects the Wadden Sea to the small harbour of Noordpolderzijl. The harbour basin has a length of about 200 m and a width of about 30 m. The intertidal mud flats at Noordpolderzijl are relatively high near the dike and are only flooded during storm conditions, while the northern areas away from the dike are flooded more

Report Phase 1A-B

28 June 2022

MUSA

frequently. The harbour of Noordpolderzijl suffers from sedimentation and both the channel and harbour basin are dry during low water. The seabed level of the channel and the basin is approximately equal to Mean Sea Level (MSL). A more detailed impression of the sampling locations at Noordpolderzijl is provided in Appendix A.
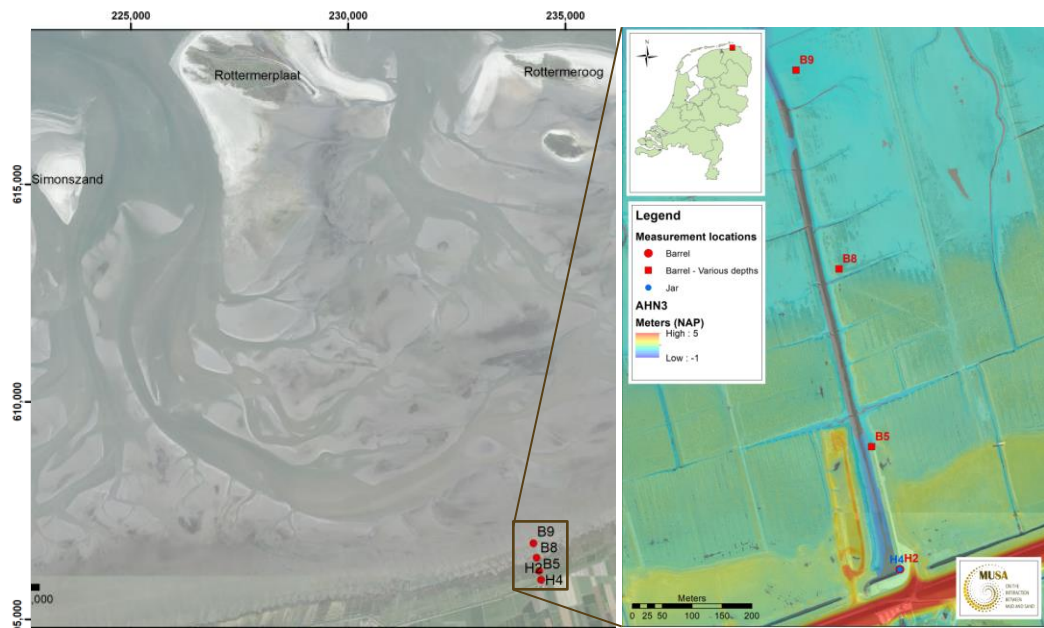


*Figure 3-1: Plan view and sampling location at Noordpolderzijl – Wadden Sea, NL.*



*Figure 3-2: Overview photos of Noordpolderzijl during sampling (Source: WaterProof).*

### 3.2.2 Western Scheldt (WS)

The Western Scheldt is a fluvial-tidal estuary that connects the Scheldt River to the North Sea. It is an important estuary as it functions as the entrance to the Harbour of Antwerp, and also is a physical and political boundary between the Netherlands and Belgium. The Western Scheldt was chosen due to its environmental-economical relevance, and because of its known variety of sub-environments containing different distributions of sand and mud which is a key characteristic for this research. In general, the intertidal higher areas are mud-rich with a soft top layer especially near the salt marshes. Sandy horizons are more abundant in the absence of vegetation and near active channels. In addition to the sand and mud distribution, the intertidal flats are rich in shells, seagrass, pebbles, stones, bedforms and organic matter in the form of peat and marshes. This wide variety of sediment characteristics and environments makes the Western Scheldt a key site for the MUSA research.

Most samples from the intertidal mud flats of the Western Scheldt were collected during a 4-days field campaign of WaterProof together with the MONEOS monitoring project of Rijkswaterstaat (Figure 3-3).

Report Phase 1A-B

28 June 2022

In Figure 3-4 to Figure 3-6 photos are presented of a number of sampling locations. Detailed GIS maps of all sampling locations at each individual site and site-photos are included in Appendix A.

Hereafter, a more detailed description of the site characteristics is given (Photographs in Appendix A):

South bank (Western Scheldt)

- Paulina Polder (PPW); sandy mud site with bed ripples, shells and patches of seagrass; soft upper layer with mud and peat in upper 3 cm;
- Terneuzen (TE); sandy mud site with bed ripples, shells and patches of vegetation; soft upper layer with mud and peat in upper 3 cm;
- Griete Harbour (GR); soft muddy site along banks inside small harbour area (marina; fishing boats);
- Hulst (HU); very firm sandy mud site (yellow-brown colour), ripples, shells and patches of vegetation;
- Baalhoek (BH); muddy site with soft upper layer at toe of dike; patches of vegetation;
- Paal harbour (PA); muddy site along banks inside small marina/harbour;

North bank (Western Scheldt)

- Zweemersdam (ZW); sandy mud site with soft upper layer; patches of seagrass near dike;
- Baarland (BA); sandy mud site with soft upper layer at toe of dike;
- Waarde-west (WAW); sandy mud site with soft upper muddy layer of 0.1 m;
- Bath Pump (Bath); muddy site with soft upper layer between new groins and between groins of pumping station outlet; very sandy site west of pumping station with thin muddy layer (< 10 mm);
- Appelzak south of Bath (APP); sandy mud site with soft muddy upper layer of 0.05 to 0.1 m
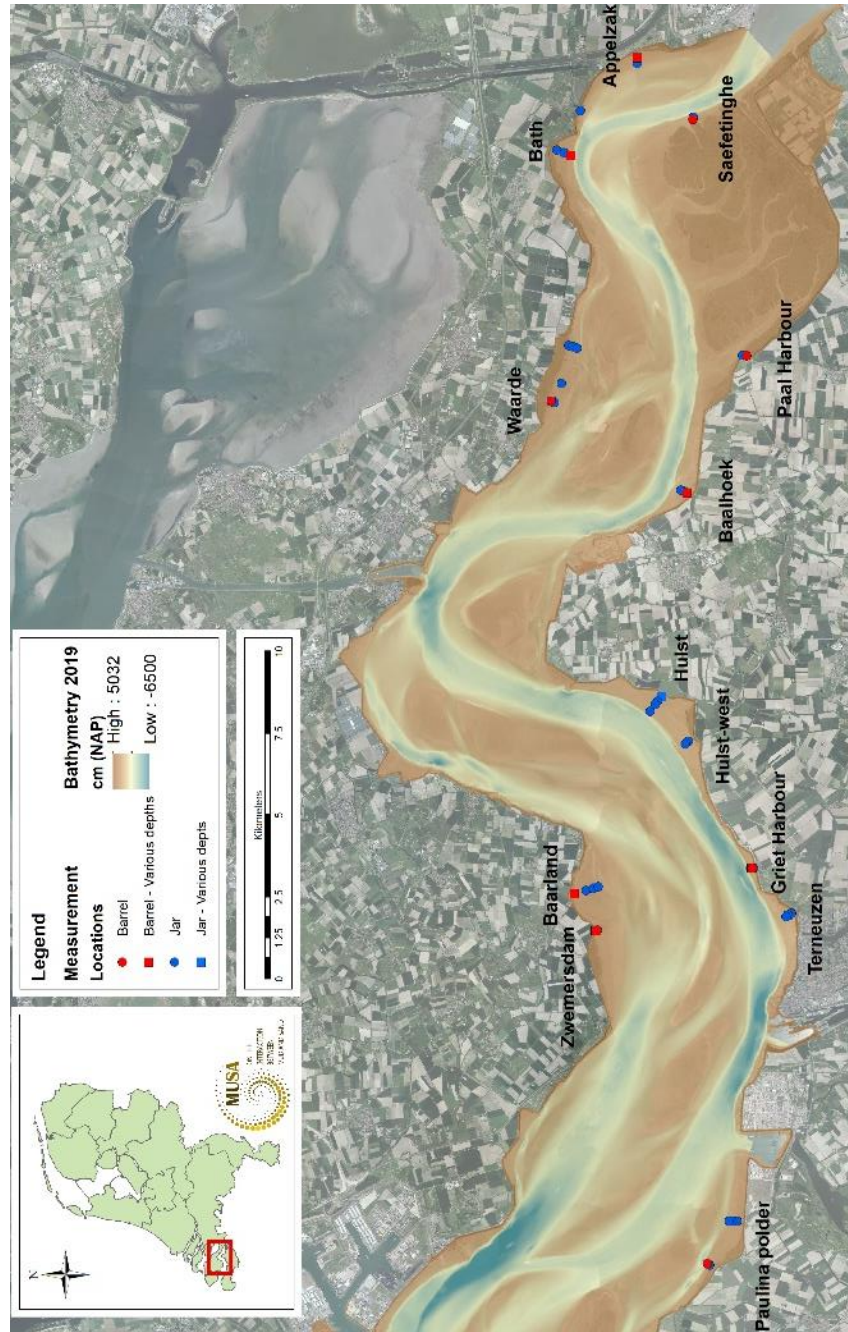
Report Phase 1A-B

28 June 2022

MUSA

*Figure 3-3: Map view of the Western Scheldt including the sampling stations.*

*Figure 3-4: Muddy sampling location Zweemersdam (ZW) along northern bank of Western Scheldt taken from the dyke (left). Mud sampling location at this location (right)*



*Figure 3-5: Very sandy tidal flat along northern bank near Bath (west of pumping station) of Western Scheldt*



*Figure 3-6: Muddy sampling location Bath-south (Appelzak) along north bank of Western Scheldt*

Report Phase 1A-B

28 June 2022

### 3.2.3 Scheldt River

The Scheldt River originates at St. Quentin (France) and has a catchment area of approximately 20.000 (150x150 ) km², which is drained by the river and its branches to the sea. The river Scheldt is situated in the northeast of France, the west of Belgium (Flanders), and the southwest of The Netherlands. The river with length of about 350 km can be divided into the non-tidal Upper Scheldt and the tidally influenced part which extends from the sluices at Gent until the mouth at Vlissingen (160 km). The tidal range in the Scheldt river near Antwerp goes up to about 6 m due to amplification effects. From the Dutch/Belgian border, the tidal river is called Sea Scheldt which is further divided into the Lower Sea Scheldt, stretching from the border until Antwerp, and the Upper Sea Scheldt, stretching from Antwerp to the upstream boundary at Gent. Three main rivers join the Scheldt: the Dender, the Durme, and the Rupel.

The wider tidal estuary seaward of the mouth of the Scheldt river is located in the Netherlands and is known as the Western Scheldt.

On the left bank of the tidal Scheldt River (near Oosterweel), Antwerp, sediment samples were collected over 1 transect from the dike towards the channel. In total 3 large samples were taken from the Scheldt site as courtesy from DEME.
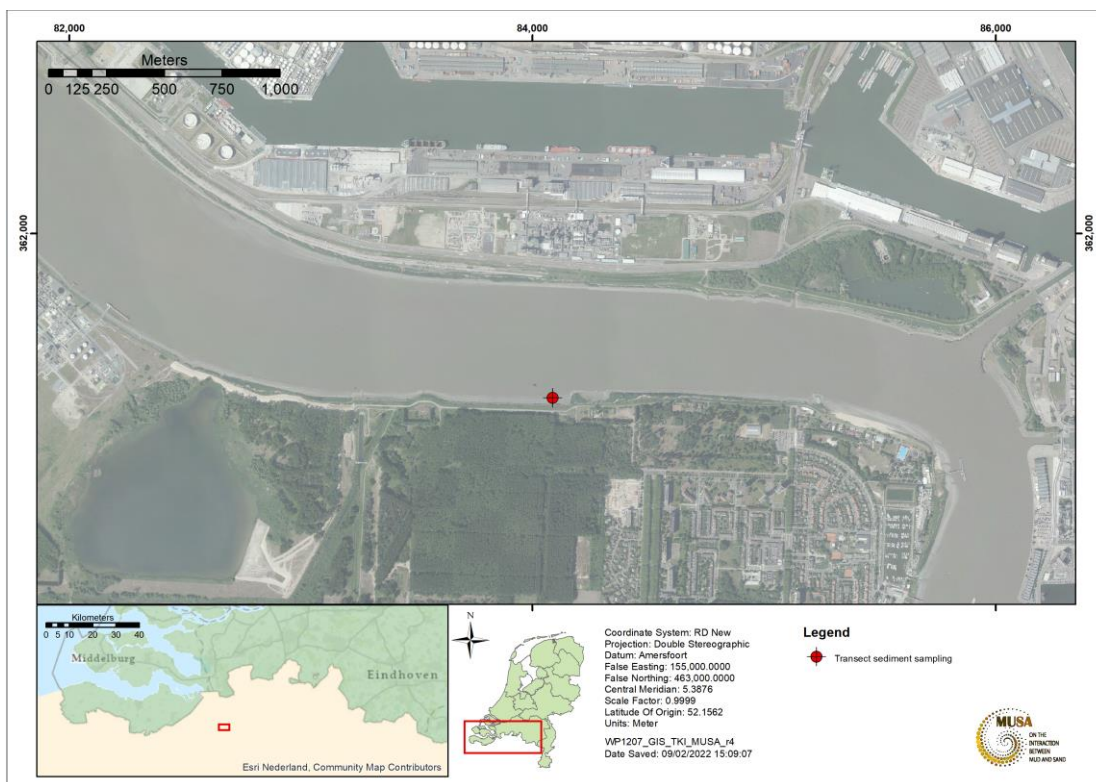


*Figure 3-7: Location for sampling at Oosterweel near Antwerp.*

*Figure 3-8: Sediment sampling at the Scheldt, courtesy of Thijs Cornu - DEME*

### 3.2.4 Bengal Bay

Four large sediment samples were collected by Jan de Nul at the Bengal Bay area in the vicinity of the Ganges-Brahmaputra delta. The location and site description are disclosed due to confidentiality terms.

### 3.2.5 Plymouth Estuary (UK)

In the tidal part of the river Plym near Plymouth (UK), various mud-sand samples from the intertidal banks (sites 1 to 5) were collected by Professor Dr. Andrew Manning (HR Wallingford) on May 2021, see Figure 3.9.

Located in Devon on the south-western peninsula of England, the Plym Estuary is a tidal river estuary that drains into Plymouth Sound at the estuary mouth. Collectively, Plymouth Sound and Estuaries have the following general characteristics:

- Marine areas, Sea inlets (50%)
- Tidal rivers, Estuaries, Mud flats, Sand flats, Lagoons including saltwork basins (40%)
- Salt marshes, Salt pastures, Salt steppes (5%)
- Coastal sand dunes, Sand beaches, Machair (2%)
- Shingle, Sea cliffs, Islets (3%)

The river's sediment source is around 450 meters above sea level on Dartmoor, in an upland marshy area called Plym Head. From the upper reaches, which contain antiquities and mining remains, the river flows roughly southwest past clay workings at Shaugh Prior to The Dewerstone, where it meets the River Meavy. The course then changes to run southwards, between Plymouth and Plympton passing through the National Trust owned Plymbridge Woods and under the ancient Plym Bridge.

The Plym Estuary experiences semi-diurnal tides with mean neap and spring ranges of 2.2 m and 4.7 m, respectively. This classifies the Plym Estuary as mesotidal. Above Laira Bridge the valley widens and the river channel shallows abruptly. Two wide bays, one on each side, were reclaimed by the erection of embankments early in the nineteenth century. The reclaimed land on the east side, known as Chelson Meadow, is drained by a series of ditches which harbour a characteristic brackish water fauna, grading inland into that of fresh water. The existing stretch of the estuary at Laira includes some extensive stretches of soft mud containing a large ingredient of China clay (predominantly kaolinite) washings carried down by the Torry and Plym.

MUSA

Five sampling sites are defined where surface samples and subsurface samples (10, 20, 30 and 40 cm below surface) have been collected (Figure 3.10):

- PLUK1 is mostly muddy;
- PLUK2 (intermediate sample between 1 and 3);
- PLUK3 is less cohesive;
- PLUK4 is muddy with organic materials;
- PLUK5 is sandy with coarse grains, little mud.

Sites PLUK2, 3, 5 are near Saltram Beach and sites PLUK1, 4 are near Chelson Meadow Recycling Centre, 250 m and 140 m wide, respectively.



*Figure 3-9: Sample sites Plym Estuary*
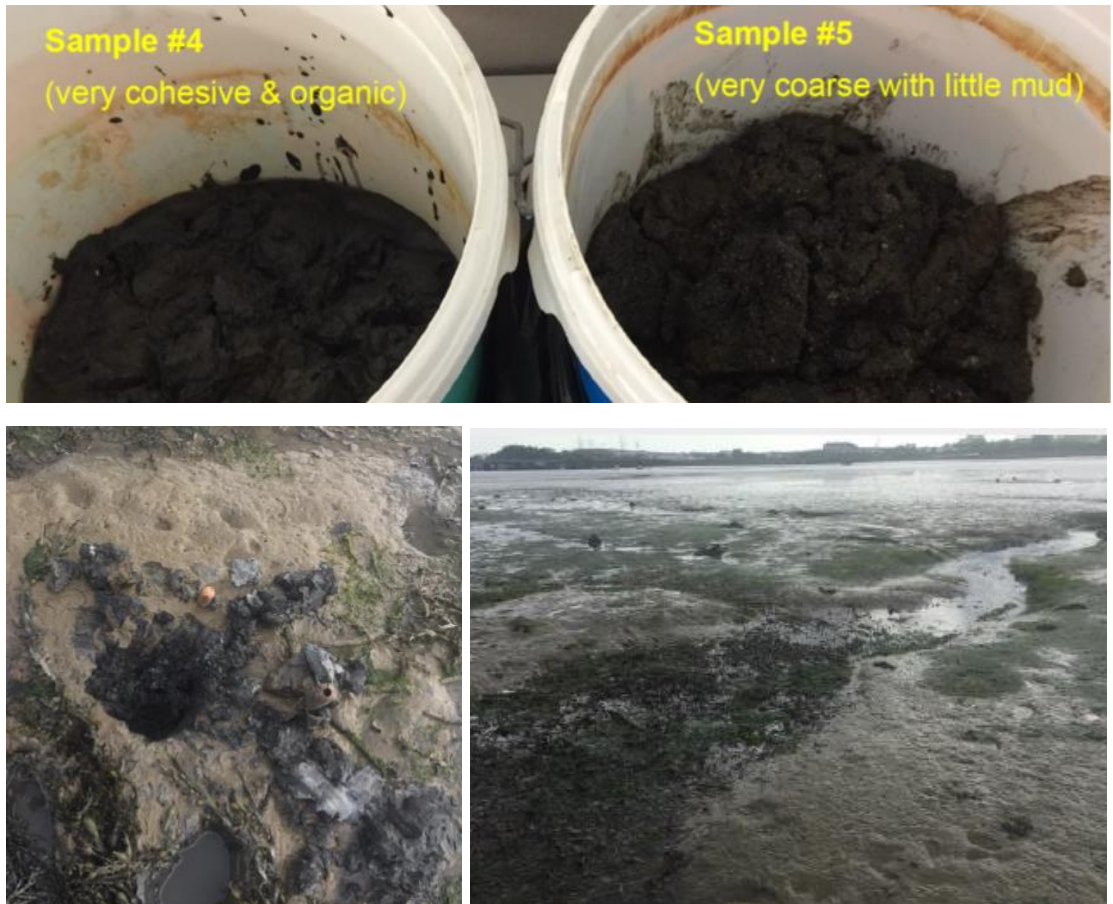
Report Phase 1A-B

28 June 2022

*Figure 3-10: Sample photos from the Plym Estuary (UK)*

## 3.3 Laboratory and Physical Experiments methodology

Under this section we briefly describe the methodology of all analyses and experiments. The detailed procedures are described in the measurement plan (Perk and Van Rijn, 2020 – Report 11204950_02A_CONCEPT2). The mud characteristics (section 3.3.1) were mainly determined by third-party laboratory analyses from Utrecht University and Wiertsema. While the other tests and the flume experiments were performed at WaterProof.

### 3.3.1 Mud characteristics and properties

Differences in the mud composition and characteristics, especially regarding the clay fraction, influences the behaviour of the sand-mud mixtures. In order to assess whether there are relationships between the erosion behaviour and the mud characteristics, we investigated the mineralogy, plasticity and strength of selected mud-rich samples.

Mud characteristics and properties were determined by analyses performed at Wiertsema (Tolbert, NL) and Utrecht University (NL). The analyses included:

- Mineral composition (Utrecht University)
- Plasticity index and Atterberg limits (Wiertsema)
- Remoulded yield strength (Wiertsema)

A detailed description of these test results is given in MUSA Report: *Literature Review-Measuring and interpretation of settling velocity and particle size, 2022.* Herein, a brief summary is given (see below).

**Mineral composition**

The cohesive and plasticity properties of clays are (to some extent) related to the physical-chemical characteristics of the clay minerals and the relative proportions of the minerals in the soil. Common clay minerals are kaolinite, illite and montmorillonite, which belong to the group of layered silicate minerals and often occur in nature as intermixed minerals in the soil.

Kaolinite is a soft, white mineral produced by chemical weathering of silicate minerals like feldspar. It has a low shrink-swell capacity in contact with water. Similarly, Illite is a non-expanding (non-swelling) layered silicate mineral. It occurs as aggregates of small to grey crystals produced by chemical weathering of other silicate minerals like feldspar. Illite is the most common clay mineral. Montmorillonite is a subclass of the smectite minerals consisting of plate-shaped particles. The individual crystals of Montmorillonite and water can easily intervene causing this clay to swell (increase of volume due to absorption of water). Chemically, it is a sodium (Na)-Calcium (Ca) based clay. Bentonite is a typical example of Montmorillonite clay, which is used as a viscous mud slurry in soil drilling industry (for cooling of drilling equipment and removing of drilling solids).

**Plasticity Index**

The degree of cohesivity of the samples can be expressed in terms of the Plasticity Index (PI) based on the Atterberg limits (Atterberg tests). The type of clay minerals and the relative proportions of the clay mineral in a soil may have a major influence on the degree of plasticity of a soil as determined by standard Atterberg tests.

The plasticity index of a soil is the numerical difference between the liquid limit and the plastic limit, which are known as the Atterberg limits. Both limits basically are moisture contents (in %). These limits define ranges in moisture content at which a soil will behave as solid, plastic of liquid materials. Typical PI-ranges are:
- PI<30: low plasticity (sandy soils);
- 30<PI<50: intermediate plasticity (silty/loamy soils);
- PI>50: high plasticity (clayey soils).

The test followed the NEN-EN-ISO-17892-12 protocol of Atterberg test.

**Remoulded yield strength**

The yield stress (undrained shear strength) is a parameter related to the internal resistance of mud-sand samples which can be determined by a vane *in-situ* test or in the laboratory using a soil sample. The vane/spindle is pushed into the soil and the spindle is rotated at slow rate ($5^{\circ}$ to $10^{\circ}$ degree per minute). The torque of the instrument is measured at regular time intervals (Figure 3-11). If the soil fails, the rotation rate will suddenly increase, and the torque will decrease to a lower constant value which is used as an estimate of the undrained remoulded shear strength. The yield stress is the stress just before initiation of viscous deformation (creep). The yield stress of the MUSA-samples was determined using the Brookfield Rheometer DV3T with a vane-type spindle at the Soil Mechanics Laboratory of Wiertsema (Tolbert, Groningen).

MUSA

*Figure 3-11: Shear stress results of vane experiment.*

### 3.3.2 Bulk Densities

The bulk density can have an important effect on the behaviour of sand-mud mixtures. Generally, lower density sediments with the same sand-mud characteristics can be eroded at lower critical shear stresses. Moreover, the densities give a good indication on the compaction of the sediment. Therefore, the dry and wet densities of all samples are analysed.

First, the wet bulk density of small samples was determined in-situ by either taking a sediment sample using a ring (dense material) or small container (softer materials) with known volume. The density was then determined by weighing the known volume of sediment. The wet density of the larger samples was determined by taking subsamples with known volume in the laboratory.

The dry bulk density was determined by 2 different methods: (1) weighing the samples after drying at 70 to 90ºC in an oven, and (2) computed from

$$\rho_{dry} = \frac{\rho_{wet} - \rho_w}{1 - (\frac{\rho_w}{\rho_s})}$$
Equation 1

where:

$\rho_{dry}$ = dry bulk density (kg/m³);
$\rho_{wet}$ = wet bulk density (kg/m³);
$\rho_w$ = water density – here 1020 kg/m³;
$\rho_s$ = sediment density – here 2650 kg/m³.

### 3.3.3 Grain size distribution

The grain size distribution has a large effect on the physical behaviour of the sediment. To analyse the grain size distribution of the sediment samples we applied different methods for the sand and mud fractions. At the WaterProof laboratory we performed sieving in combination with hydrometer and tap/pipet analyses without pre-treatment of samples (no removal of calcareous and organic materials). In addition, samples were also analysed with Laser Diffraction at Utrecht University, Sedigraph at Wiertsema Soil Mechanics Laboratory and video analyses from HR Wallingford.

First, the sand fractions (> 63 µm) were sorted from the fine (mud) fractions by means of wet sieving; the sample was washed over a sieve mesh of 63 µm where the sand fraction was retained while the finer content was washed into a container. After this sorting, the sand fraction was dried, and the grain size

Report Phase 1A-B

28 June 2022

**MUSA**

distribution was obtained by dry sieving. The grain size distribution of the finer particles was obtained with two methods, namely 1) the hydrometer test and 2) the TAP/Pipet test.

Beside these methods, the outcomes of the Laser Diffraction and Sedigraph tests provided a grainsize distribution of the full samples. Under Phase 1E, HR Wallingford will also analyse the grain size distribution based on a video-based method. Important to note that methods such as the tap/pipet, hydrometer and Sedigraph are based on settling velocity while the Laser Diffraction and the Video Observation method directly measure the particle sizes. Therefore, the settling velocity methods indirectly quantify the particle size while they capture the effective settling velocity (that is relevant for the depositional behaviour) while the direct methods are able to directly measure the particle size but do not assess the settling behaviour.

The hydrometer and TAP/Pipet tests have been extensively compared by Van Rijn and Koudstaal (2021). The methods are briefly described below.

### 3.3.3.1 Grain size distribution of sand particles > 63 µm

The grain size distribution of sand, *i.e.* sediment particles > 63 µm, was obtained by dry sieving. A Haver & Boecker sieving machine was used with 10 sieve meshes (Figure 3-12). The sieve mesh choice consisted of ½ phi, *i.e.* phi is the $\log_2$(diameter in millimeter), interval between medium sand and silt while the coarser fractions were sieved in 1 phi intervals up to very coarse sand. The grain size classes follow the Wentworth (1922) distribution with the following sieve meshes: 2000, 1000, 500, 355, 250, 212, 125, 90, 63 and 45 µm.



*Figure 3-12: Haver & Boecker sieve stack*

### 3.3.3.2 Grain size distribution of fine particles < 63 µm, method 1: Hydrometer test

The hydrometer test measures the settling velocities by means of the buoyancy of a floating body to obtain the grain size distribution of the finer (<63 µm) fractions. The method is based on the settling of suspended particles in a standing column of water. A float type ASTM152H:E100 (Figure 3-13) was used to measure the density of the slurry consisting of water and sediment in suspension. A temperature sensor and heating system was applied to maintain the water temperature at a fixed level (20 degrees).
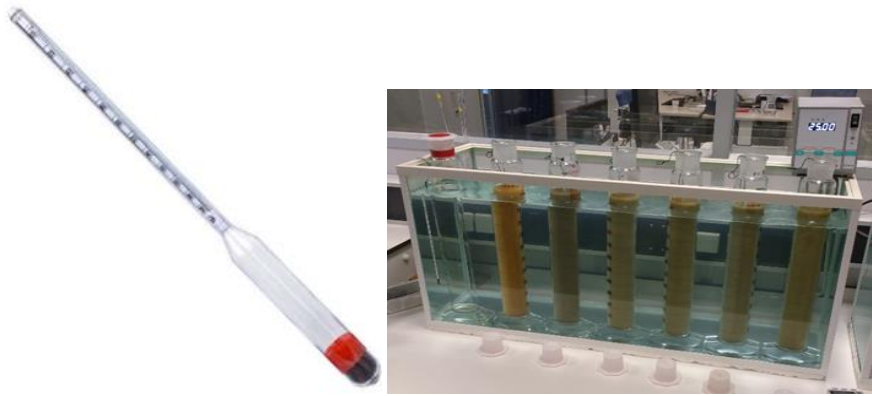
*Figure 3-13: Hydrometer float type ASTM152H:E100 (left) and water basin in which temperature is remained constant (right).*

The float measures the slurry density on the upper part of the water column. Since particles of different sizes settle with different velocities, and therefore time, the density of the suspension decreases with time by the sedimentation of relatively larger particles. By knowing the time in which a particular grain size class of sediment settles it is possible to indirectly derive a grain size distribution (Stokes particle size distribution). The theoretical settling velocity is based on the Stokes formulation, which reads as;

$$w_s = \frac{(s-1)g.D_{stokes}^2}{18\upsilon} \qquad \text{Equation 2}$$

that can be transformed into

$$D_{stokes} = \sqrt{\frac{18\upsilon}{(s-1)g}.\frac{h_e}{t}} \qquad \text{Equation 3}$$

where,

$D_{stokes}$ = Stokes settling diameter (m);
$w_s$ = settling velocity (m/s) = $h_e/t$;
$h_e$ = effective settling height (m);
$t$ = time (s);
$g$ = acceleration of gravity, here 9.81 m/s$^2$;
$\rho_s$ = sediment density, here 2650 kg/m$^3$;
$\rho_m$ = fluid mixture density, here 1010 kg/m$^3$;
$s$ = relative density, here $\rho_s/\rho_m$ = 2650/1010=2.623 (-);
$\upsilon$ = kinematic fluid density depending on temperature (m$^2$/s)

In the testing cylinder a sediment suspension of about 1L with a concentration was prepared between 20 and 30 g/L of sediment in combination with 125 mL of dispersing agents (i.e. Calgon) consisting of 35 g of sodium polyphosphate and 7 g of sodium carbonate on 1L demi water. This mixture of sediment and dispersing agents (DA) was prepared at least 18 hours before the start of experiment and was kept under constant temperature immerse in water. The temperature was measured by a separate thermometer during the entire extent of the test. Immediately before the test, the suspension was mixed thoroughly. Along the test the density and temperature were documented at predetermined times: 18 s, 40 s, 2 min, 5 min, 15 min, 30 min, 60 min, 4 hours, and minimum of 20 hours.

During the experiment, except for the first measurements, the hydrometer was removed to prevent that particles settle on the hydrometer and distort the measurement. Meanwhile the hydrometer was cleaned in demi water and stored in a DA solution of 125 mL Calgon diluted in 1L of demi water. Detailed information on procedures of the hydrometer method is given in the MUSA-report by Van Rijn and Koudstaal (2021).

### 3.3.3.3 Grain size distribution of fine particles < 63 μm, method 2: Pipet/TAP method

Similarly to the Hydrometer method, the Pipet/TAP method is based on the settling of suspended particles in a settling column (Figure 3-14). The advantage of the Pipet/TAP method is that concentrations in the range between 50 and 1000 mg/L can be tested while the hydrometer experiments requires higher concentrations (20.000 – 30.000 mg/L). Small samples are taken from the prepared mixture of water, sediment and DA at calculated times based on the Stokes settling law. The sediment distribution is computed from the amount of sediment collected in these small samples over time.
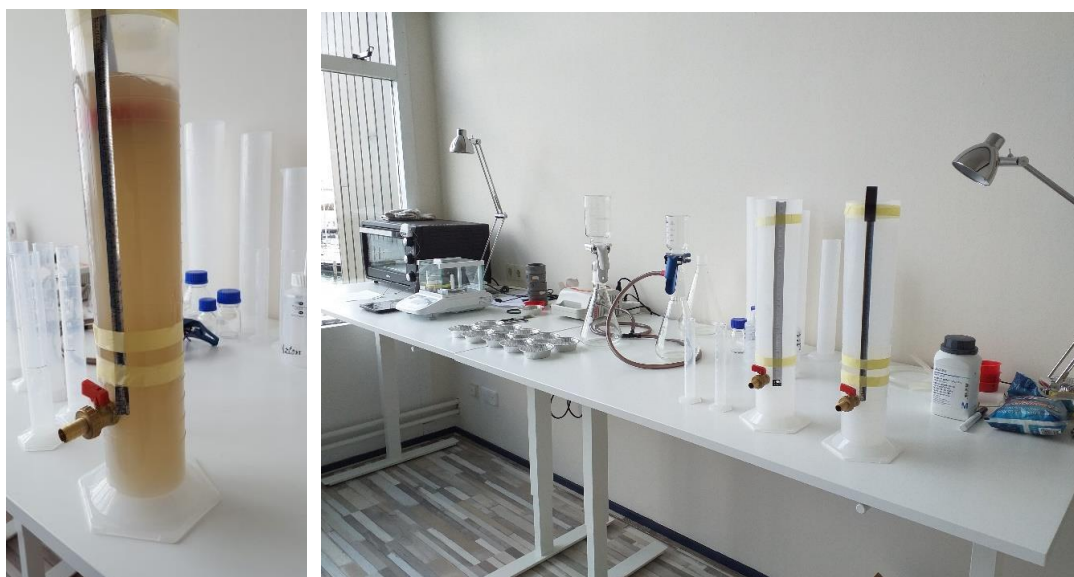


*Figure 3-14: Photo of the settling cylinder used for the Pipet/TAP test.*

The settling column consists of a Perspex cylinder with an internal diameter of 90 mm and a height of about 45.5 cm. A small tap is located about 80 mm above the base of the column. A 2L suspension with DA was made for sediment concentrations between 500 and 1000 mg/L. This mixture was prepared a minimum of 18 hours before the start of experiment. The suspension was mixed thoroughly before the start of the test.

During the test samples of 50 mL were collected from the suspension at predetermined moments, which were 0, 1, 3, 5, 10, 30, 60, 120, 180, 360 minutes, and 1080 minutes. After each withdrawal of a sample the water surface level of the settling column above the tap was documented. The 50 mL subsamples were filtrated in a vacuum pump through Vos nylon filters of 0,45 μm and a diameter of 47 mm. The filters were weighed before and after filtration to obtain the accurate amount of retained sediments. By knowing the amount of extracted volume and weight of sediment at the predetermined measurement moments the concentration in the settling column over time can be obtained. Using the measured settling velocity and the Stokes settling formula, the equivalent spherical grain size distribution of the mud fraction can be determined. The Pipet/TAP test was always executed in duplicates for later comparison of accuracy. Details are given in MUSA-Report by Van Rijn & Koudstaal (2021).

### 3.3.3.4 Grain size distribution of fine particles < 63 μm, method 3: video observation system

As an additional and novel method to analyse fine particles (< 63 μm), samples will be tested through a Video Observation System developed by Prof. Andrew Manning. This method allows, among other outputs, the quantification of settling velocities and related grain size distribution accounting for the presence of flocs among the cohesive particles.

Two instruments designed by Andrew Manning and HR Wallingford will be used: (1) the LabSFLOC instrument for measuring the flocculation characteristics in the laboratory, and (2) its field counterpart, the INSSEV-LF.

The LabSFLOC-2 (Laboratory Spectral Flocculation Characteristics) instrument utilizes a low-intrusive, high-resolution, monochrome digital video camera to observe flocs as they settle in a 32 cm high Perspex settling column (square section of 10 x 10 cm). This setup can measure flocs in high concentrated

conditions as high as 100-200 g/L. For the measurement, a floc-sample is directly extracted from its original environment to the column where the flocs are measured through the camera system combined with LED back-illumined where the flocs appear as silhouettes. This novel method permits minimal disturbance of the floc structure.

LabSFLOC-2 can measure floc sizes of 8 mm in diameter and settling velocities approaching 45 mm/s, providing the flexibility to measure both pure mud and mud–sand mixtures. The complete analyses enclose individual floc porosity, fractal dimensions, floc dry mass and the mass settling flux distribution of a floc population.

The portability of the LabSFLOC instrument has led to the development of the INSSEV-LF: IN-Situ Settling Velocity instrument (see Manning et al., 2017). The INSSEV-LF permits floc samples to be collected and analysed in a field deployment. The INSSEV-LF is a hybrid system that combines the low-intrusive characteristics of the LabSFLOC with an *in-situ* sampler unit. The sampler consists of a 2.2L van Dorn horizontal sampling tube (or Niskin tube) that can collect water samples at a nominal height above the bed. More information on this method will be described in Phase 1E.

### 3.3.3.5 Laser Diffraction

Laser Diffraction tests were executed at Utrecht University using a Malvern Mastersizer 2000 to obtain the full sample's grainsize distribution as the equipment covers the size range between 0.02 and 2000 µm nominal diameter. Laser Diffraction is based on the relation between particle size and the angle and distribution of scattered light as described in the Mie Scattering Theory. Laser Diffraction measures the angular variation in intensity of light scattered as a large beam is passes through a dispersed particulate sample. Light scatters off at a higher intensity and smaller angles from large particles, whereas smaller particles scatter light at a lower intensity and higher angles compared to the laser beam. Based on the data of angular scattering intensity, the size of the particles creating this scattering can be calculated.

The LD analyses were performed for both bulk (raw samples) and treated sample were the organic matter and carbonates were previously removed by hydrogen peroxide and HCl, respectively. All samples were suspended in deionized water added with dispersion agent (44.6g of $Na_4P_2O_7\cdot10H_2O$ + 4.24g $Na_2CO_3$ for 1L $H_2O$).

### 3.3.3.6 Sedigraph

The Sedigraph-instrument of Wiertsema Soil Mechanics Laboratory has been used. This instrument consists of a small cell-type container which is filled with a mud suspension and the mud concentrations are determined by direct (pre-calibrated) x-ray absorption inside a narrow beam. Using the known settling height, the decreasing mud concentrations in time are converted to settling velocities and to equivalent (spherical) sediment diameters with the Stokes settling formula. Deflocculation agents (peptiser) are used to fully disperse the samples (Protocols: NEN-EN-ISO17892-4/13317-3). For routine sample analysis, organic and calcareous materials are not removed.

### 3.3.4 Consolidation test parameters

Consolidation tests are performed to measure the sediment bulk density increase over time. Based on this, the hindered settling velocity, the contraction concentration and the bulk density increase over time can be determined. The contraction concentration is the transitional point from hindered settling phase to the consolidation phase (Figure 3-15). The hindered settling velocity is calculated by means of the hindered settling height and the settling time involved. The settling height is the height between the water surface and the (sinking) mud interface during the hindered settling phase.

The consolidation tests were performed on 2 litre settling cylinders with saline water (native seawater) added with different sediment concentrations, here 10, 20, 50, 100, 200 and 300 kg/m³ (Figure 3-16).

The water-sediment slurry was thoroughly mixed at the start of the test and during the test the position of the interface between the clear water and the suspension was measured at predetermined time steps over a period of 7 days. Based on this, time series of concentration (or dry density) are computed from the relative settling height and the initial dry density. These values represent the average dry density over the height of settled sediments (height below interface).
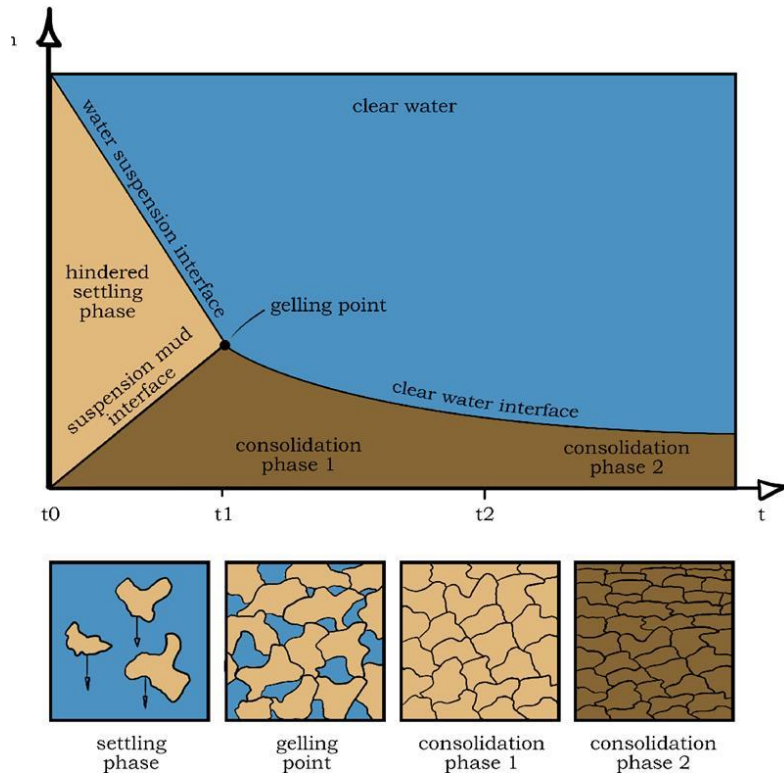
MUSA

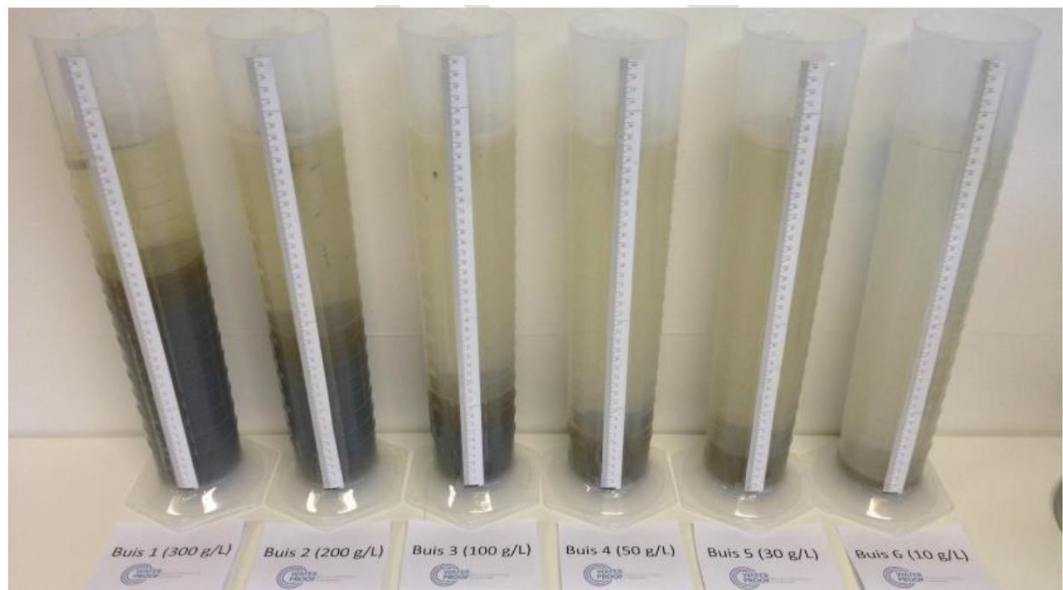*Figure 3-15: Evolution of a Consolidation test (source: van den Bosch, 2016).*



*Figure 3-16: Consolidation test with increasing concentrations from right to left (10, 20, 50, 100, 200, 300 kg/m³).*

### 3.3.5 Organic matter content

The content of organic matter was obtained by the Loss-On-Ignition (LOI) method. The LOI method consist of burning the organic matter in high temperatures furnaces (Figure 3-17). Samples of about 5 g were pre-dried, mashed with a pestle in a mortar and divided into two smaller subsamples. The test trays were weighed 3 times before and after they were filled with the sample. The samples were then placed in the furnace for 20 hours at 550°C, not including preheated and cooling. The content of organic matter was then computed by the difference in weight before and after the ignition of the organic matter. Using

MUSA

this method, some of the calcareous materials may also be lost (calcium carbonate decomposes when the temperature is higher than about 850 °C).



*Figure 3-17: Furnace used to quantify the organic matter content through the LOI-method.*

### 3.3.6 Critical shear stress and erosion rate based on Flume experiments

To determine the critical bed shear stress of erosion under flow, flume experiments were performed. The sediment was placed in a small compartment in the bottom of the flume, and the flow velocities were increased in gentle steps, here 5 cm/s, while observing the behaviour of the sediment within the compartment.

The flume is 5 m long, 0.3 m wide and 0.3 m high and can reach 1.5 m/s of flow velocity. A wall of plexiglass is present in the middle of the flume, which can be adjusted to different flume widths. The water depth is about 0.13 m. The sediment samples were placed in the mid-portion of the flume by means of sample trays (Figure 3-18). For velocities up to 1.0 m/s a wide tray was used (14.6 x 15.7 cm), while for higher velocities the flume width was reduced, and a narrow tray was used (14.6 x 10.9 cm). Bottom roughness was introduced by means of 250 µm sand attached to the bottom along the entire flume length. A sediment trap was placed downstream from the sample compartment in order to trap sand particles that move as bed load. The trapped sand is further used to evaluate the amount of bed load sediment transport.
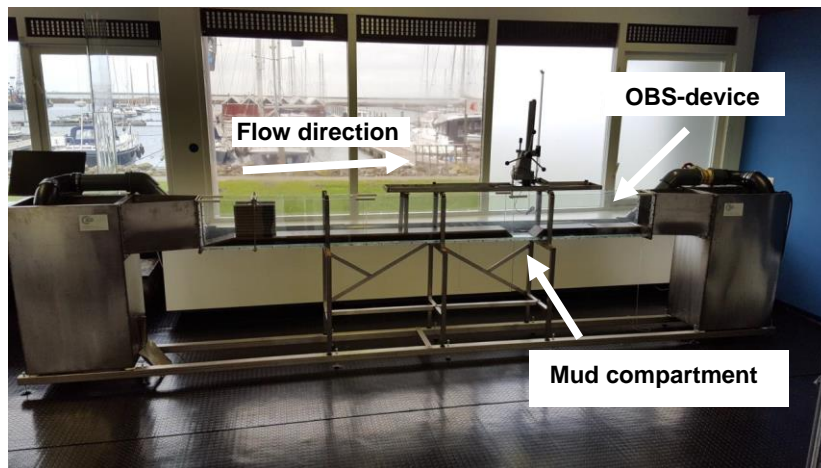


*Figure 3-18: Photo of the flume at the laboratory facility of WaterProof.*

### 3.3.6.1 Sample preparation

The density of samples was varied by using the base density as present in the base containers and lower densities by diluting of samples using native water (see Equation 1). After the dilution, the samples were let to settle for approximately 16 hours. The wet bulk density was measured before and after the test. For

Report Phase 1A-B

28 June 2022

the flume experiments, the excess layer on top of the sample tray was scraped off, making the sample level with the flume bottom. After the placement of the sample tray into the flume, the bed roughness height (i.e. $k_s$) was estimated from the surface irregularities observed on the top of the sample (mostly <0.5 mm).

The surface of the sample was prepared flush with the flume bottom to minimize abrupt changes in bed levels. However, minor variations in bed roughness at both transitions between the mud compartment and the adjacent bottom could not always be avoided. In tests with relatively soft mud, the mud surface was sometimes a few millimetres below the adjacent flume bottom due to previous consolidation (overnight) processes. These uneven bed transitions cause minor vortices and local velocity accelerations initiating erosion, particularly at the upstream transition. Therefore, we defined initiation of surface erosion as the creation of erosion marks (grooves, craters) in the middle of the mud compartment and away from the sides. Erosion spots at the upstream transition were neglected. Although the main objective of these tests was the determination of the critical bed-shear stress for erosion, in some tests the total erosion volume at the end of the test was also measured to get an estimate of the erosion rate.

### 3.3.6.2 Experimental procedure

The flume experiments were performed by increasing the flow velocity in steps of 5 cm/s. The water level was maintained at 13 cm by means of a downstream weir. The flow velocity was measured by a Vectrino device located 1.5 meter upstream from the sample and measured the flow velocity at a level of 5 cm above the flume bottom (*i.e.* 0.4*h* – corresponding to the depth averaged velocity) above the bed level. The measured velocity was converted to bed shear stress through:

$$\tau = g\rho_w \left[ \frac{u}{18\log\left(\frac{12h}{k_s}\right)} \right]^2 \qquad \text{Equation 4}$$

where:

$\tau$ = bed shear stress (N/m$^2$),
$g$ = gravitational acceleration, here 9.81 m/s$^2$;
$\rho_w$ = water density, here 1000 kg/m$^3$;
$h$ = water level (m); mostly approx. 0.13 m;
$u$ = depth averaged flow velocity (m/s), *i.e.* flow velocity at 0.4*h* height;
$k_s$ = bed roughness (m);
C=18log(12h/k$_s$)= Chézy-coefficient (C≅70 m$^{0.5}$/s for h=0.13 m and ks=0.0002 m) .

Dedicated velocity profile measurements have been done earlier to compare the bed-shear stress derived from Equation 4 to values derived from measured velocity profiles, see Table 3-3.

Equation 4 yields realistic results for smooth beds (k$_s$ in the range of 0.0001 to 0.0005 m).

MUSA

Table 3-3: Hydrodynamic measurements from the small flow-flume, and the computation of bed shear stresses at water depth of 0.13 m.

| | Height above bottom [m] | Flow velocity at height z [m/s] | Water depth [m] | Bed-shear velocity u* [m/s] | Bed-shear stress $\tau_b$ [N/m²] | Kinematic viscosity $\upsilon$ [m²/s] | Zero velocity level $z_0$ [m/s] | Nikuradse roughness $\kappa_s$ [m] | Reynolds number $u^*\kappa_s/\upsilon$ | Velocity at z = 0.4h [m/s] | Chezy coefficient C [m^0.5/s] |
|---|---|---|---|---|---|---|---|---|---|---|---|
| Depth-average velocity = 0.2 m/s | 0.005 | 0.153 | | | | | | | | | |
| | 0.010 | 0.166 | | | | | | | | | |
| | 0.015 | 0.171 | 0.13 | 0.0071 | 0.05 | 1.05E-06 | 9.30E-07 | ≤ 0.0001 | < 5 (hydraulic smooth regime) | 0.2 | 88.1 |
| | 0.020 | 0.178 | | | | | | | | | |
| | 0.025 | 0.182 | | | | | | | | | |
| | 0.050 | 0.196 | | | | | | | | | |
| Depth-average velocity = 0.43 m/s | 0.005 | 0.334 | | | | | | | | | |
| | 0.010 | 0.343 | | | | | | | | | |
| | 0.015 | 0.390 | 0.13 | 0.02 | 0.39 | 1.05E-06 | 5.80E-06 | ≤ 0.0001 | < 5 (hydraulic smooth regime) | 0.43 | 67.3 |
| | 0.020 | 0.405 | | | | | | | | | |
| | 0.025 | 0.412 | | | | | | | | | |
| | 0.050 | 0.429 | | | | | | | | | |
| Depth-average velocity = 0.92 m/s | 0.005 | 0.693 | | | | | | | | | |
| | 0.010 | 0.726 | | | | | | | | | |
| | 0.015 | 0.759 | 0.13 | 0.0384 | 1.47 | 1.05E-06 | 4.70E-06 | ≤ 0.0001 | < 5 (hydraulic smooth regime) | 0.92 | 75 |
| | 0.020 | 0.788 | | | | | | | | | |
| | 0.025 | 0.815 | | | | | | | | | |
| | 0.050 | 0.916 | | | | | | | | | |

The sediment concentration was measured by an OBS3+ device placed downstream from the sample at the middle of the water column (Figure 3-18). The OBS output unit (counts/NTU) was calibrated to concentration (*e.g.* mg/L) based on the samples from the Western Scheldt. The samples were dried and then weighed and brought into homogeneous suspension into 5-Liter containers of water with different sediment concentrations. The OBS NTU unit was then correlated to suspended sediment concentrations with the following empirical relation:

$$C_{sus} = -0.0015 C_{ntu}^2 + 1.7162 C_{ntu} - 18.83 \qquad \text{Equation 5}$$

where $C_{sus}$ is the sediment concentration in *mg/L* and $C_{ntu}$ is the measured NTU from the OBS instrument.

During the test with increasing flow velocity, the sediment motion, type of erosion and the mode of sediment transport were observed and recorded. The bed load sediment transport of sand was measured from the sediment trap placed in the flume.

The main experimental aim was to determine the critical bed-shear stress of erosion as follows:

- **Surface erosion**: When the shear stress is larger than the critical shear stress for surface erosion ($\tau > \tau_{cr,se}$), several layers of particles are put into motion, which takes place near the surface. This is generally taken to be the moment when grooves start to form on the surface. Erosion rates during surface erosion are in the magnitude of less than 1 g/m²s.
- **Mass erosion**: When the shear stress is larger than the critical shear stress for mass erosion ($\tau > \tau_{cr,me}$), mass erosion occurs. This is recognized by the sudden release of large quantities of bed material, which may occur in an irregular fashion and allows sediment to be suspended over the entire water column. Initiation of mass erosion is taken as the last observation before mass erosion occurs. Erosion rates in this phase are larger than 1 g/m²s.

The visual observations were complemented with the sediment concentration measured by the OBS sensor. The transition from no or very modest sediment transport to surface erosion can be identified by a slow increase in the concentration. The transition from surface to mass erosion corresponds to a

MUSA

subsequent and sudden large increase in the concentration values. Lastly, all experiments were video-recorded, allowing for revisiting the *in-situ* observations.

### 3.3.6.3 Data analysis

In order to quantify the critical shear stress and erosion rates we combined the flow measurements, sediment concentration and the observed erosion behaviour of the sample along the test. Both sediment concentration and flow velocities were filtered by a moving average to filter spikes and to retain the average conditions between each step. In addition, the sediment concentration was corrected for background sediment concentrations by means of subtracting the measured concentration right before the onset of the experiment. The measured values were then compared with the type of erosion (surface and mass erosion) determined by visual observation (also video-recorded) and by the inspection of the measured concentration curve over time. Consequently, we determined the critical shear stress for surface and mass erosion based on the joint observation of the sample with the underlaying flow conditions.

These measurements also allow for estimating the erosion rates that occur during mass erosion. We applied two methods to estimate the erosion rates related to mass erosion, as follows:

1. From the increase of the sediment concentration over time. However, this method was not sufficiently accurate as the concentration may not be homogeneously suspended over the water column.
2. From measuring the volume of sediment eroded from the sample. This method assumes that most of the erosion happens during the mass erosion stage, and therefore, the erosion during the stage of surface erosion is negligible. The eroded volume was determined in two different ways:

   i)   Measuring the dimensions (width, length and depth) of the scour marks to further compute the volume, and

   ii)  removing or adding water above the sample with scour marks and measuring the volume of added/removed water.

During experiments with very soft sediment, the erosion volume quantification method of adding/removing water was not used to prevent sample disturbance (mentioned in the data tables).

In order to compute the erosion rate, it is important to quantify the erosion duration. The erosion duration is the time between the beginning of mass erosion (i.e. knickpoint in sediment concentration – see Figure 3-19) and the end of the experiment. For example, the erosion duration in the experiment depicted in Figure 3-19 is about 60 seconds.
The erosion rate is then calculated as:

$$E = \frac{(V * \rho_{dry,bulk})/\rho_w}{A * t} \qquad \text{Equation 6}$$

In which:

$E$ = erosion rate (kg/m$^2$s);
$V$ = the eroded volume (m$^3$);
$\rho_{dry,bulk}$ = dry sediment density after the flume experiment (kg/m$^3$),
$\rho_w$ = water density, here 1022 kg/m$^3$,
$A$ = sample surface area (m$^2$);
$t$ = duration of mass erosion (s).

MUSA
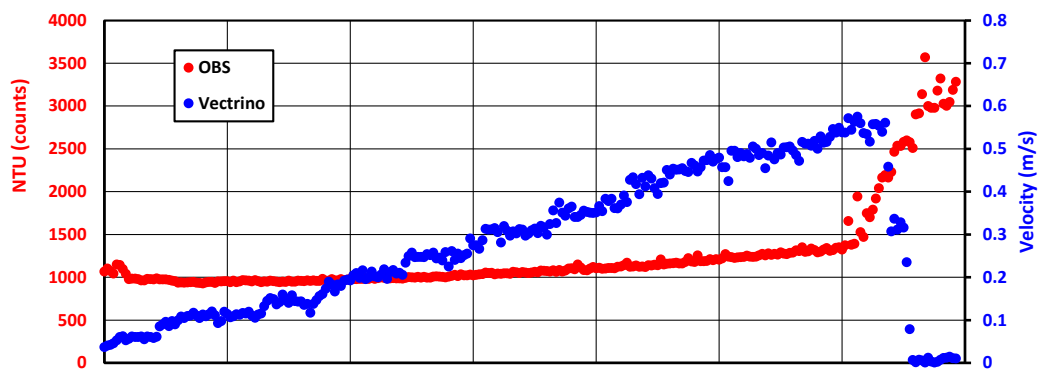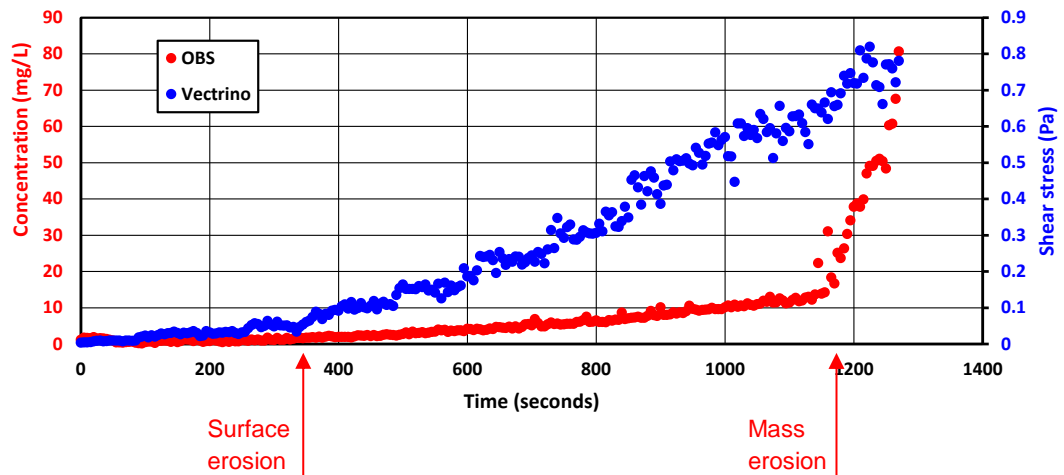
*Figure 3-19: Flume test results with (upper) raw data of flume test H2-261 with sediment concentration in NTU-unit and velocity depicted over time. (lower) The sediment concentration in mg/L versus the computed bed shear stress during the same flume experiment. The arrows indicate the critical shear stress for surface and mass erosion, respectively.*

The method applied to estimate the erosion rate during mass erosion intends to provide an initial estimation. For more accurate determination of the erosion rates in future experiments, we advise the execution of dedicated experiments. Such experiments should be performed with a stepwise increase of the bed-shear stress. The steps should be kept at a certain level until the sediment concentration has adapted to the flow condition. With constant bed-shear stress, the increase in sediment concentration $C$ (dC/dt, as sediment is recirculating) provides data on the value of the erosion mass. Now, it is not possible to isolate which part of the erosion is related to the mass erosion, from the critical bed-shear stress, and the increase in strength in the bed. However, the current adopted approach is the only viable option when the amount of sediment in the bed is limited. Another option, to be tested, is by means of controlling the sample height (e.g. lifting tray) which allows for eroding the bed for longer time while keeping the sediment bed at the equal heights with respect to the bed of the flume. A small high-precision echo-sounding may also be tested for this purpose.

### 3.3.7 Critical bed-shear stress based on EROMES experiments

The EROMES device consists of a cylinder in which circular flow motion on top of sediment surface is generated by a small propeller. The advantage of the EROMES is that the device is rather simple and portable, which enables to test samples in-situ. The EROMES device is placed on top of a sediment surface/sample (i.e. sample bed) and the user-defined rotation of the propeller creates circular flow motion and the erosion of the sample can be observed and correlated to the (calibrated) bed-shear stress, similarly to the flume, for assessing the critical shear stress. The advantage here is to minimize the sediment disturbance due to handling and the ability to obtain faster and in-situ results during field campaigns.

### 3.3.7.1 Setup

The EROMES device consists of a transparent cylinder of 0.4 m high in which a propeller is installed. The sediment concentration during the experiment was recorded with an optical NEP152-sensor, similar to the OBS-device. The EROMES propeller is placed above the sample (see Figure 3-20) before the experiment. The propeller brings the water in motion, while the NEP-device measures the sediment suspended concentration.

Report Phase 1A-B

28 June 2022
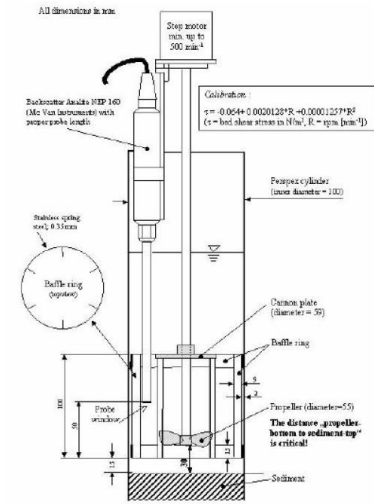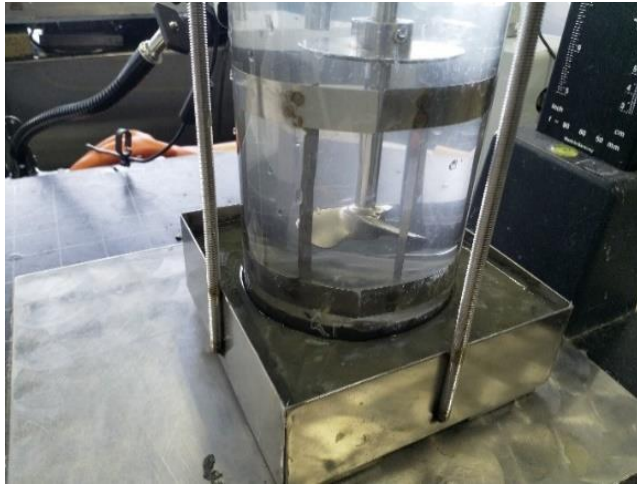
*Figure 3-20: The EROMES erosion instrument in laboratory setting*

### 3.3.7.2 Preparation

Similar to the flume test, the sample was prepared 16 hours in advance and with the same target bed densities as used in the flume experiments. The sediment was placed into a tray and let to rest overnight. After that, the tube was slowly pressed into the tray and secured with a watertight connection. The propeller was set at 3 cm above the sample and the tube was filled with 17 cm of saline water (approx. 1.5 litres). Comparable to the flume experiments, the wet bulk density of the sediment was determined using the method described under Section 3.3.2.

### 3.3.7.3 Calibration of EROMES

Several calibrations were performed prior to the experiments:

- RPM calibrations: discrepancies between the input and delivered RPMs
- Bed shear stress calibration: a new bed shear stress calibration was performed. This new calibration was based on the observations of the initiation of motion for sand beds with known sizes (100 to 1000 µm for propeller height at 3 cm)
- Concentration calibrations of NEP sensor for mud samples from both locations (i.e. Noordpolderzijl and Western Scheldt sediments), several calibration sets with known concentrations were made to calibrate the NEP, similarly to the NTU measurements from the flume.

*RPM calibrations*

The EROMES experiment uses a user-defined rotation of the propeller (in rotations per minute, RPM). By comparing the measured RPM output versus the user-defined RPM, it was found that the user-defined and measured RPM are very comparable up to 700 RPM and that the maximum RPM of the propeller is 720 RPM. This is an important parameter as the RPMs are used to compute the bed shear stress, similar to the depth averaged velocity measurements from the flume.

*Bed shear stress calibration*

The conversion of EROMES RPM to bed shear stress was initially performed according to the Van Rijn (2018, 2020) curve (Figure 3-24). This curve derived from measurements of the shear stress by a hot film anemometer, and on observations of the initiation of motion of sediment beds with known grain sizes. The original curve was adjusted based on new measurements performed during the MUSA project by measuring the initiation of motion of a sand bed with known grain size (range of 0.1 to 1.5 mm) and for propeller heights of 3 and 4 cm. A comparison between the old (HTS) and the new results for a propeller height of 3 cm is shown in Figure 3-21. The comparison between the new results for a propeller height of 3 and 4 cm is shown in Figure 3-22.

The following remarks are made:

- New curves show slightly higher RPMs than the HTS curves (for the same mode of motion);

Report Phase 1A-B

28 June 2022

**MUSA**

- Remarkable effect of propeller height on the bed-shear stress and initiation of motion. This highlights the importance of correctly setting the propeller height.
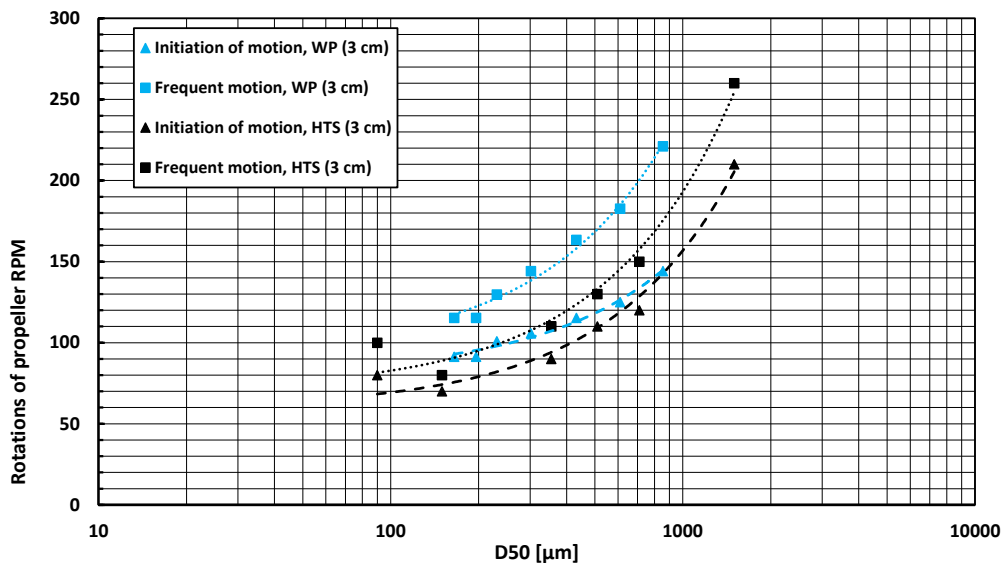


*Figure 3-21: Relation between (1) initiation of motion and (2) frequent motion against RPM for various well-sorted sand sizes. Comparison between calibration results of WaterProof (WP in blue) and calibration results of HTS (HTS in black) from Van Rijn (2018)*
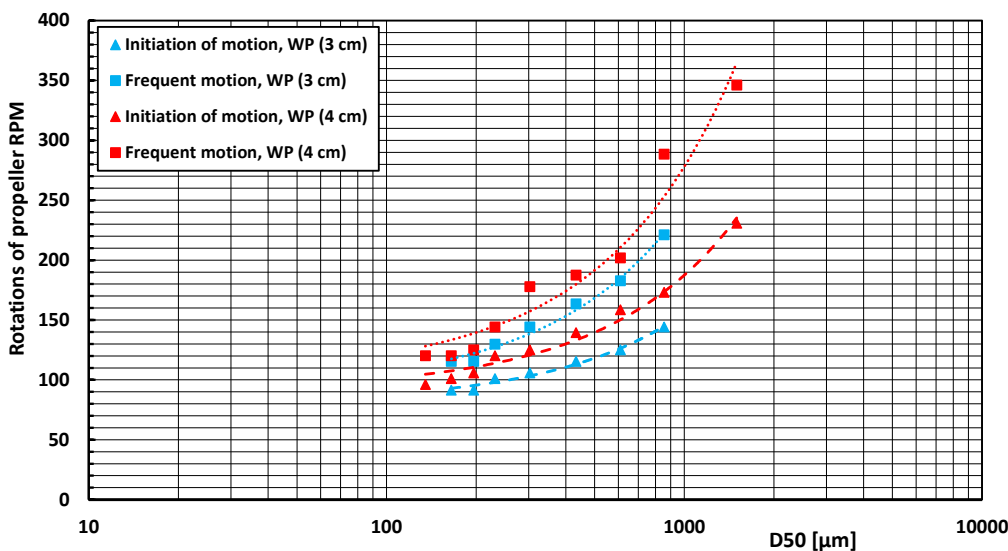


*Figure 3-22: Relation between (1) initiation of motion and (2) frequent motion against RPM for various well-sorted sand sizes and 2 propeller heights (3 and 4 cm above the bed).*

The results of Figure 3-22 were converted into a bed-shear stress using the Shields equation for initiation of motion and for frequent motion. These bed shear stresses and earlier results from Van Rijn (2018) are shown in Figure 3-23 and Figure 3-24.

The new observations agree with the early anemometer results from Van Rijn (2018). However, no observations could be made for the higher RPM ranges, as no coarser sediment was available. Therefore, the new calibration curve, as used in this research, is mostly based on the anemometer results. The bed-shear stress for a propeller height of 3 cm can be determined by:

$$\tau_{bed} = 1 * 10^{-8} RPM^3 + 3 * 10^{-6} RPM^2 + 4 * 10^{-4} RPM \qquad \textbf{Equation 7}$$

Report Phase 1A-B

28 June 2022

With $\tau_{bed}$ = bed shear stress in [N/m²] and $RPM$ is Rotations Per Minute.

Compared to these results, the bed-shear stress for a propeller height of 4 cm is (maximum) 30% smaller.
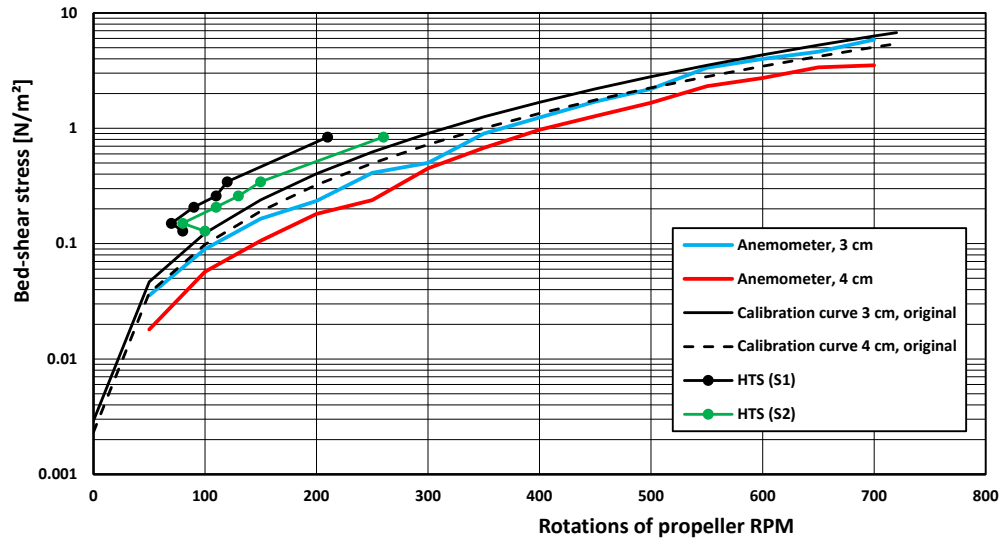


*Figure 3-23: Original EROMES calibration curve (black lines). The HTS data series are initiation of motion and frequent motion experiments from Van Rijn (2018). The blue and red line are the anemometer results from Van Rijn (2018).*
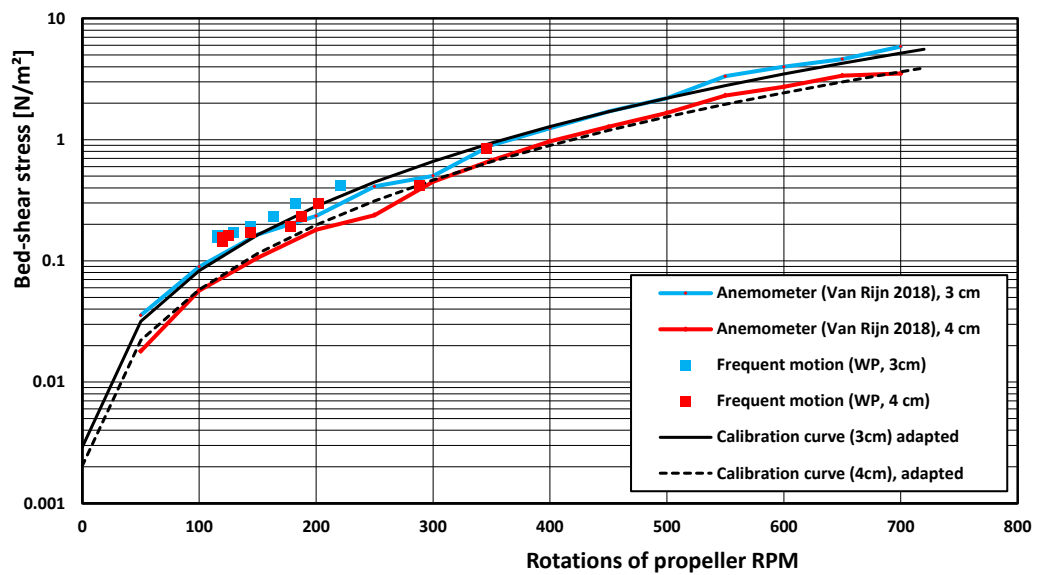


*Figure 3-24: New EROMES calibration curve (black lines), as used in this research. For the new calibration, both initiation of motion and frequent motion are observed while increasing the RPM of the EROMES for a propeller height of 3- and 4 cm. The blue and red line are the anemometer results from Van Rijn (2018).*

*Concentration calibration*

The output of the NEP-sensor (NTU) was calibrated in the same manner as the calibration of the OBS-device used in the flume experiments. The NEP was calibrated for sediment concentrations based on several sediment dilutions derived from both Noordpolderzijl samples and Western Scheldt samples (Figure 3-25). Non-linear calibration curves are used herein to cover the full range of low and high concentrations. It is noted that the data are fairly linear in the low concentration range.

The Western Scheldt conversion follows:

$$C = 1.9 * 10^{-3} \, NTU^2 + 0.618 \, NTU \qquad \text{Equation 8}$$

While Noordpolderzijl

$$C = 1.6 * 10^{-3} \, NTU^2 + 1.147 \, NTU \qquad \text{Equation 9}$$

Where *C* is the concentration in mg/L and *NTU* is the input from the NEP-sensor in NTU units.
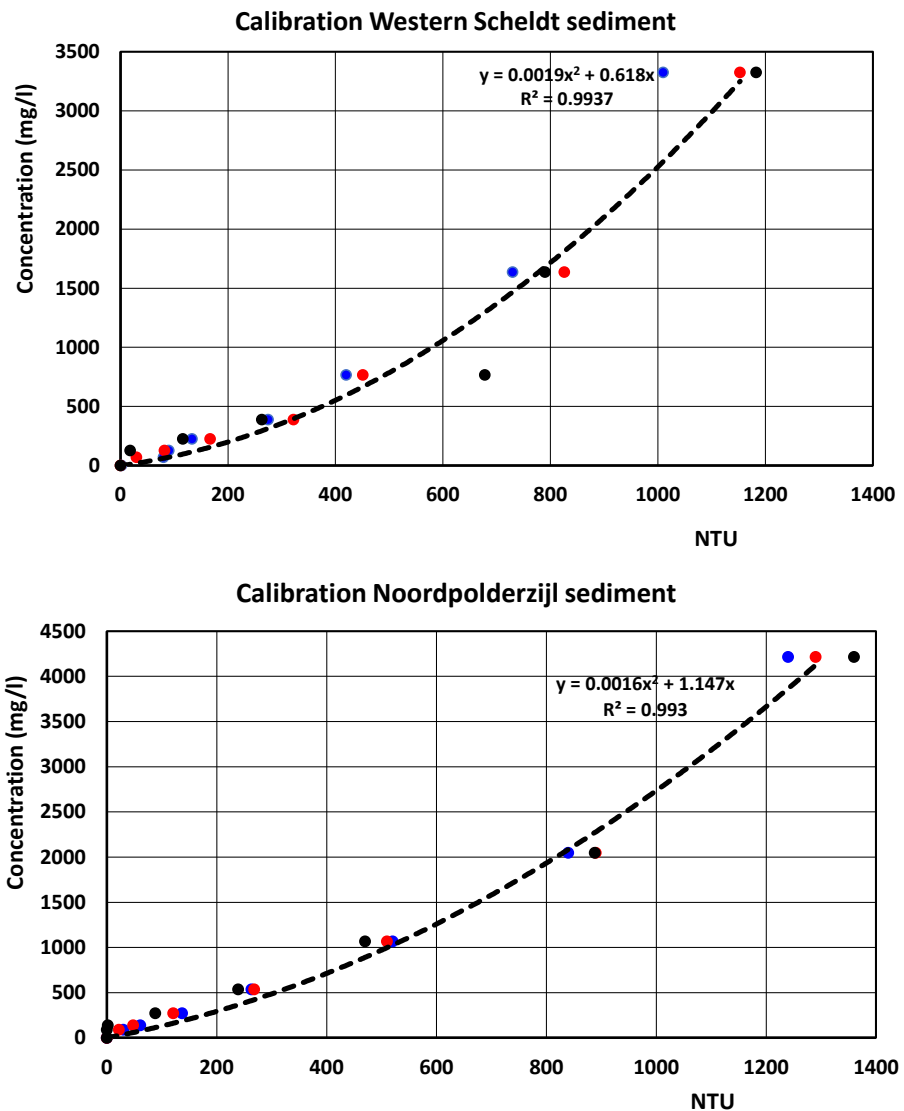


*Figure 3-25: Calibration curves of the NEP-sensor for both Noordpolderzijl (upper) and the Western Scheldt (lower). The different colors depict different subsequent series of calibration experiments.*

#### 3.3.7.4 Test setup

For the EROMES experiments, the Rotations Per Minute (RPM) were increased by 10 every 20 seconds. The test was stopped either when the sediment concentration measured with the NEP was saturated or when the maximum RPM was reached.

An example of the result of an EROMES experiment is shown in Figure 3-26. The rotations (RPM) were converted to bed shear stress using Equation 7. The stepwise increase in bed shear stress is the result of the stepwise increase in RPM. The red line shows the measured concentration by the NEP sensor, which was located 10 cm above the bed.
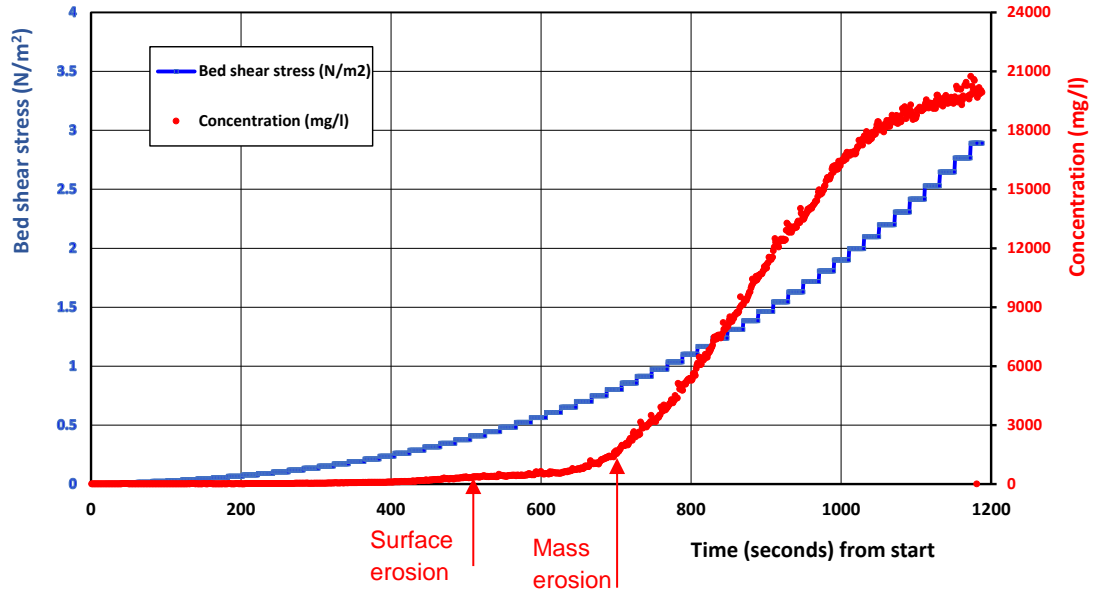


*Figure 3-26: EROMES test results WAW1 with measured concentration by NEP (mg/l) and bed shear stress as derived from relation with RPM (Equation 7). The arrows indicate the critical shear stress for respectively surface- and mass erosion, comparable with the Flume results (see Figure 3-19)*

We tested whether the NEP concentration measurements could also be used to assess the erosion rate (kg/m²/s) of the sediment. However, after a thorough analysis of the results we concluded that this is unreliable because in some experiments the sediment concentrations went up extremely fast after the start of mass erosion. The reason for this is that the sediment is being suspended in only 1.5 L of water and the NEP gets saturated instantly resulting in unreliable erosion rate estimates. Therefore, another method was used (in later tests) by taking water samples at fixed intervals in time. These samples were filtered to obtain the concentration of suspended solids. Based on the increase in concentration, the erosion rate was estimated. These measurement results were much more in line with the results of the flume experiments.

Report Phase 1A-B

28 June 2022

## 3.4 Results of Sediment analyses and physical experiments

### 3.4.1 Distribution of sand percentage and densities in collected samples

For the MUSA project we are interested in sediment samples which cover the complete range between sand and mud. For all samples the percentage of sand was determined by wet sieving the sediment over a 63 µm sieve. The results of the Western Scheldt samples are presented in Figure 3-27. A table with all results is provided in the MUSA database spreadsheet (11204950_TKI-MUSA_02B_Database_phase1A.xlsx).

The sediment samples collected at Noordpolderzijl and Western Scheldt (The Netherlands), Bengal Bay and Plymouth Estuary (United Kingdom), covered a wide range of sand-mud percentages. Sand percentages ranged between 1% and 99%. The highest contents of fines < 63 µm were found at the northern margin of the Western Scheldt and at the harbour areas (Paal Harbour & Griete Harbour) as well as at Bengal Bay. A visual presentation of the results for Western Scheldt is presented in Figure 3-28.
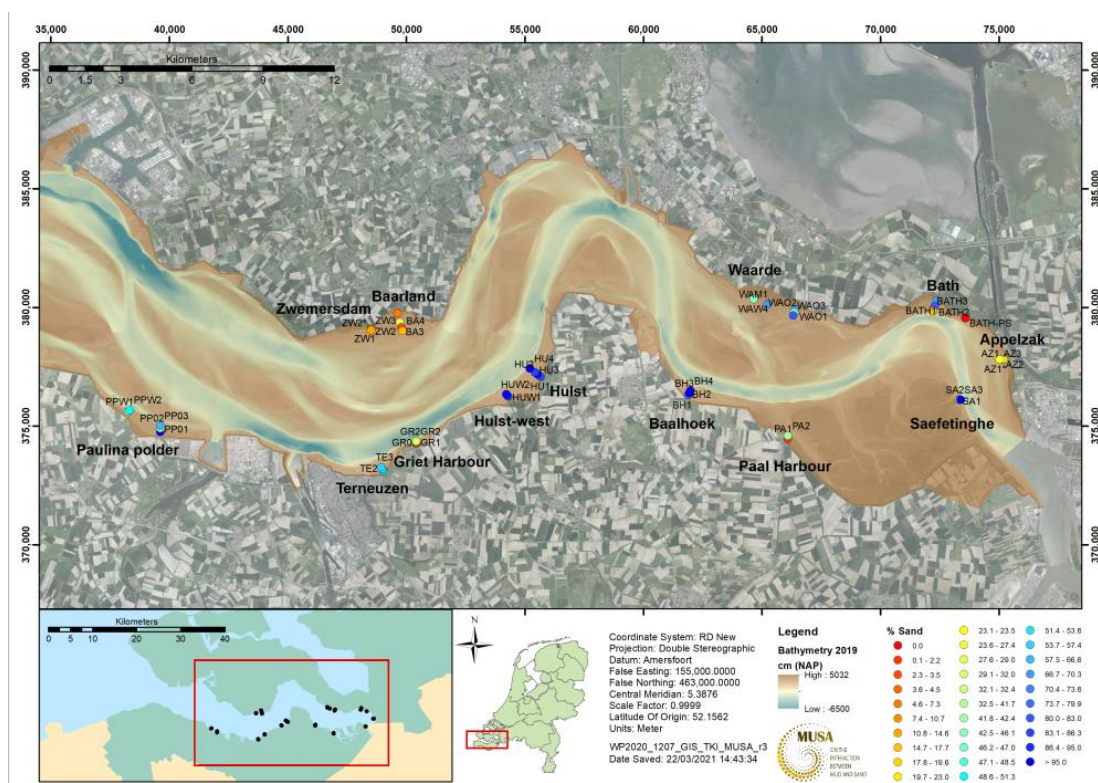


*Figure 3-27: Overview map of sand percentages derived from the surface-samples along the Western Scheldt*
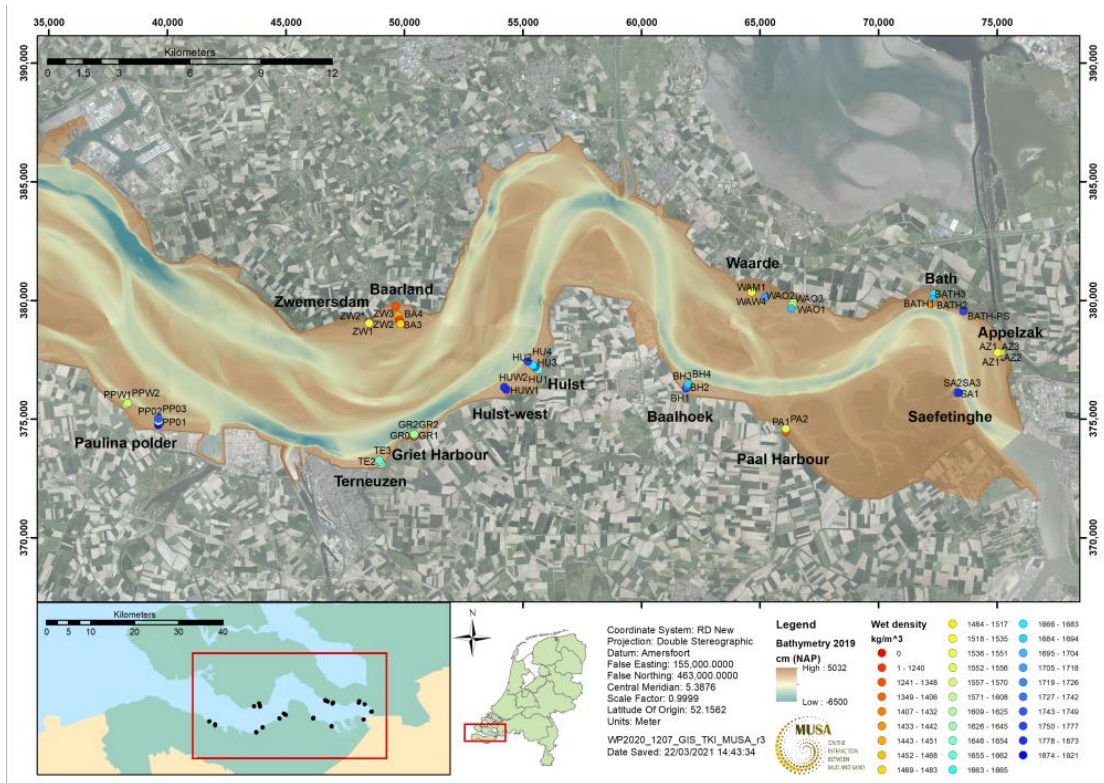
*Figure 3-28:Overview map of wet-density of collected surface-samples along the Western Scheldt.*

In general, the dry density increases for increasing percentages of sand. A relation between the dry-density and the percentage of sand based on the small samples is presented in Figure 3-29. The very silty samples from Bengal Bay (2 blue symbols in upper left corner) have a relatively high dry density at a low percentage of sand and deviate from the other samples. Furthermore, these silty samples from Bengal Bay showed a high level of compaction, low water content and almost no organic materials.
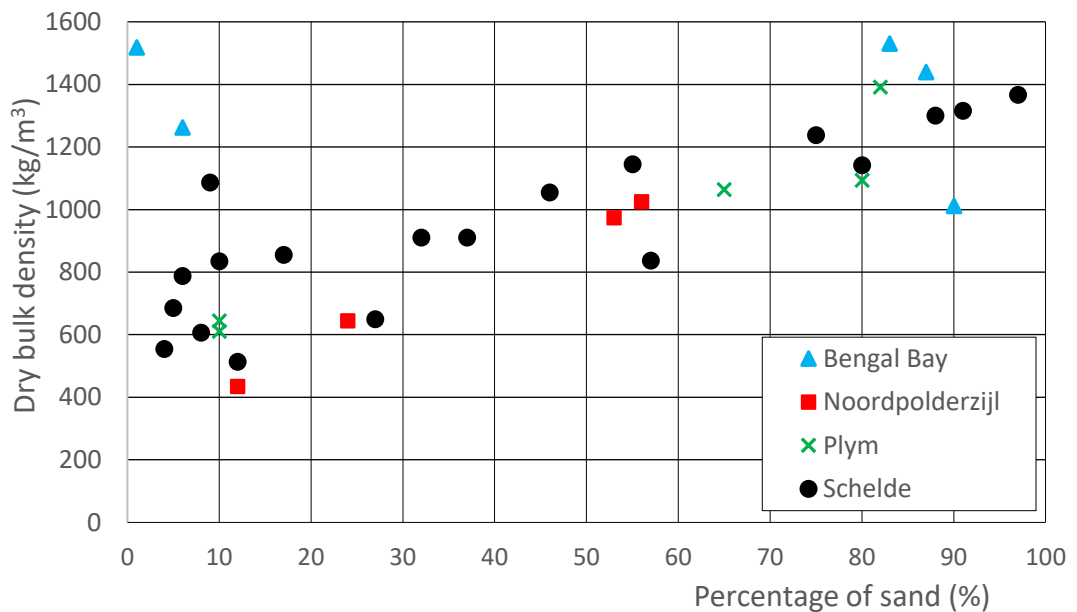


*Figure 3-29: Dry density versus sand percentage of all small samples at Noordpolderzijl, Western Scheldt, Plymouth Estuary and Bengal Bay*

Report Phase 1A-B

28 June 2022

MUSA

### 3.4.2 Distribution of density over depth

To get an indication on the variation of percentage of sand and densities over depth, sediment samples were taken from the upper 40 cm of the bed at various locations/sites of the Western Scheldt area (see Figure 3-3).Table 3-4 presents the percentage of sand for these samples. The results have been arranged in ascending order of sand percentages of the surface samples. It can be seen that:

- the sand percentage in the sub-surface samples is generally larger than the surface samples
- the sand percentage can strongly vary with depth
- the density generally increases with depth. However, the variation is large

Table 3-4: Distribution of sand percentage (%), wet density (kg/m³) and dry density (kg/m³) in the sediment samples in the first 0.5 m below the surface

| Sample | Surface (1-3cm) | 10cm below surface | 20cm below surface | 30cm below surface | 40cm below surface |
|---|---|---|---|---|---|
| WS-ZW1 | 3.5% 1348; 530 | 9.1% 1513; 800 | 48.9% 1708; 1115 | 13.7% 1487; 755 | 34.0% 1642; 1010 |
| WS-GR1.5 | 4.5% 1446; 690 | 2.5% 1454; 705 | 5.1% 1469; 725 | 13.2% 1503; 780 | |
| WS-BA1 | 7.3% 1335; 510 | 17.4% 1501; 780 | 10.6% 1499; 775 | 19.3% 1530; 825 | |
| WS-BATH3 | 16.1% 1442; 685 | 70.2% 1291; 435 | | | |
| NPZ-B5 | 18.8% 1440; 680 | 25.42% 1430; 605 | 21.5% 1400; 615 | 38.0% 1355; 540 | 56.2% 1500; 780 |
| WS-ZW2 | 23.0% 1551; 860 | 30.3% 1730; 1150 | 33.5% 1689; 1085 | 54.2% 1646; 1015 | |
| WS-AZ1 | 27.5% 1662; 1040 | 42.2% 1729; 1150 | >95% 1846; 1340 | >95% 1831; 1315 | 58.8% 1321; 485 |
| WS-WAW1 | 31.8% 1535; 835 | 64.7% 1766; 1210 | 44.0% 1699; 1100 | 46.5% 1707; 1115 | 48.5% 1718; 1130 |
| NPZ-B8 | 41.1% 1430; 665 | 36.3% 1300; 450 | 40.5% 1315; 475 | 36.1% 1300; 450 | 39.1% 1285; 430 |
| WS-BH1 | 50.7% 1640; 1005 | 58.1% 1696; 1100 | 41.0% 1666; 1050 | 58.8% 1768; 1215 | 77.1% 1775; 1225 |
| WS-TE2 | 51.3% 1604; 950 | 83.6% 1958; 1525 | >95% 1904; 1435 | | |
| NPZ-B9 | 53.6% 1570; 890 | 66.3% 1615; 965 | 65.3% 1640; 1005 | 59.9% 1570; 890 | 71.3% 1640; 1005 |
| WS-HU1 | 86.2% 1851; 1350 | 90.5% 1843; 1335 | 78.8% 1788; 1245 | 48.6% 1697; 1100 | 53.5% 1707; 1115 |
| UK-PLUK4 | 11.4% 1441;682 | 8.0% 197;936 | 4.3% 1647;1018 | 4.7% 1627;984 | 36.0% 1686;1084 |
| UK-PLUK5 | 52.2% 1810;1285 | 57.8% 1754;1226 | 51.9% 1741;1199 | 40.0% 1734;1181 | 37.0% 1707;1154 |

Report Phase 1A-B

28 June 2022

MUSA

### 3.4.3 Mud characteristics

**Mineral Composition**

The mineral composition clearly reflected the origin of sediments (Table 3-5; description of all minerals present in the samples).

The Dutch samples from PA1, B5, SO3, BATH and APP were dominated by Illite, The Bengal Bay samples (BB2 and BB3) were predominantly composed of Chlorite and Illite with a provenance from the Himalaya. The Plym samples, PLUK1 and 4, from UK are mainly composed by Kaolinite from the Cornish granites.

Remarks are:

- Samples B5 (Noordpolderzijl) and BAPU (Western Scheldt) are very similar; minerals are: calcite, aragonite, quartz, illite/mica,K-feldspar, 14Å clay (smectite, chlorite), halite
- Samples PLUK1 and PLUK4 are very similar; Minerals: quartz, illite/mica, K-feldspar, kaolinite,14Å clay, halite (marine salt);
- Samples PA1, BAPU, APP and SO3 are similar (Scheldt samples); Minerals: calcite, aragonite, quartz, illite/mica, K-feldspar, 14Å clay, halite;
- Samples BB2 and BB3 are very similar; minerals are: quartz, illite/mica, plagioclase feldspar, amphibole, 14Å clay (chlorite), halite
- Grain size analysis: B5 and BAPU are similar; B5 exhibits a sharper peak in the very fine sand fraction, whereas the distribution of BAPU is more platykurtic; PLUK1 and PLUK 4 are very similar.

Table 3-5: Mineralogical properties of samples (analysis performed at University of Utrecht). 14Å clay is (either smectite or chlorite); halite is marine salt from the water derived from the bulk sample (dried and crushed); Ca = Carbonate materials. The dominant minerals are marked in **bold**.

| Location | Sample | % sand | % mud | % Ca | Minerology Composition |
|---|---|---|---|---|---|
| Noordpolderzijl channel (NL) | B5 | 33 | 43 | 22 | calcite, aragonite, quartz, **illite**/mica, K-feldspar, 14Å clay, halite |
| Westerschelde en Zeeschelde (NL, BE) | PA1 | 9 | 47 | 30 | calcite, aragonite, quartz, **illite**/mica, K-feldspar, 14Å clay, halite |
| | BAPU | 29 | 42 | 23 | calcite, aragonite, quartz, (**illite**/mica), K-feldspar, 14Å clay, halite |
| | APP | 86 | 9 | 10 | calcite, aragonite, quartz, (**illite**/mica), K-feldspar, 14Å clay |
| | SO3 | 61 | 26 | 20 | calcite, aragonite, quartz, **illite**/mica, K-feldspar, 14Å clay |
| Plymouth Estuary (UK) | PLUK1 | 11 | 64 | 7 | quartz, illite/mica, K-feldspar, **kaolinite**, 14Å clay, halite |
| | PLUK4 | 8 | 68 | 10 | quartz, illite/mica, K-feldspar, **kaolinite**, 14Å clay, halite |
| Bengal Bay | BB2 | 8 | 64 | 10 | quartz, **illite**/mica, plagioclase feldspar, amphibole, 14Å clay (**chlorite**), halite |
| | BB3 | 9 | 64 | 11 | quartz, **illite**/mica, plagioclase feldspar, amphibole, 14Å clay (**chlorite**), halite |

Report Phase 1A-B

28 June 2022

**Plasticity Index**

Clays with relatively large proportions of Montmorillonite minerals with significant swelling capacity generally have relatively high PI values, in particular sodium-based Montmorillonite clays. A very high PI value (>70) m is therefore an indication of the presence of a relatively high content of Montmorillonite minerals. Clays with high content of kaolinite minerals without much swelling capacity generally have low PI values.

The measured values of the MUSA-samples are given in Table 3-6, Figure 3-30 and Figure 3-31 show the PI-results of MUSA-samples (Table 3-6) as function of the percentage of clay < 2 $\mu$m and clayey materials < 8 $\mu$m. For comparison, the PI-values of Kaolinite, Illite and Montmorillonite-dominated clays and three geological clays found in the UK (Skempton, 1953) are also shown in Figure 3-30. The sandy samples (Bath-APP, SO3 and PLUK2) have relatively low PI-values between 12 and 22. The silty samples (PLUK1, PLUK4, BB1, BB3) have PI-values between 15 and 30. The clayey samples (Bath-BAPU, PA1, B%) have relatively high PI-values between 45 and 60 in the range of the Montmorillonite (Ca) clays. Figure 3-31 shows that 8 samples (except the very silty samples BB2, BB3 from Bengal Bay) can be represented by linear trendline: PI=$p_{<8\ \mu m}$ with $p_{<8\ \mu m}$ =percentage of sediment < 8 $\mu$m.

Gyamera et al. (2014) reported many PI-values in the range of 25 to 35 for very sandy/silty/loamy samples with $p_{clay<2um}$ in the range of 10 to 30 from the Ghana coast in Africa (see Figure 3-30).

The sandy samples (Bath-APP, SO3, PLUK2) have relatively low PI-values between 12 and 22.
The silty samples (PLUK1, PLUK4, BB1, BB3) have PI-values between 15 and 30.
The clayey samples (Bath-BAPU, PA1, B%) have relatively high PI-values between 45 and 60 in the range of the Montmorillonite (Ca) clays.
Analysis of results shows that 8 samples (except the very silty samples BB2, BB3 from Bengal Bay) can be represented by linear trendline: PI=$p_{<8\ \mu m}$ with $p_{<8\ \mu m}$ =percentage of sediment < 8 $\mu$m. The relatively low PI-values of the BB-samples are most likely related to the low content of cohesive and organic materials.

Table 3-6: Liquid and plasticity limits (Atterberg Limits) and Plasticity Index. Water content=[(wet density-dry density)/dry density] x 100%; Percentage < 2 $\mu$m and Percentage < 8 $\mu$m based on SE/HY-methods.

| Sample | Percentage < 2, 8, 63 $\mu$m | Water content | Liquid Limit WL | Plasticity Limit WP | Plasticity Index PI=WL-Wp | Classification |
|---|---|---|---|---|---|---|
| | % | % | % | % | % | - |
| WS-Bath-APP dd=1100±100 | 7, 12, 24 | 63 | 30.6 | 17.2 | 13.4 | clay; low plasticity |
| WS-Bath-BAPU dd=670±30 | 27, 40, 70 | 107 | 68.9 | 24.4 | 44.4 | clay; high plasticity |
| WS-PA1 dd=600±30 | 38, 60, 95 | 136 | 94.3 | 34.2 | 60.1 | clay; very high plasticity |
| WS-SO3 dd=850±30 | 14, 22, 43 | 80 | 48.5 | 27.0 | 21.5 | clay; medium plasticity |
| NPZ-B5 dd=600±30 | 25, 40, 72 | 117 | 83.1 | 30.3 | 52.8 | clay; very high plasticity |
| PLUK1 dd=670±30 | 17, 29, 87 | 108 | 65.6 | 37.5 | 28.1 | silt; high plasticity |
| PLUK2 dd=1050±30 | 10, 15, 37 | 58 | 33.9 | 21.2 | 12.7 | clay; low plasticity |
| PLUK4 dd=630±30 | 18, 28, 80 | 119 | 66.1 | 40.4 | 25.7 | silt; high plasticity |
| BB2 dd=1500±50 | 21, 42, 88 | 28 | 40.9 | 25.7 | 15.2 | silt; medium plasticity |
| BB3 dd=1200±50 | 19, 35, 94 | 39 | 41.3 | 24.1 | 17.2 | clay-silt; medium plasticity |

Report Phase 1A-B

28 June 2022
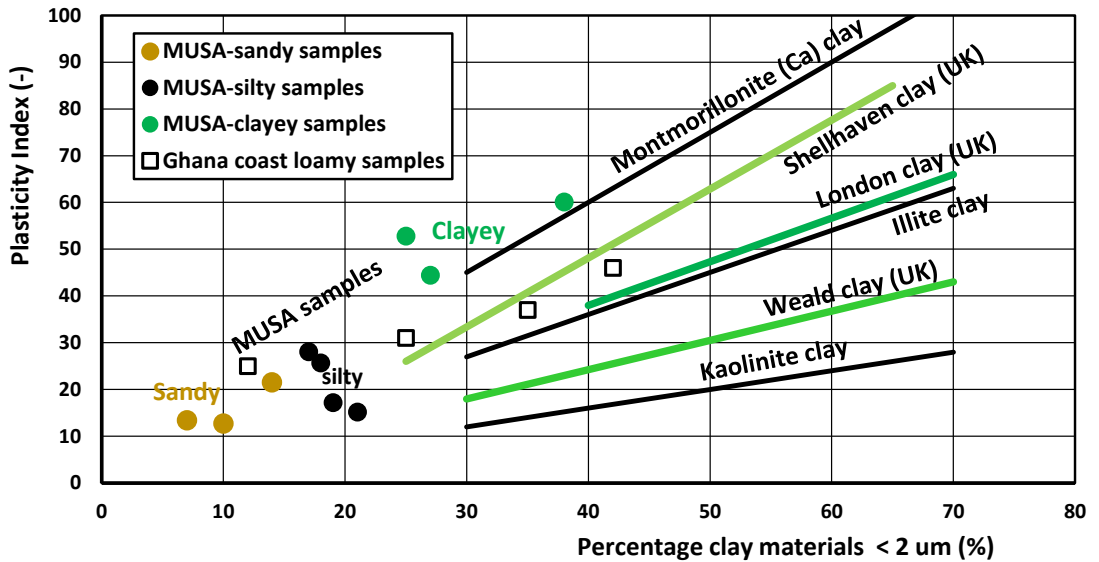
*Figure 3-30: Plasticity Index as function of percentage clay (< 2 μm).*
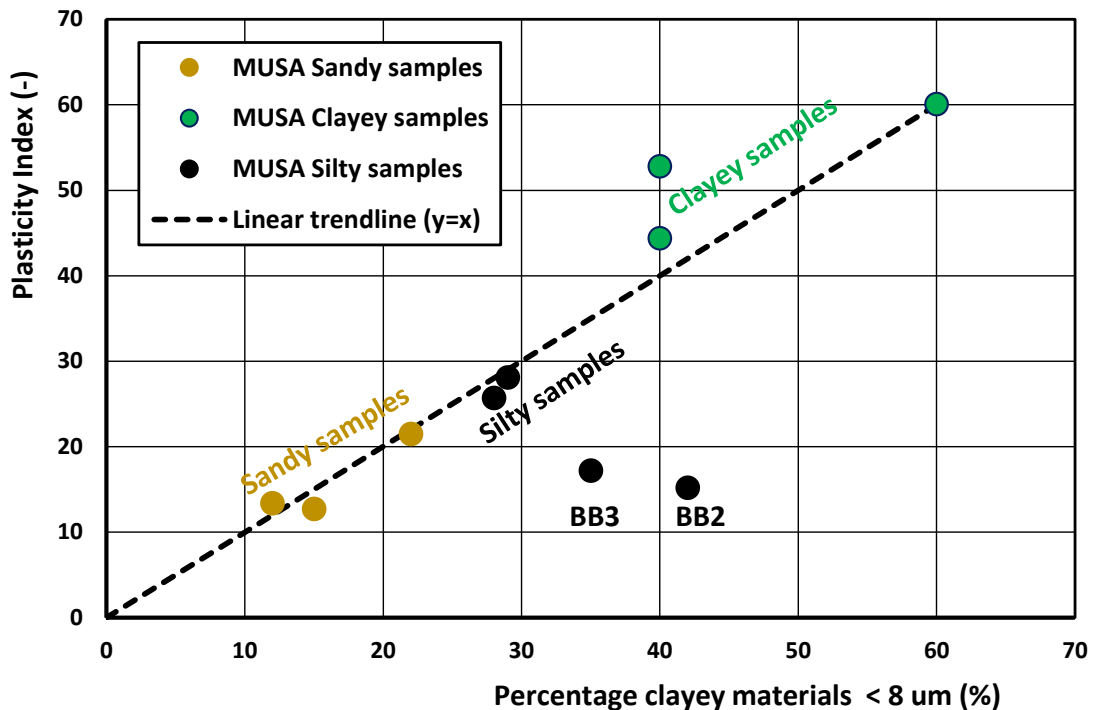


*Figure 3-31: Plasticity Index as function of percentage clayey materials (< 8 μm).*

**Yield strength**

The summary of the yield strength results is given in Table 3-7. Figure 3-32 shows three typical examples of the measured shear stress versus the measured strain of the sample (output data of Brookkfield Rheometer). The yield stress is derived from stress-strain curves.

Figure 3-33 shows the yield stress results of all tests and the envelope curves of the data from the Literature for marine and estuarine muds (Deltares, 1991; Wurpts, 2005; Wurpts and Greiser, 2005; McAnally, 2007; Seifert and Kopf, 2010). The yield stress values show an increasing trend for increasing dry density of the mud-sand mixture in agreement with the data envelope curves. The yield stress values of the clayey MUSA-samples with low sand content (<30%) are close together and mostly within the

envelope curves. These results are most reliable as the sand particles are well buried within the mud matrix. The yield stress values of the silty samples are in the low range of the envelope curves. Two samples with a relatively high sand content >60% to 70% are significantly above the envelope curves, which may be the effect of high internal friction between the sand particles.

It is noted that the yield stress values for a mixture with dry density of 100 kg/m$^3$ are less reliable as segregation of mud, silt and sand particles may easily occur during the test procedure.

*Table 3-7: Yield stress values of MUSA-samples.*

| Sample | Dry density | Percentage < 2, 8, 63 µm | Water content= $(\rho_{wet}-d_{ry})/\rho_{dry}$x100 | Yield stress at $\rho$ = 100, 200, 300 kg/m$^3$ |
|--------|-------------|--------------------------|---------------------------------------------------|------------------------------------------------|
|        | kg/m³       | %                        | %                                                 | N/m²                                           |
| WS-APP | 1100±100 | 7, 12, 24 | 63 | 2.7; 9.3; 49.2 |
| WS-BAPU | 670±30 | 27, 40, 70 | 107 | 0.9; 3.4; 47.4 |
| WS-PA1 | 600±30 | 38, 60, 95 | 117 | 0.08; 2.2; 3.1 |
| WS-SO3 | 850±30 | 14, 22, 43 | 80 | 0.08; 0.16; 2.6 |
| NPZ-B5 | 600±30 | 25, 40, 72 | 136 | 0,24; 3.1; 21.2 |
| PLUK1 | 670±30 | 17, 29, 87 | 108 | 0.11; 1; 3.6 |
| PLUK2 | 1050±30 | 10, 15, 37 | 58 | 0.08; 28.7; 59.8 |
| PLUK4 | 630±30 | 18, 28, 80 | 119 | 0.1; 0.2; 3 |
| BB2 | 1500±50 | 21, 42, 88 | 28 | 0.08; 0.24; 0.8 |
| BB3 | 1200±50 | 19, 35, 94 | 39 | 0.08; 2.3; 9.8 |
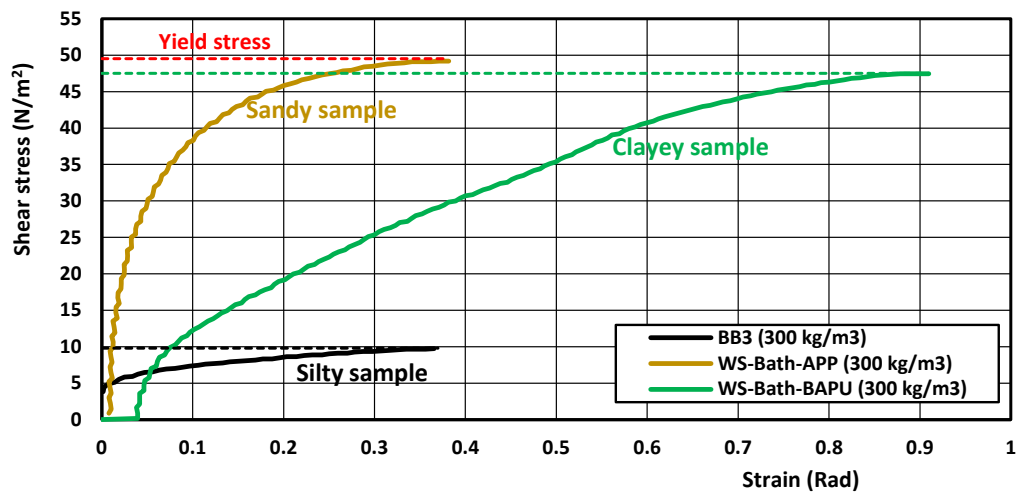


*Figure 3-32: Shear stress against Strain for three mud samples (MUSA samples) at dry density of 300 kg/m³.*
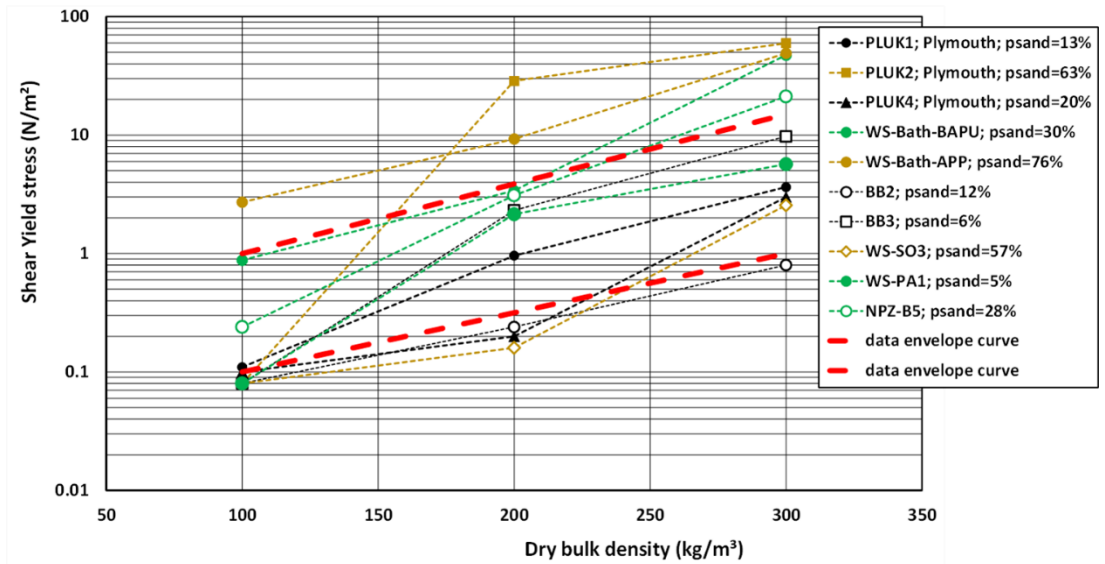
*Figure 3-33: Yield stress as function of dry density for MUSA-samples.*

### 3.4.4 Initial grain size analyses and sample selection for further analysis

Table 3-8 shows the 33 collected large volume (Barrel) samples in ascending order of sand percentage. The samples from the Western Scheldt, Wadden Sea (Noordpolderzijl), Plymouth Estuary (UK), Scheldt River (BE) and Bengal Bay cover a range between about 3% and 97% of sand content and dry bulk densities between approximately 435 to 1500 kg/m$^3$. Note that there exists a wide range in dry bulk density (between 435 and 1262 kg/m$^3$) for sediment samples with a relatively small percentage of sand (< 15%) while for the samples with larger percentages of sand (> 30%) the differences are smaller. This is related to the percentage of clay, silt and organic materials in each sample.

From the large samples, we selected 15 samples (Bold underlined samples; Table 3-8) to be analysed in more detail (Section 3.4.5 to 3.4.10). The selection was made based on the following considerations:

- Select a wide range of sand percentage;
- Select samples both from Noordpolderzijl and Western Scheldt which have similar percentage of sand (NPZ-H2 and WS-ZW2).

*Table 3-8: Sand percentages in ascending order, wet bulk density and dry bulk density for 33 samples. Selected samples in **Bold**.*

| Location | Sample | wet bulk density (kg/m³) | dry bulk density (kg/m³) | Sand percentage (%) |
|---|---|---|---|---|
| Bengal Bay | BB2-mud | 1944 | 1518 | <5 |
| **W. Scheldt** | **GR1** | **1408** | **685** | **5** |
| **W. Scheldt** | **PA1** | **1332** | **554** | **4** |
| W. Scheldt | GR1,5 | 1478 | 788 | 6 |
| **Bengal Bay** | **BB3** | **1760** | **1262** | **6** |
| W. Scheldt | BA1 | 1378 | 607 | 8 |
| W. Scheldt | SA1 | 1686 | 1086 | 9 |
| **W. Scheldt.** | **ZW2** | **1516** | **835** | **10** |
| **Plymouth Es.** | **PLUK1** | **1407** | **644** | **10** |
| **Plymouth Es.** | **PLUK4** | **1373** | **611** | **10** |

MUSA

| W. Scheldt | BATH3 | 1336 | 514 | 12 |
|---|---|---|---|---|
| **NPZ** | **H2** | **1275** | **435** | **12** |
| W. Scheldt | ZW1 | 1512 | 855 | 17 |
| **NPZ** | **B5** | **1391** | **644** | **24** |
| **W. Scheldt** | **BAPU** | **1405** | **650** | **27** |
| W. Scheldt | AZ1 | 1580 | (calc.) 910 | 32 |
| **W. Scheldt** | **WAW1** | **1581** | **(calc.) 910** | **37** |
| W. Scheldt | PPW2 | 1646 | 1055 | 46 |
| NPZ | B8 | 1602 | 974 | 53 |
| **W. Scheldt** | **BH1** | **1712** | **1145** | **55** |
| NPZ | B9 | 1606 | 1025 | 56 |
| **Scheldt River** | **SO3** | **1507** | **837** | **57** |
| Plymouth Es. | PLUK2 | 1684 | 1064 | 65 |
| **W. Scheldt** | **APP** | **1785** | **1238** | **75** |
| Plymouth Es. | PLUK3 | 1672 | 1094 | 80 |
| Scheldt River | SO1 | 1703 | 1142 | 80 |
| Plymouth Es. | PLUK5 | 1863 | 1391 | 82 |
| Bengal Bay | BB2_sand | 1880 | 1531 | 83 |
| Bengal Bay | BB1 | 1719 | 1439 | 87 |
| Bengal Bay | BB4 | 1170 | 1012 | 90 |
| **W. Scheldt** | **HU1** | **1797** | **1300** | **88** |
| Scheldt River | SO2 | 1777 | 1316 | 91 |
| **W. Scheldt** | **BA4** | **1594** | **1367** | **97** |

In general, the dry density increases for increasing percentages of sand at all sites (Figure 3-34). The very silty samples from Bengal Bay (2 blue symbols in upper left corner) have a relatively high dry density at a low percentage of sand and deviate from the other samples.

Figure 3-34 shows the measured dry bulk density (Table 3-8) compared to the empirical equation of Van Rijn and Barth (2018) which computes the dry bulk density based on percentages of organic matter ($p_{org}$), clay ($p_{clay}$), silt ($p_{silt}$) and sand ($p_{sand}$) as follows

$$\rho_{dry} = (1-p_{org}/100) \left[400\ p_{clay}/100 + 800\ p_{silt}/100 + 1600\ p_{sand}/100\right] \qquad \text{Equation 10}$$

Based on the premise that $p_{org}+p_{clay}+p_{silt}+p_{sand}=100\%$.

Using: $p_{silt}/100=1 - p_{org}/100 - p_{clay}/100 - p_{sand}/100$, and $p_{org}=5\%$, Equation 10 can be rearranged into:

$\rho_{dry}= 0.95 \left[760-400\ p_{clay}/100 + 800\ p_{sand}/100\right]$, which is shown in Figure 3-34.

This formulation was able to predict the dry bulk density with a root mean square error of 200kg/m³ when considering all samples, and RMS of 120 kg/m³ when excluding the BB-sample (the outlier) from the analyses (Figure 3-35). The prediction capacity is better for high densities, i.e. sandy samples, as the mineral composition and porosity in the sand range is less variable when compared to the mud fractions. It is noted that the dry bulk density values of the small samples were excluded from this analysis as they may have inaccurate (lower) density values. The reason for this is attributed to the inaccuracy of

Report Phase 1A-B

28 June 2022

MUSA

quantifying the wet bulk density by filling the small sample jars (i.e. 71 mL). During this process air pockets could be entrained and, due to the small sample volume, this would result in an underestimation of the bulk densities.
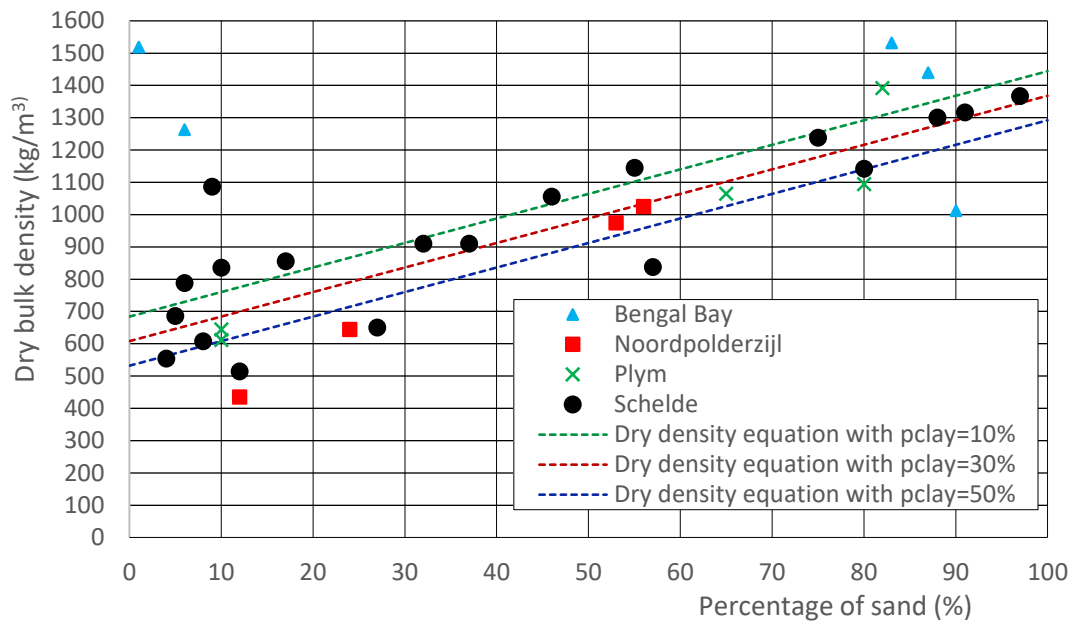


Figure 3-34: Dry bulk density of mud-sand bed samples (large samples; see Table 3-8) as a function of sand percentage.
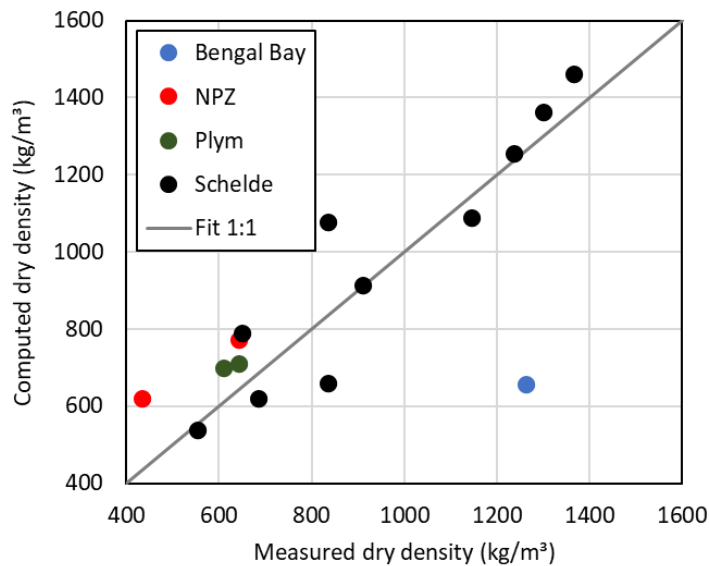


Figure 3-35: Comparison between measured and computed dry bulk density.

### 3.4.5 Grain size analyses of selected samples

The detailed grain size distribution of the selected samples was performed using dry sieving for the sand fraction (see Section 3.3.3) and the hydrometer test for the silt and clay fraction (see Section 3.3.3.2). We preferred the hydrometer experiments due to the ease of execution and the fact that the Hydrometer-

Report Phase 1A-B

28 June 2022

method yields similar results as the Pipet/TAP-method (Van Rijn and Koudstaal, 2021 – Report 11204950_01B_CONCEPT1.pdf).

The combined grain size distributions of sand and mud fractions are presented in Figure 3-36 and in Table 3-9.
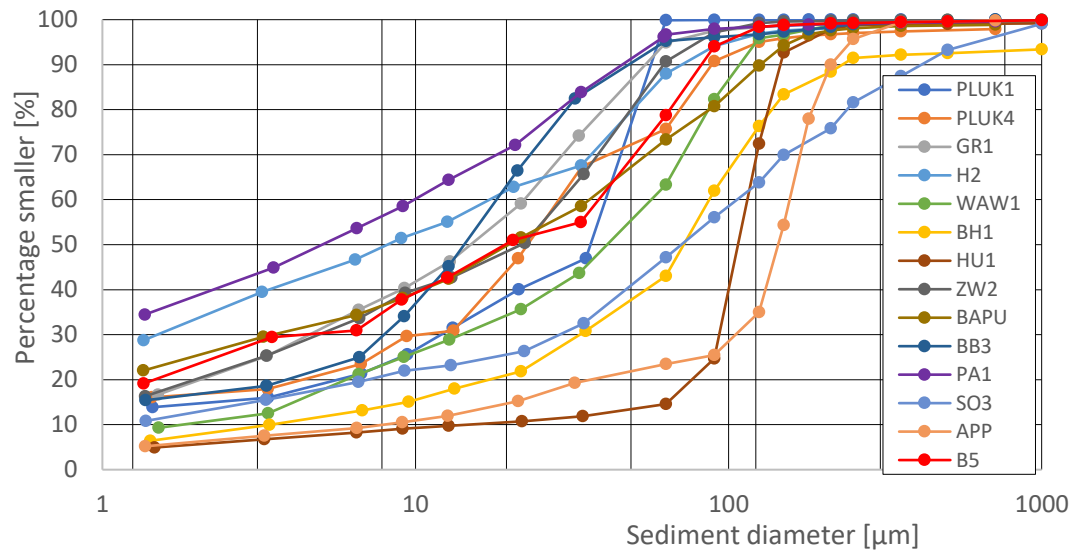


*Figure 3-36: Grain size distribution derived from hydrometer experiments for all locations*

The selected samples cover a large range of *in-situ* bulk densities and mud-sand ratios (Table 3-9). The results show that our selected samples encompass wet bulk densities between 1275 and 1800 kg/m³ and dry densities from 435 to 1300 kg/m³. The sand percentages vary from 5 to 99 %, and the organic matter content is between 1.9 and 10.5%. The highest organic matter quantities occur in the samples collected in the Western Scheldt near the De Paal harbour (*i.e.* PA1) and at Plymouth Estuary (*i.e.* PLUK1 and PLUK4) which are also associated with higher percentages of mud.

*Table 3-9 Summary of sediment analyses for the selected samples*

| Location | Sample | $d_{50}$ $d_{90}$ | Wet density | Dry density | > 63 µm (Sand) | < 63 µm (Silt+clay) | < 8µm | < 2µm | Organic matter |
|---|---|---|---|---|---|---|---|---|---|
| | | µm | kg/m³ | kg/m³ | % | % | % | % | % |
| Bengal Bay | BB3 | 14.8 52.6 | 1262 | 1760 | 6 | 94 | 29.8 | 16.4 | 3 |
| Western Scheldt | GR1 | 15 55 | 1408 | 680 | 5 | 95 | 37 | 17 | 6.7 |
| | ZW2 | 22 65 | 1516 | 835 | 10 | 90 | 37 | 23 | 4.8 |
| | WAW1 | 40 110 | 1581 | 910* | 37 | 63 | 24 | 11 | 4.7 |
| | BH1 | 70 230 | 1712 | 1145 | 55 | 45 | 14 | 8 | 3.2 |
| | HU1 | 150 190 | 1797 | 1300 | 88 | 12 | 8 | 5 | 1.9 |
| | BAPU | 20.3 126.2 | 1405 | 650 | 28.8 | 71.2 | 36.6 | 24.6 | 8.8 |
| | APP | 144.4 | 1785 | 1238 | 77 | 23 | 10 | 5 | 4.9 |

Report Phase 1A-B

28 June 2022

MUSA

|  |  | 212 |  |  |  |  |  |  |  |
| --- | --- | --- | --- | --- | --- | --- | --- | --- | --- |
|  | BA4 | 126.7 170.8 | 1594 | 1367 | 99.8 | 0.2 | 0 | 0 | 2.3 |
|  | SO3 | 77.5 418.5 | 1507 | 837 | 56.1 | 43.9 | 20.8 | 12.3 | 6 |
|  | PA1 | 5.5 54.7 | 1332 | 554 | 6.3 | 93.7 | 56.4 | 37.5 | 13 |
| Plymouth | PLUK1 | 37.5 69.8 | 1407 | 644 | 12.7 | 87.3 | 23 | 14.2 | 10.2 |
|  | PLUK4 | 23.4 88.6 | 1373 | 611 | 22.3 | 77.7 | 26.5 | 16.6 | 10.5 |
| NPZ | H2 | 8 75 | 1275 | 435 | 12 | 88 | 51 | 38 | 7.7 |
|  | B5 | 19.5 85.1 | 1391 | 644 | 28.1 | 71.9 | 35 | 22.3 | 10 |

Report Phase 1A-B

28 June 2022

MUSA

### 3.4.6 Consolidation

The consolidation process of soft materials consists of three distinct phases:

1. hindered settling phase (initial hours),
2. primary (short-term) consolidation phase accompanied by large strains (weeks to months);
3. secondary (long-term) consolidation phase accompanied by small strains (months to years)

In this section we provide the results of the first two phases (hindered settling phase and primary consolidation phase). Detailed results are only shown for sample GR1 as an example. The consolidation results for all samples are provided in Appendix B. Moreover, we present a first comparison between the results of the various samples.

The consolidation experiments were performed by diluting the original sample. For sample GR1, the base sample had a dry density of 679 kg/m³ (in-situ density). For the consolidation tests with varying initial concentrations, the original density was reduced after dilutions with native sea water with a density of 1022 kg/m³.

The consolidation test results are depicted in Table 3-10 and Figure 3-37 and Figure 3-38. The time series of concentration (or dry density) shown in these plots are computed from the relative settling height and the initial dry density and thus represent the average dry density over the height of settled sediments (height below interface).

The dry density after 7 days represents the end density of the primary consolidation phase. The end density depends on the initial dry density and the layer thickness. The highest end density of sample GR1 with initial dry density of 100 kg/m³ is about 400 kg/m³ after 7 days. The end density of the test with initial dry density of 300 kg/m³ is 450 kg/m³ (10% higher than starting with initial density of 100 kg/m³). These end density values of the primary consolidation phase are much smaller than the in-situ dry density of the base mud GR1 at the intertidal flat (679 kg/m³). Generally, the end density of the primary consolidation phase of a sample with initial dry density of 100 kg/m³ is about 50% to 70% of the in-situ density of top layer of intertidal flats (see Table 3-11). The end density of the primary consolidation phase is reached after 1 day for the sandy samples and after 7 days for the muddy samples. The higher in-situ density values of the top layer of the intertidal flats point to a longer consolidation period of months to years at the intertidal flats (secondary consolidation phase).

*Table 3-10: Consolidation data for 6 different initial dry density values for GR1 (Western Scheldt)*

| Original dry density after dilution (kg/m³) | Initial settling height (cm) | Hindered settling duration (s) | Hindered settling height (cm) | Hindered settling velocity (mm/s) | Contraction conc. (kg/m³) | Total settling height (cm) | Dry density after 3 hours (kg/m³) | Dry density after 168 hours (kg/m³) |
|---|---|---|---|---|---|---|---|---|
| 10 | 37.8 | 600 | 33.6 | 0.560 | 90 | 37.8 | 180 | 261 |
| 20 | 37.8 | 1260 | 29.7 | 0.236 | 93 | 35.5 | 76 | 194 |
| 50 | 37.5 | 3600 | 23.2 | 0.064 | 131 | 32 | 179 | 399 |
| 100 | 37.5 | 6780 | 19.7 | 0.029 | 211 | 28.2 | 229 | 403 |
| 200 | 37.5 | 74580 | 15 | 0.002 | 333 | 20.5 | 204 | 441 |
| 300 | 37.6 | 0 | 0 | 0 | 0 | 9.6 | 302 | 403 |

MUSA

Estimates of the contraction concentration are reported in Table 3-10. The contraction concentration is by definition the concentration at which a space-filling network is formed (i.e. material property). What is referred to in Table 3-10 as contraction concentration is actually the concentration at the transition from the hindered settling phase to the primary consolidation phase (transition from concave to convex curve in Figure 3-37). We consider this to be a reasonable estimate of the contraction concentration as a material property. Contraction concentration estimates are in the range of about 100 to 200 kg/m³ with original concentrations of 10 to 100 kg/m³ for sample GR1. For the initial concentrations of 200 and 300 kg/m³ no clear transition from concave to convex is found, as hindered settling does not occur at these high concentrations and consolidation occurs primarily by dewatering from the pores.

Hindered settling velocities derived from the settling of the mud interface range between 0.002 and 0.560 mm/s for GR1 (concentration of 100 kg/m³) and are highest with low mud concentrations. All hindered settling data are shown in Figure 3-41.
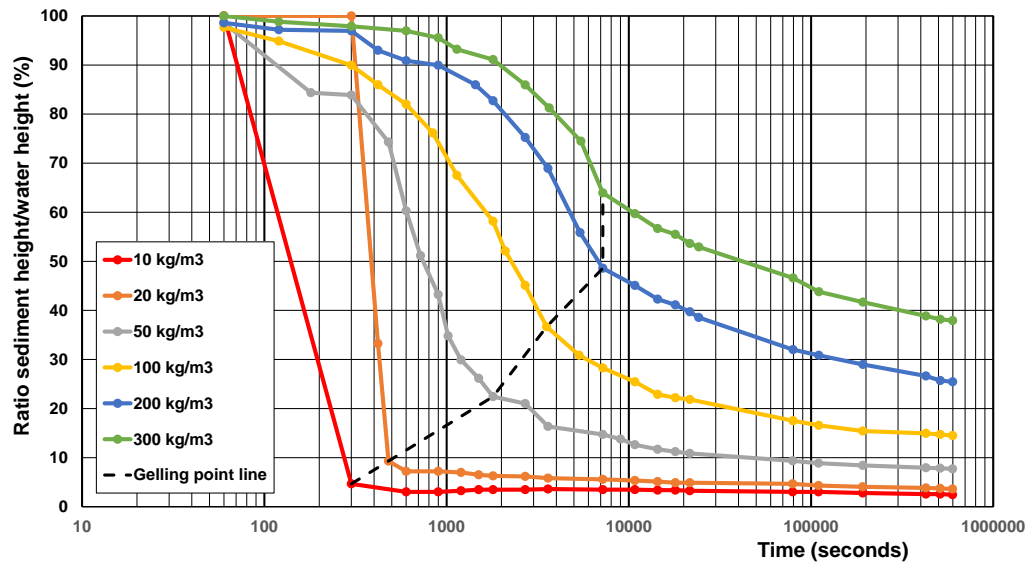


Figure 3-37: Settling height as function of time based on consolidation test for GR1; initial dry density of 10 to 300 kg/m³; dashed line as contraction points
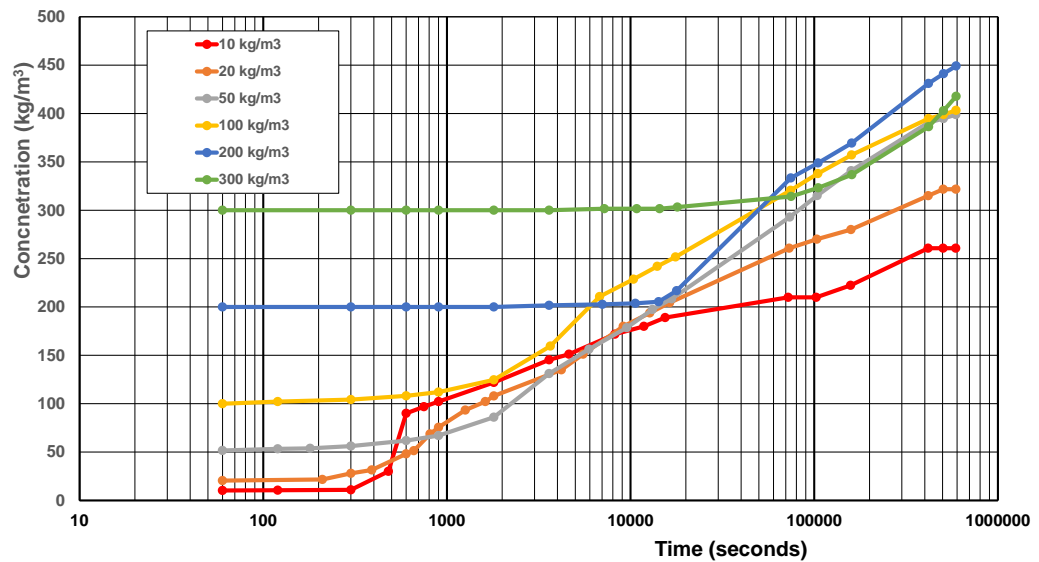


Figure 3-38: Dry mud density as function of time based on consolidation test for GR1; initial dry density of 10 to 300 kg/m³

MUSA

In order to compare the results among the different samples, the consolidation results of all selected samples with an initial density of 100 kg/m$^3$ are shown in Table 3-11, Figure 3-39 and Figure 3-40. The samples with a higher sand percentage consolidate at a faster pace, see the hindered settling velocities in Table 3-11. Generally, the final dry density values are higher for the samples with a higher sand percentage.

The only exception is the sample H2 (sample from harbour area of Noordpolderzijl), with higher percentage of clay (51%, see Table 3-9) and a relatively low final dry density compared to similar sand-content samples such as the ZW2. The dewatering process in samples with high clay content proceeds relatively slow.

*Table 3-11 Consolidation results for the selected samples with initial dry density of 100 kg/m$^3$ (column 6 also gives percentage with respect to in-situ density of column 1)*

| Sample (in-situ density; kg/m$^3$) | Percentage sand > 63um; clay < 8um (%) | Hindered settling duration (sec) | Hindered settling velocity (mm/s) | Contraction density (kg/m$^3$) | Dry density after 3 hours (kg/m$^3$) | Dry density after 7 days (kg/m$^3$) |
|---|---|---|---|---|---|---|
| NPZ-H2 (435) | 12; 51 | 7200 | 0.021 | 168 | 180 | 286 (65%) |
| WS-GR1 (685) | 5; 37 | 6780 | 0.029 | 211 | 229 | 403 (60%) |
| WS-ZW2 (835) | 10; 37 | 7200 | 0.028 | 212 | 199 | 431 (52%) |
| WS-WAW1 (910) | 37; 24 | 6840 | 0.031 | 230 | 119 | 436 (48%) |
| WS-BH1 (1145) | 55; 14 | 3540 | 0.077 | 273 | 393 | 690 (60%) |
| WS-HU1 (1300) | 88; 8 | 900 | 0.031 | 293 | 188 | 782 (60%) |
| WS-SO3 (837) | 57; 21 | 3600 | 0.057 | 248 | 331 | 568 (68%) |
| BB3 (1262) | 6; 30 | 3600 | 0.069 | 380 | 486 | 704 (56%) |
| NPZ-B5 (644) | 25; 35 | 1800 | 0.123 | 143 | 218 | 386 (62%) |
| WS-PA1 (554) | 5; 56 | 3600 | 0.041 | 174 | 223 | 400 (62%) |
| PLUK1 (644) | 10; 23 | 1800 | 0.121 | 277 | 404 | 517 (80%) |
| PLUK4 (611) | 10; 27 | 1800 | 0.120 | 278 | 423 | 563 (92%) |
| WS-BAPU (650) | 27; 37 | 3600 | 0.044 | 185 | 255 | 447 (69%) |
| WS-BA4 (1367) | 97; 0 | 60 | 5.233 | 1263 | 1137 | 1176 (86%) |
| WS-APP (1238) | 75; 10 | 600 | 0.363 | 279 | 586 | 850 (69%) |

Report Phase 1A-B

28 June 2022

MUSA
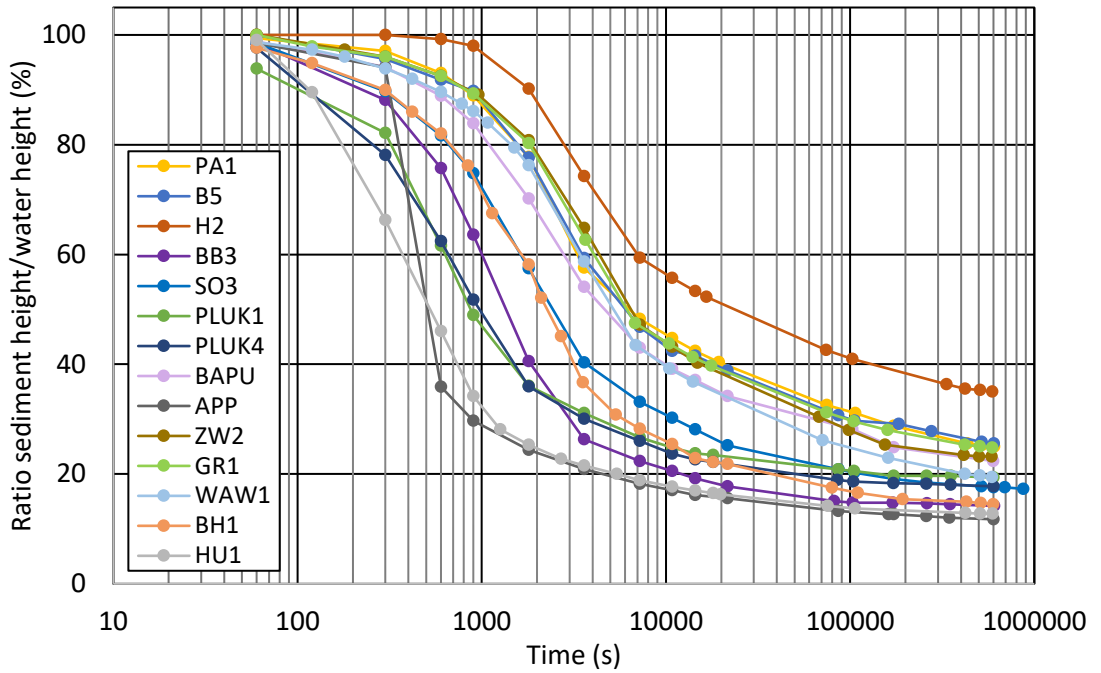
*Figure 3-39 Settling height as function of time based on consolidation test for all samples with initial dry density of 100 kg/m³, with the dashed line as contraction point line.*
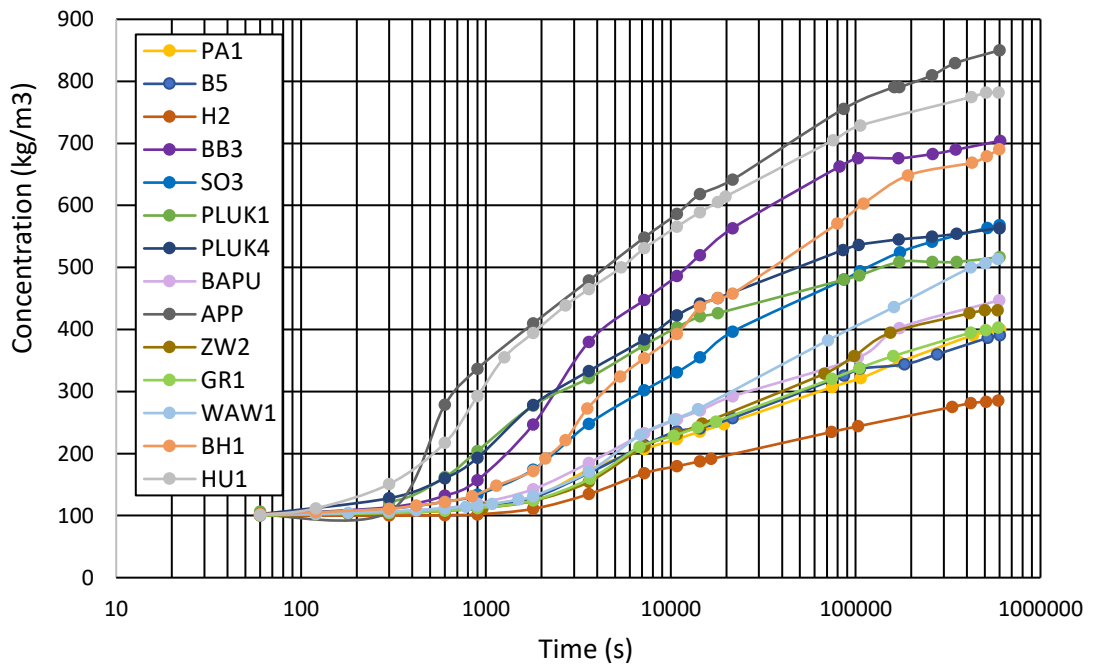


*Figure 3-40: Dry mud density as function of time based on consolidation for all samples with initial dry density of 100 kg/m³*

Figure 3-41 shows the measured hindered settling velocity values of the samples from Noordpolderzijl and Western Scheldt together with other representative samples for the Dutch coasts. The present data from Noordpolderzijl and Western Scheldt, are in good agreement with the data from elsewhere with exception of sample HU1, which contains a the highest percentage of sand (83%) and the lowest percentage of clay (5%) resulting in high settling velocities. Another sample (WS-APP) with a high percentage of sand (77%) has lower settling velocities at high concentrations. This may be related to the sand grain sizes involved.
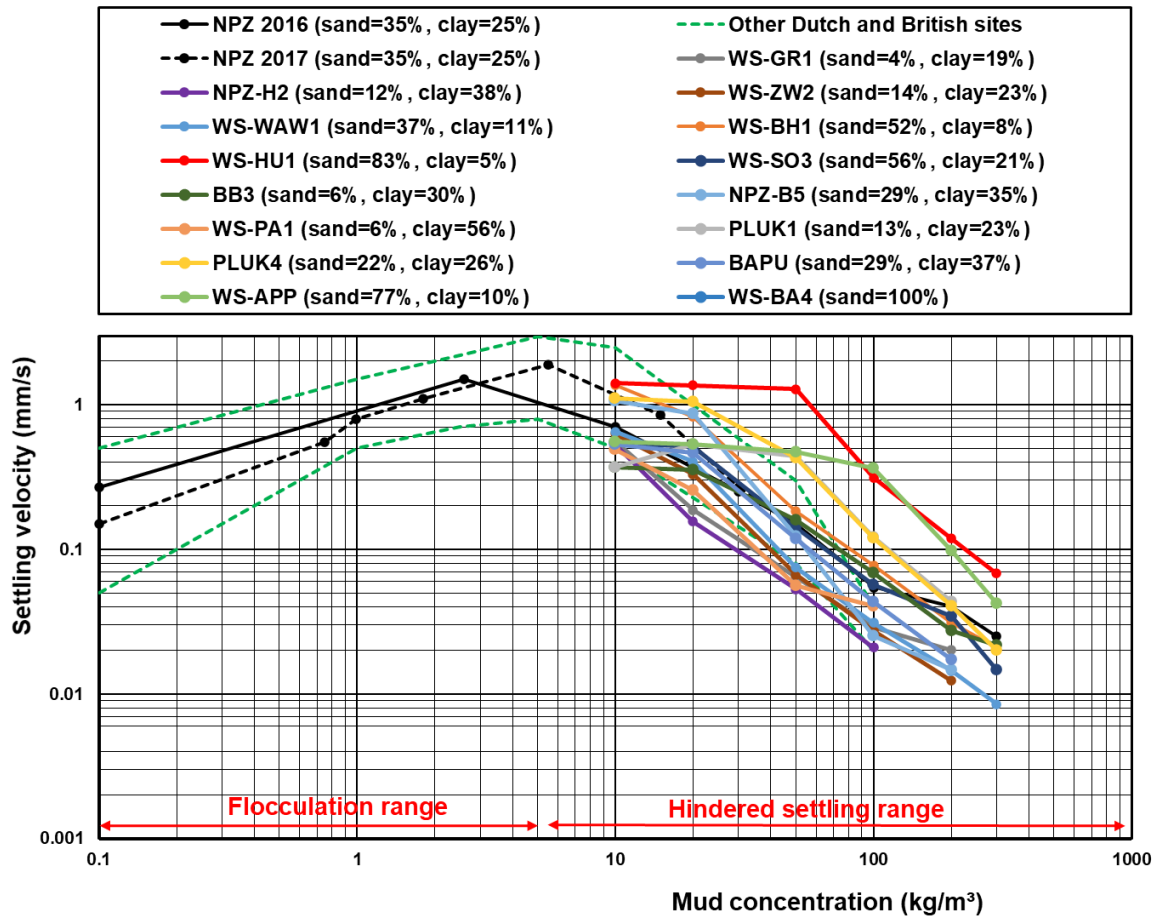
MUSA

*Figure 3-41: Settling velocity as function of diluted mud concentration for samples from MUSA in comparison to other data (Dutch and British sites).*

### 3.4.7 Critical shear stress and erosion rate of mud-sand bed samples based on flume tests

Flow flume experiments were performed to derive the critical bed-shear stresses and erosion rates for the selected sediment. Some samples were diluted to obtain smaller density values. We reduced the sediment bulk density of a sample by diluting the base mud sample with native seawater which creates a new remoulded sample with the desired bulk density. Some samples were also tested in the EROMES-apparatus (perspex-tube with propeller) to determine the critical bed-shear stress. All densities which have been tested in the flume and the EROMES are presented in Table 3-12.

*Table 3-12: Densities considered for the flume experiments and EROMES experiments. The experiments are ranked in order of increasing sand content. NPZ=Noordpolderzijl; WS= Western Scheldt.*

| Sample | Target density (kg/m³) | Flume density (kg/m³) | | EROMES density (kg/m³) |
|---|---|---|---|---|
| | | Before test | After test | Directly upfront test |
| NPZ-H2 | 250 | 263 | 284 | 234 |
| | 325 | 298 | 340 | 319 |
| | 400 | | 377 | 386 |
| WS-GR1 | 250 | | 363 | 337 |
| | 400 | 414 | 411 | 421 |
| | Original (685) | 646 | 718 | 682 |
| WS-ZW2 | 250 | | 292 | 420 |
| | 400 | 397 | 413 | 412 |
| | 600 | 556 | 574 | 550 |
| | Original (835) | | 754 | 756 |
| WS-WAW1 | 400 | | 521 | 623 |
| | 600 | 524 | 583 | 618 |
| | Original (910) | 848 | 868 | 818 |
| WS-BH1 | 400 | 548 | 747 | 712 |
| | 600 | | 712 | 784 |
| | Original (1145) | 1095 | 1146 | 1157 |
| WS-HU1 | 400 | | 1087 | 956 |
| | 600 | | 1007 | 991 |
| | Original (1300) | 1275 | 1310 | 1244 |

Table 3-12 shows slightly different initial densities in comparison with the measured target densities, due to sampling errors and due to consolidation of the sample over the 16-hour resting period between the preparation of the sample and the execution of the experiment. Furthermore, there is often a slight difference between the bulk densities measured in the EROMES in comparison with the flume. This deviation is mostly attributed to different procedures of measuring the sediment bulk density between the two devices. The density of the sediment in the EROMES is determined by taking the sediment from the top layer which is levelled with the bottom frame immediately before the experiment commenced and then sampled. While the sample from the flow-flume is taken from the bed directly after the experiment.

MUSA
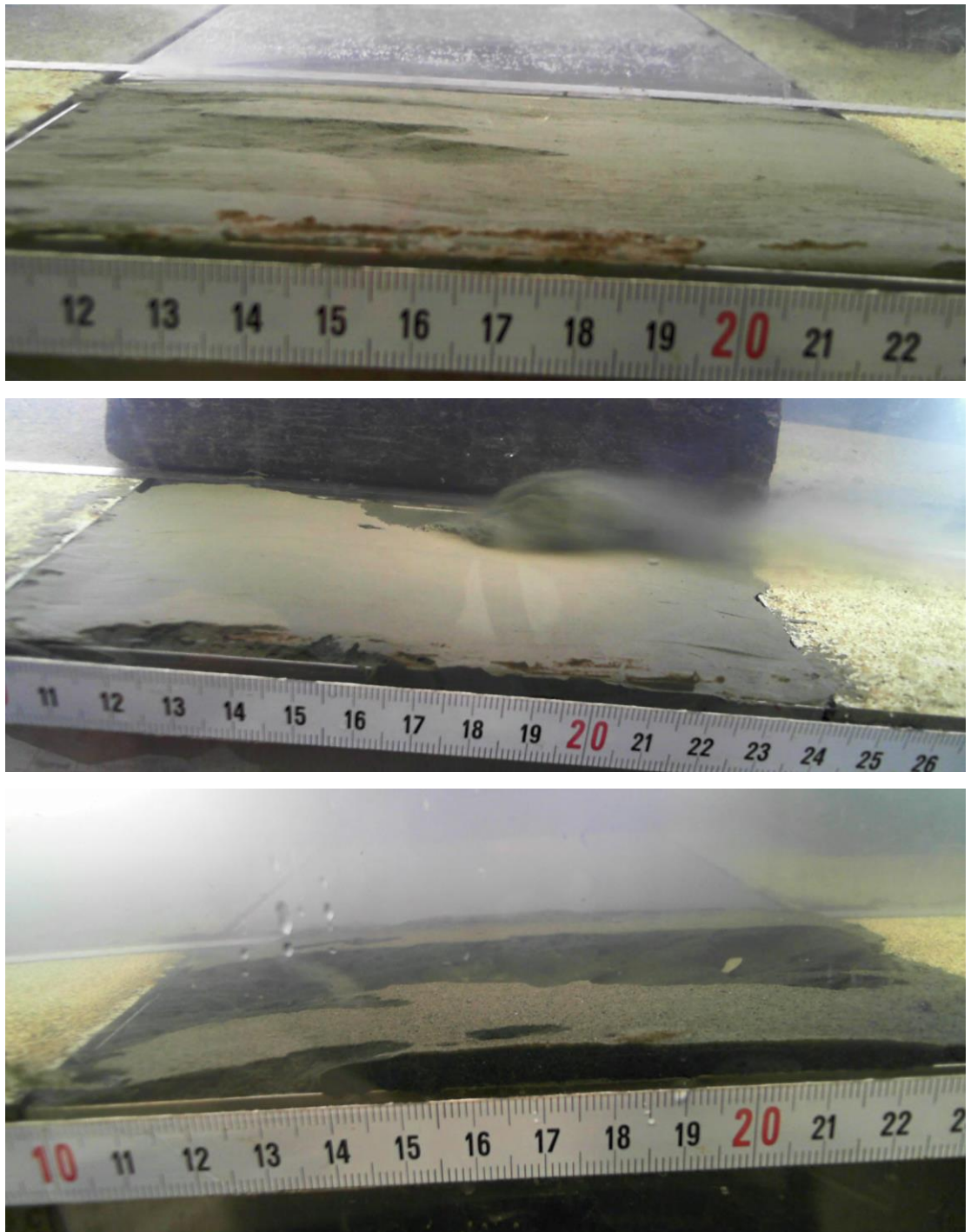
*Figure 3-42: Photos from the sediment tray during the flow-flume experiments. Upper panel WAW1 base mud, middle panel GR1 base mud, lower panel HU1 base mud*

The relation between bed shear stress, erosion rate and sediment concentration is shown in Figure 3-43 and Figure 3-44 for the flume experiments performed for GR1 and ZW2, respectively. Figure 3-43 presents the results for sample GR1 with 3 different dry bulk densities, namely 350, 415 and 682 kg/m³. Figure 3-44 shows similar flume test results for sample ZW2 with dry bulk densities; 356, 413, 560 and 755 kg/m³.

Report Phase 1A-B

28 June 2022
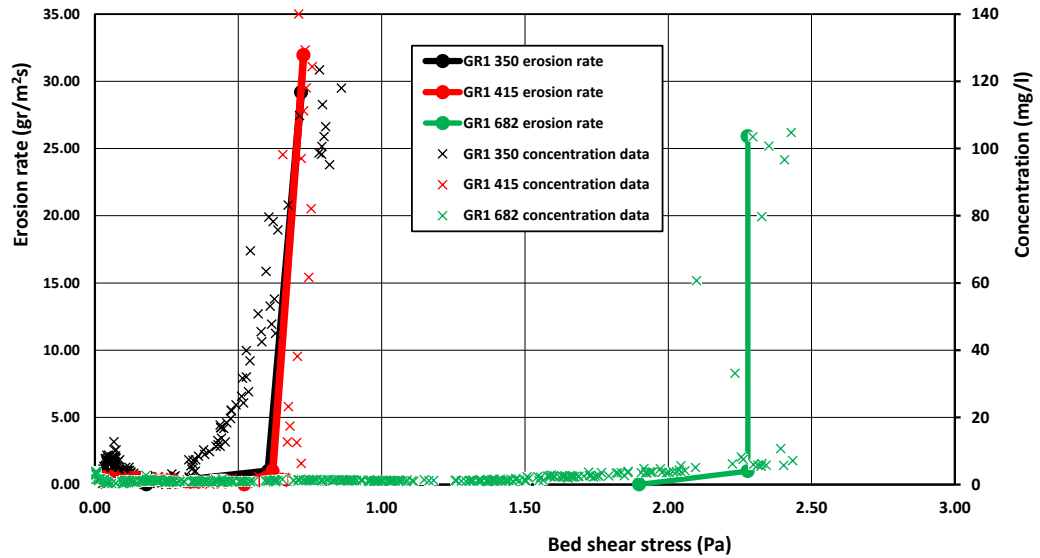
*Figure 3-43: Erosion rate and bed shear stress for flume tests of GR1 with dry bulk densities of 350, 415 and 682 kg/m3. The knickpoint is the onset of mass erosion.*
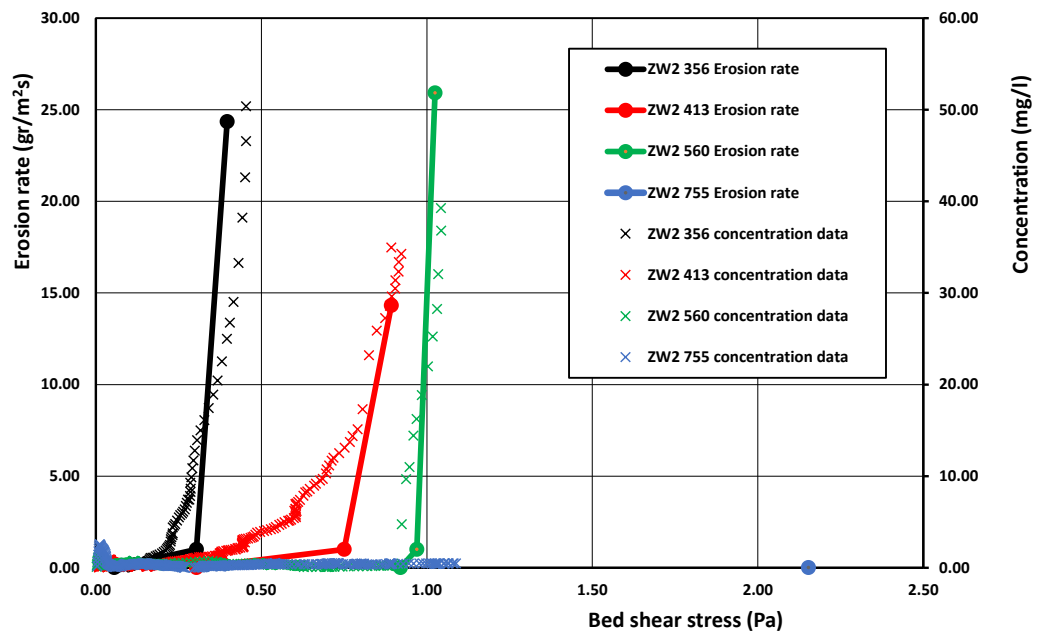


*Figure 3-44: Erosion rate and bed shear stress for flume tests of ZW2 with dry bulk densities of 356, 413, 560, 755 kg/m3 (lower). The knickpoint on the erosion rate curves is the onset of mass erosion; Mud-sand sample in flume before testing (upper).*

It can be seen from Figure 3-43 and Figure 3-44 that the erosion rate curves present a clear knickpoint that coincides with the bed shear stress above which the sediment concentrations sharply increases in value. This knickpoint is less pronounced for the low-density samples. With lower density sediments the increase is more gradual and the transition to mass erosion can hardly be identified based on visual observations. Most likely, the transition between surface and mass erosion is more gradual for low density samples in comparison with the higher density sediment samples.

In total 28 flume experiments are executed using base mud-sand samples and diluted samples as described in Chapter 3.4.7. The erosion parameters for all flow-flume experiments are given in Table 3-13 (se=surface erosion; me=mass erosion).

Report Phase 1A-B

28 June 2022

*Table 3-13: Erosion parameters derived from flow-flume experiments (WS=Western Scheldt Estuary and River; NPZ=Noordpolderzijl harbour/channel; DD=dry density measured from a subsample from the top layer at the end of the test; base mud data with in-situ density in **BOLD**)*

| | Dry density (kg/m³) | Organic content (%) | $P_{fines}$ <63 | $P_{clay}$ <8 | silt/clay ratio (-) | $\tau_{cr,se}$ Flume (Pa) | $\tau_{cr,me}$ Flume (Pa) | Erosion rate flume (gr/m²/s) |
|---|---|---|---|---|---|---|---|---|
| **NPZ B5** | **620** | **10** | **76** | **35** | **1.4** | **1.5** | **>3** | |
| **WS PA1** | **560** | **13** | **96** | **56** | **1.0** | **1.3** | **2.2** | **110** |
| **WS SO3** | **837** | **6** | **43** | **21** | **1.5** | **0.7** | **1.8** | **30** |
| **Bengal Bay BB3** | **1262** | **3** | **94** | **30** | **2.6** | **1.5** | **>3** | |
| **Plymouth PLUK1** | **644** | **10.2** | **90** | **23** | **3.2** | **0.9** | **1.5** | **2.3** |
| **Plymouth PLUK4** | **611** | **10.5** | **90** | **27** | **2.2** | **0.9** | **1.5** | **1.9** |
| **WS BAPU** | **650** | **8.8** | **73** | **37** | **1.2** | **1.3** | **2.0** | **0.7** |
| **WS APP** | **1238** | **4.9** | **25** | **10** | **1.7** | **1.3** | **2.2** | **2.5** |
| **WS BA4** | **1367** | **2.3** | **3** | **0** | **-** | **0.3** | **1.4** | **30** |
| NPZ H2 | 260 | 7.7 | 88 | 51 | 1.7 | 0.2 | 0.7 | 9 |
| | 320 | 7.7 | 88 | 51 | 1.7 | 0.7 | 1.6 | 5 |
| | **380** | **7.7** | **88** | **51** | **1.7** | **0.8** | **2** | **6** |
| WS GR1 | 350 | 6.7 | 95 | 37 | 2.6 | 0.35 | 0.65 | 14 |
| | 415 | 6.7 | 95 | 37 | 2.6 | 0.45 | 0.7 | 14 |
| | **680** | **6.7** | **95** | **37** | **2.6** | **0.8** | **2.5** | **32** |
| WS WAW1 | 570 | 4.7 | 63 | 24 | 2.6 | 0.5 | 0.8 | 7 |
| | 575 | 4.7 | 63 | 24 | 2.6 | 0.8 | 1.2 | 13 |
| | **845** | **4.7** | **63** | **24** | **2.6** | **1.3** | **2.5** | **230** |
| WS BH1 | 670 | 3.2 | 45 | 14 | 3.4 | 0.6 | 0.9 | 17 |
| | 750 | 3.2 | 45 | 14 | 3.4 | 0.5 | 0.8 | 16 |
| | **1135** | **3.2** | **45** | **14** | **3.4** | **1.6** | **>3** | **-** |
| WS HU1 | 1000 | 1.9 | 12 | 8 | 2.1 | 0.4 | 0.8 | 66 |
| | 1020 | 1.9 | 12 | 8 | 2.1 | 0.4 | 0.8 | 41 |
| | **1275** | **1.9** | **12** | **8** | **2.1** | **1.3** | **2.2** | **47** |
| WS ZW2 | 355 | 4.8 | 90 | 37 | 2.3 | 0.15 | 0.3 | 24 |
| | 410 | 4.8 | 90 | 37 | 2.3 | 0.5 | 0.8 | 4 |
| | 560 | 4.8 | 90 | 37 | 2.3 | 0.8 | 1 | 18 |
| | 755 | 4.8 | 90 | 37 | 2.3 | 1.2 | >2.5 | - |

### 3.4.8 Critical shear stress and erosion rate of mud-sand samples based on EROMES tests

A selection of 6 samples (ZW2, HU1, BH1, WAW1, GR1 and H2) with different densities were tested in the EROMES. The method is described in Section 3.3.7. Like the methods used in the flume experiments, the surface erosion (SE) and mass erosion (ME) were determined by (1) visual observation; closely observing the movement of particles within the instrument during the experiment, and (2) using the

Report Phase 1A-B

28 June 2022

MUSA

sediment concentration measurements from the NEP optical sensor. In Figure 3-45, the results of EROMES experiments from the sample GR1-350 (350 kg/m³) are shown. This figure presents the suspended sediment concentration as a function of bed shear stress.
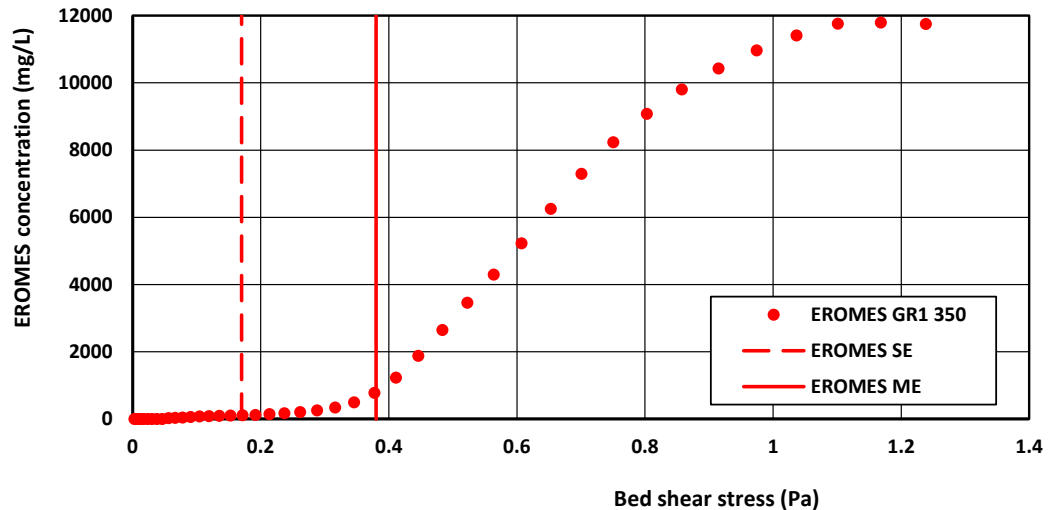


*Figure 3-45: Concentration as a function of bed shear stress for EROMES test GR1-350. The red dots indicate concentration measurements during the EROMES experiments. The dashed and solid lines depict the critical shear stresses for respectively surface (SE)- and mass erosion (ME).*

In general, the observations at the moment of surface erosion (SE) and mass erosion (ME) coincide well with the development of the concentration profile in time. The SE and ME values for all tested samples are presented in Table 3-14.

Contrary to the flow flume experiments, results of the erosion rate of surface and mass erosion were not determined for the EROMES experiments due to inaccuracy. In theory, the erosion rate can be estimated from the development of the measured concentrations over time. The theoretical conception relates the amount of sediment measured in suspension with the erosion, considering that the water volume in the EROMES is known and constant. However, during the experiments we noticed that the measured concentrations are not reliable for this purpose. We hypothesize that small irregularities in the bed during the test cause sudden bursts on suspended sediment concentrations jeopardizing the computation of realistic erosion rates. Moreover, the relatively small volume of the EROMES (i.e. 1.5 litre) quickly saturates the water after the start of mass erosion. The higher suspended concentrations in the EROMES saturates the NEP-sensor, and consequently the recorded values are unreliable after the beginning of mass erosion.

In order to better estimate the erosion rate from the EROMES, during later experiments we collected two water samples during the experiments. The first sample was collected immediately after the water was saturated with sediments, just before mass-erosion took place, and the second sample a couple of minutes after the mass erosion started. Based on the sediment concentration of these two samples and the time between the 2 sampling moments, we were able to perform an initial estimation of the erosion rates in the EROMES.

The critical bed shear stresses for surface erosion and mass erosion are presented in Table 3-14. It is important to note that contrary to the flume experiments, the critical shear stress results from the EROMES are only valid for a flat and smooth bed surface. The effect of bed roughness on the bed-shear stress cannot be taken into account in the present EROMES experiments. Additional and detailed calibrations including varying bed roughness are required for this purpose.

MUSA

*Table 3-14: Erosion parameters derived from EROMES experiments (WZ= Western Scheldt; NPZ=Noordpolderzijl; DD= dry density as measured from a subsample from the top layer before the test;) base mud data with in-situ density in **BOLD**.*

| Name | DD (kg/m³) | LOI (%) | $P_{fines}$ (<63 $\mu m$) | $P_{clay}$ (<8 $\mu m$) | silt/clay ratio | $\tau_{cr,se}$ EROMES (Pa) | $\tau_{cr,me}$ EROMES (Pa) |
|---|---|---|---|---|---|---|---|
| NPZ H2 | 260 | 7.7 | 88 | 51 | 1.7 | 0.15 | 0.35 |
| NPZ H2 | 320 | 7.7 | 88 | 51 | 1.7 | 0.35 | 0.6 |
| **NPZ H2** | **380** | **7.7** | **88** | **51** | **1.7** | **0.5** | **0.9** |
| WS GR1 | 350 | 6.7 | 95 | 37 | 2.6 | 0.2 | 0.4 |
| WS GR1 | 415 | 6.7 | 95 | 37 | 2.6 | 0.5 | 0.8 |
| **WS GR1** | **680** | **6.7** | **95** | **37** | **2.6** | **3.2** | **5.3** |
| WS ZW2 | 355 | 4.8 | 90 | 37 | 2.3 | 0.14 | 0.35 |
| WS ZW2 | 410 | 4.8 | 90 | 37 | 2.3 | 0.21 | 0.35 |
| WS ZW2 | 560 | 4.8 | 90 | 37 | 2.3 | 1.0 | 1.3 |
| **WS ZW2** | **755** | **4.8** | **90** | **37** | **2.3** | **5.3** | **5.5** |
| WS WAW1 | 570 | 4.7 | 63 | 24 | 2.6 | 0.3 | 0.7 |
| WS WAW1 | 575 | 4.7 | 63 | 24 | 2.6 | 0.2 | 1.5 |
| **WS WAW1** | **845** | **4.7** | **63** | **24** | **2.6** | **4.7** | **5.6** |
| WS BH1 | 670 | 3.2 | 45 | 14 | 3.4 | 0.14 | 0.6 |
| WS BH1 | 750 | 3.2 | 45 | 14 | 3.4 | 0.6 | 0.8 |
| **WS BH1** | **1135** | **3.2** | **45** | **14** | **3.4** | **3.5** | **5.3** |
| WS HU1 | 1000 | 1.9 | 12 | 8 | 2.1 | 0.12 | 0.22 |
| WS HU1 | 1020 | 1.9 | 12 | 8 | 2.1 | 0.1 | 0.24 |
| **WS HU1** | **1275** | **1.9** | **12** | **8** | **2.1** | **2** | **2.5** |

### 3.4.9 Comparison of critical bed-shear stress of flow-flume and EROMES experiments

To compare the critical bed-shear stress measured in the flume experiments and in the EROMES-cylinder, we plotted the measured values for surface erosion and mass erosion of both methods together in Figure 3-46. To study the effect of density, we divided the mud-sand samples in 4 dry density classes:

- LD: Low density samples: < 300 kg/m³
- LMD: Low-Medium density samples: 400 – 800 kg/m³
- MHD: Medium-high density samples: 800 – 1200 kg/m³

Report Phase 1A-B

28 June 2022

MUSA

- HD:     High density samples:          > 1200 kg/m³

The critical bed-shear stresses (surface erosion) of the EROMES-tests and the flume tests show large differences up to factor of 5, which may be related to differences in the type of flow (radial and vertical flows in EROMES), differences in roughness of the bed surface (smooth in EROMES and more irregular and variable in Flume), side wall effects and inaccuracy of the EROMES-calibration. The variability of the EROMES results is higher with critical shear stresses in the range of 0.1 to 5.4 N/m², while the critical shear stresses of the flume tests are in the range of 0.15 to 3 N/m². Given these results, the critical shear stresses of the flume tests are assumed to be more valid than those of the EROMES tests.
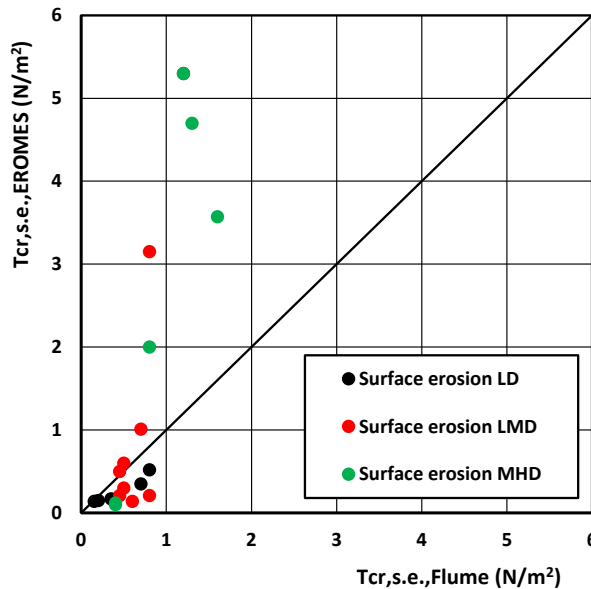


Figure 3-46: Critical bed-shear stresses for surface erosion of flume and EROMES tests. The black line is the line of perfect agreement.

### 3.4.10  Relation between density and critical bed shear stress

The critical bed-shear stresses ($\tau_{cr,se}$) for surface erosion as measured in the flume tests as a function of dry bed density (base sample and diluted sample) are shown in Figure 3-47 for 6 samples: H2, GR1, ZW2, WAW1, BH1 and HU1. The critical shear stress of surface erosion increases for increasing dry density.

The dry density of the samples with $p_{fines}$ > 60% is lower than about 800 kg/m³, whereas the dry density increases to above 1200 kg/m³ for $p_{fines}$ < 20%. A clear difference can be observed in the critical bed-shear stresses values of the base mud samples and the diluted mud samples.

The samples were diluted in two steps:

1) minor dilution: the base mud samples were diluted by adding 10% to 20% native water and

2) major dilution: the base mud samples were diluted by using 20% to 40% native water.

The base mud samples ZW2, WAW1, BH1 and HU1 (bold values of Table 3-14) have a relatively high density > 700 to 800 kg/m³ resulting in a relatively high critical shear stress values > 1 N/m². When these base mud samples are diluted to make samples of lower dry density in the range of 500 to 1000 kg/m³, the $\tau_{cr,se}$-values are strongly reduced to values below 0.5 N/m², especially for samples with relative large percentage of sand (BH1 and HU1), see Figure 3-47 and Figure 3-48.

Report Phase 1A-B

28 June 2022
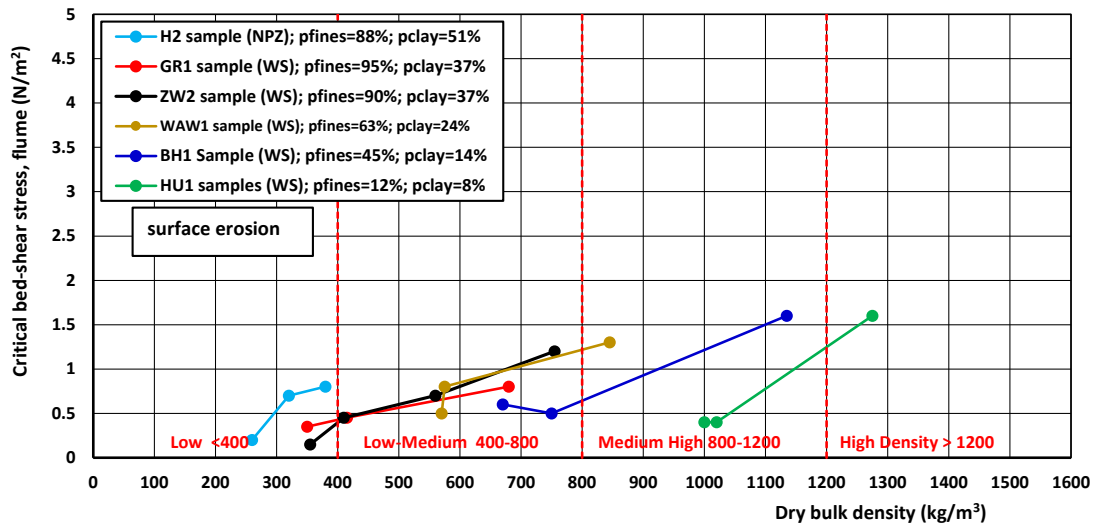
*Figure 3-47: Critical bed-shear stress for surface erosion as function of dry density; samples of Noordpolderzijl and Western Scheldt (grouped per sample location; diluted mud and base mud samples).*
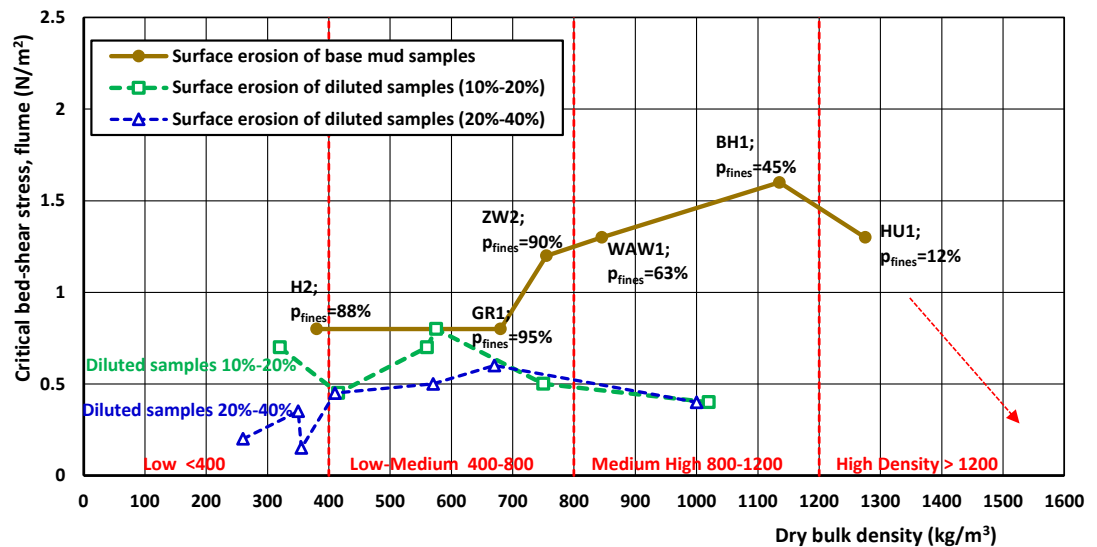


*Figure 3-48: Critical bed-shear stress for surface erosion as function of dry density; diluted and base mud samples of Noordpolderzijl and Western Scheldt (grouped as base mud and diluted samples). This figure contains only samples that were tested for dilutions.*

Figure 3-48 shows that the base samples have a much higher critical shear stress for surface erosion than the diluted samples. This strong reduction may be related to 2 processes: (1) possible segregation of sediment fractions after the placement of the sample in the flume compartment, especially for the sandier sediment samples, and (2) effects on cohesion/ interlocking of particles when more water is added to dilute the densities.

It is noted that the dilution and mixing of higher density samples to make lower density samples may disturb the internal structure of the cohesive mud particles and the internal arrangements of grains and flocs (segregation of sediment fractions, development of a fluffy top later, etc.) resulting in deviating and unreliable results when compared to natural and undisturbed samples of the same density; especially for samples with a relative high percentage of sand; BH1 (55%) and HU1 (88%).

Figure 3-49 shows the values of the critical bed-shear stresses (css) for surface erosion and mass erosion of all samples of Table 3.9 (base samples) used in the FLUME tests as function of the dry density. Although substantial variation can be observed, the critical shear stress shows an increasing tendency for increasing dry bulk density up to a dry density of about 1100-1300 kg/m$^3$ and a decreasing trend for higher dry density values. In the dry density range > 1300 kg/m$^3$, the samples are mostly sandy with a critical stress approaching to the value of pure fine sand with critical stress of about 0.2 N/m$^2$. The critical shear stress values for mass erosion ($\tau_{cr,me}$) show similar results.

For very low density values < 300 kg/m$^3$, the $\tau_{cr,se}$-value will decrease to about 0.2 N/m$^2$ as found in earlier studies (Van Rijn, 2018), (see red dashed line on the left in Figure 3-49). Similarly, the $\tau_{cr,se}$-value will decrease to that of pure sand (0.2 N/m$^2$ for sand of 0.2 mm) for a high dry density of 1600 kg/m$^3$ and p$_{fines}$ approaching to 0 (see red dashed line on the right in Figure 3-49). For p$_{fines}$ <45%, the $\tau_{cr,se}$-values gradually decrease, except for very silty samples (BB3 with high density of 1262 kg/m$^3$ in combination with high percentage of fines 94%).

The $\tau_{cr,se}$-values for mass erosion are much higher (factor 1.3 to 2) than the $\tau_{cr,se}$-vales for surface erosion.
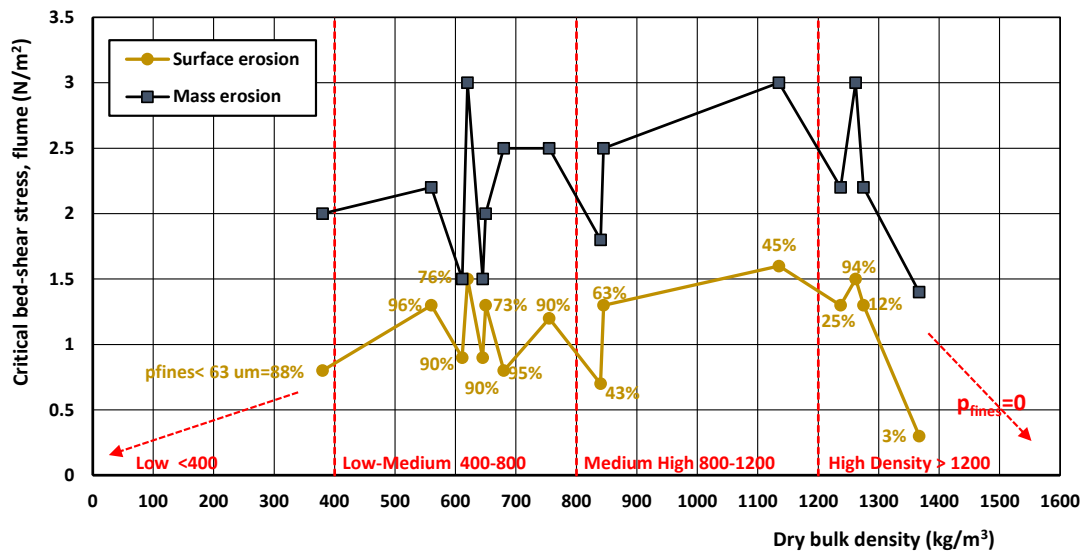


Figure 3-49: Critical bed-shear stress for surface and mass erosion as function of dry density; base mud samples. The written percentages denote the percentage of fines.

Figure 3-50 shows the $\tau_{cr,se}$ and $\tau_{cr,me}$-values for surface and mass erosion, respectively, as function of the percentage of fines. Higher $\tau_{cr,se}$ and $\tau_{cr,me}$-values are found for p$_{fines}$ in the range of 45% to 75%. The $\tau_{cr,se}$-value is relatively small for p$_{fines}$ of about 5%, but rapidly increases for p$_{fines}$ > 15%.

The erosion rate could be measured from 4 experiments (H2, GR1, WAW1 and HU1), the base mud of BH1 and ZW2 was too strong to induce mass erosion in the flume experiment. The erosion rate values vary in the range of 6 to 230 g/m$^2$/s and do not show a clear relationship with the measured bed-shear stress values. The relatively high value of 230 g/m²/s of test WAW1 is related to sudden failure of a large part of the sample compartment (see photograph of test WAW1 in Appendix C. It is advised to better study the erosion rate by e.g. using a vertical lift system installed in the floor of the flume in which the bed can be lifted when erosion takes place. In this way the erosion rate can be determined over a longer measurement period, reducing the amount of scatter due to sudden failure of the bed.
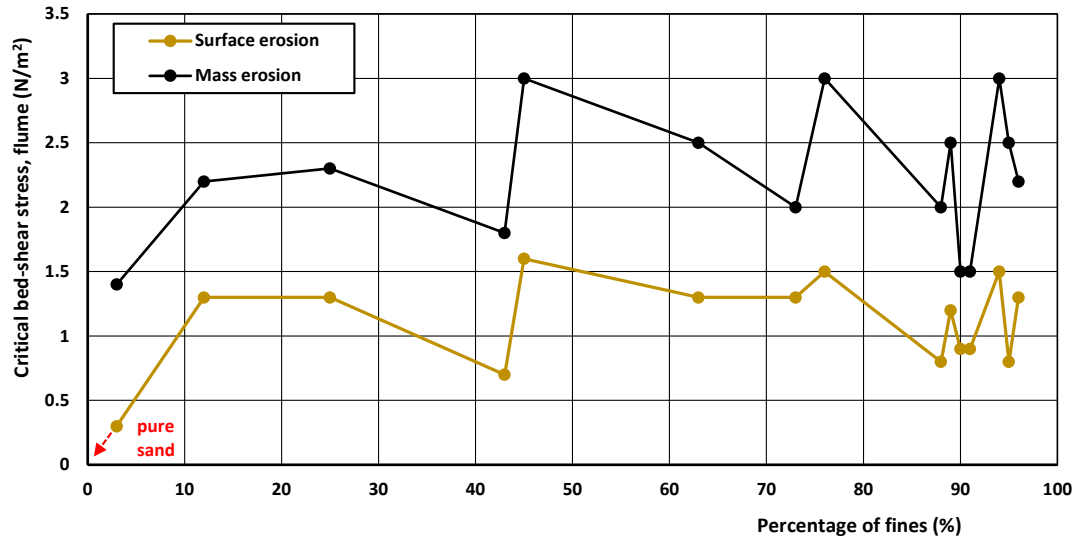
*Figure 3-50: Critical bed-shear stress for surface and mass erosion as function of percentage of fines (pclay = percentage of clay; DD= dry density in kg/m3); base mud samples of Western Scheldt and Noordpolderzijl.*

### 3.4.11 Data comparison among sites

The results of the present study are compared to earlier results of samples from Noordpolderzijl (Van Rijn, 2019) and Holwerd (WaterProof2019a,b). Most samples from the tidal channel at Noordpolderzijl (taken at the intertidal banks) are sandy muds with a relatively low percentage of fines (i.e. < 63 $\mu$m). The samples from Holwerd are muddy samples taken from the bed of the channel (samples taken from below the low water level). The measured critical bed-shear stresses of surface erosion ($\tau_{cr,se}$) for the 3 sites are summarized in Table 3-15 and in Figure 3-51.

Based on comparison of the results, the following remarks are made:

- the critical bed-shear stress ($\tau_{cr,se}$) of surface erosion shows an increasing trend from approx. 0.3 to approx. 0.7 N/m$^2$ for a dry density < 400 kg/m$^3$ (low-density range LMD);
- the critical bed-shear stresses ($\tau_{cr,se}$) of surface erosion are varying in the range of 0.7 to 2.5 N/m$^2$ for a dry density between 400 to 1200 kg/m$^3$;
- the critical bed-shear stress gradually decreases to approximately 0.2 N/m$^2$ (Shields's curve) for fine to medium fine sand with density >1300 kg/m$^3$ and almost no fines < 5%.

Van Rijn (2020) has a method to compute the critical stress for surface erosion of mud-sand mixtures. The method is briefly summarized below:

$$\tau_{cr,s} = (1 + p_{fines})^{\beta} \, \tau_{cr,silt}$$

$$\beta = [1 + (p_{clay}/p_{fines})^{\alpha 1} + (\rho_{dry}/\rho_{dry,max})]^{\alpha 2}$$

Equation 11

with:

$\tau_{cr,silt}$= critical shear stress of cohesionless silt particles ($\cong$0.1 to 0.2 N/m²);

$p_{fines}$= percentage of fines < 63 $\mu$m;

$p_{clay}$= percentage of clayey materials < 8 $\mu$m;

$\rho_{dry}$= dry bulk density of sample;

$\rho_{dry,max}$= maximum dry bulk density of sample ($\cong$1600 kg/m³).

MUSA

The method is applied for:

$\rho_{dry}$ = 300, 400, 500, 600, 700, 800, 900,1000, 1100, 1200, 1300, 1400 kg/m³;
$p_{fines}$ = 0.8, 0.8, 0.8, 0.8, 0.8, 0.7, 0.6, 0.5, 0.4, 0.3, 0.2, 0.1
$\tau_{cr,silt}$=0.2 N/m²; $\rho_{clay/pfines}$=0.3, $\alpha_1$=1 and $\alpha_2$=2

In this example computation, the percentages of fines was set to 80% from dry densities between 300 and 700 kg/m³ to account for variations in mud characteristics (e.g. water content and mineralogy). Between 800 and 1400 kg/m³ the percentage of fines was linearly decrease towards 10% representing the mixtures between fine sediments and sand, similar to the transition observed in natural samples. The results are shown in Figure 3.52. The Equation proposed by Van Rijn (2020) yields very reasonable results for mud-sand mixtures with dry density values in the range of 400 to 1000 kg/m³, but underpredicts up to factor of 2 for high-density mixtures. The data show considerable scatter in the critical shear stress for erosion. Apparently, the parameters $p_{fines}$, $p_{clay}$ and $\rho_{dry}$ are not sufficient to fully explain all effects involved across the mud-sand mixtures. This requires further (future) studies focussing on the type and percentage of clay (< 2 $\mu$m; < 8 $\mu$m) and organic materials.
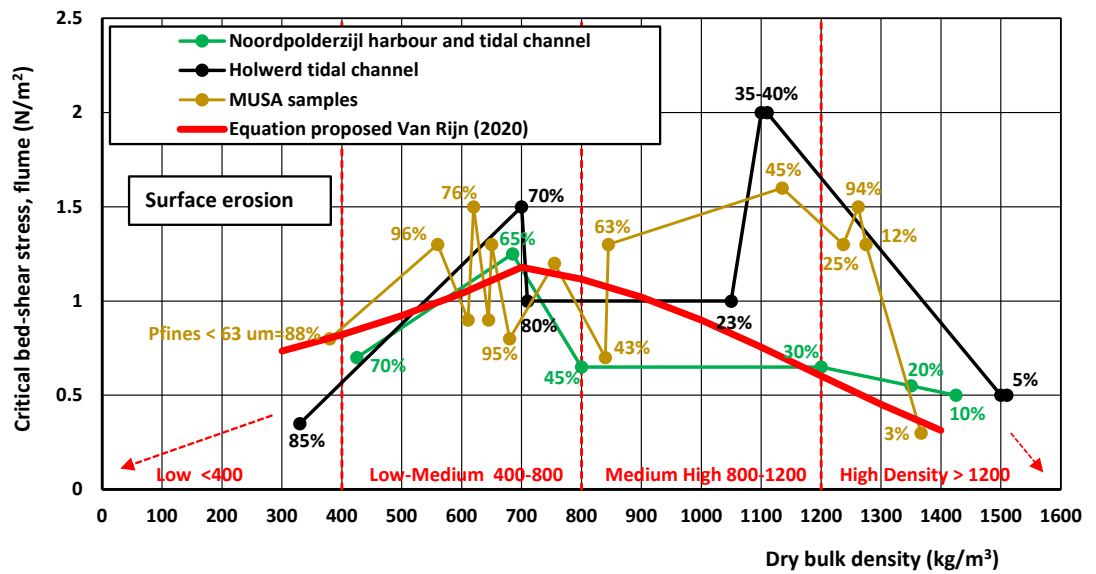


*Figure 3-51: Critical bed-shear stress for surface erosion as function of dry density and percentage of fines; base mud samples from three different sites*

*Table 3-15: Critical bed-shear stress of base mud-sand samples from three Dutch sites. WS= Intertidal flats of Western Scheldt Estuary; NPZ= Harbour and tidal channel of Noordpolderzijl; HW=tidal channel near Holwerd ferry landing (previous studies)*

| Location | In-situ dry density (kg/m³) | Percentage fines (< 63 μm) and Clay (<8 um) (%) | Critical Bed shear for SE and ME (N/m²) | Bed Roughness |
|---|---|---|---|---|
| WS GR1 | 680 | 95; 37 | 0.8; 2.5 | smooth |
| WS ZW2 | 755-835 | 90; 37 | 1.2; > 2.5 | smooth |
| WS WAW1 | 845-910 | 63; 24 | 1.3; 2.5 | smooth |
| WS BH1 | 1135-1145 | 45; 14 | 1.6; >3.0 | smooth |
| WS HU1 | 1275-1300 | 12; 8 | 1.3; 2.2 | smooth |
| NPZ H2 | 380-435 | 88; 51 | 0.8; 2 | smooth |
| NPZ H1 | 685 | 65; 25 | 1.25; 2.25 | smooth |
| NPZ H4 | 425 | 70; 25 | 0.7; 0.9 | smooth |
| NPZ B5 | 800 | 45; 15 | 0.65; >2 | smooth |
| NPZ B7 | 1200 | 30; 10 | 0.65; >2 | smooth |
| NPZ B9 | 1350 | 20; 8 | 0.55 ; 1.2 | smooth and rough with shells |
| NPZ B15 | 1425 | 10; 5 | 0.5; >2 | smooth and rough with shells |
| HW 0 km | 330 | 85; 30 | 0.35; 0.6 | smooth |
| HW 0 km | 710 | 85; 30 | 1.0; 1.4 | smooth |
| HW 1 km | 700 | 70; 25 | 1.5; 2.5 | smooth |
| HW 2 km | 1100 | 35; 10 | 2; 2.9 | smooth |
| HW 3 km | 1100 | 40 | 2; 2.9 | smooth |
| HW 4 km | 1050 | 23 | 1; 1.8 | smooth |
| HW 5 km | 1500 | 5 | 0.5 | sandy; smooth and rough |
| HW 6 km | 1500 | 5 | 0.5 | sandy; smooth and rough |

Report Phase 1A-B

28 June 2022

MUSA

## 3.5 Main conclusions and recommendations experiments Phase 1A

### 3.5.1 Main conclusions based on the first results of Phase 1A

The Phase 1A experiments of the MUSA-project encompassed the sediment sampling of mud-sand beds from the tidal harbour of Noordpolderzijl (Wadden Sea, NL), the intertidal banks of the Western Scheldt Estuary (NL) and Scheldt River (BE), the silt-rich samples from the Bengal Bay near the Ganges-Brahmaputra delta and from muddy sites in the Plymouth Estuary (UK). The samples were mainly processed and analysed at the WaterProof laboratory to determine the sediment composition, the wet and dry densities and the organic matter content. A selection of samples with a wide range of sand-mud percentages ($\cong$ 5-95% of sand) and bulk density values (dry density of 400 to 1300 kg/m$^3$) were used for the consolidation tests, and physical experiments for the determination of the critical bed-shear stress for erosion.

The findings of the study are summarized in the following conclusions:

1. the intertidal banks of the Western Scheldt Estuary and Scheldt River consist of the following type of sediments:
   - mud-rich sediments with percentages of fines (<63 $\mu$m) higher than 80% and dry densities between 500 and 800 kg/m$^3$; mostly in the top layer (< 0.1 m) of intertidal banks and in sheltered areas (harbour sites);
   - sandy mud sediments with percentage of fines (<63 $\mu$m) between 50% and 80% and dry densities between 800 and 1200 kg/m$^3$ (mostly below the top lower layer of the intertidal banks);
   - low mud sediments with percentage of fines < 50% and dry densities between 500 and 800 kg/m$^3$ (most at intertidal banks with sufficient wave activity due to wind and/or ship waves);
   - organic materials in the range of 2% to 7%;
2. the percentage of clay-type particles (< 8 $\mu$m) in the top layer of the intertidal banks of the Western Scheldt Estuary and Scheldt River varies in the range of 10% in sandy areas to 50% in very muddy areas; the ratio of fines (< 63 $\mu$m) and clay (<8 $\mu$m) is about 2.5 ($\pm$0.7);
3. the surface samples from the intertidal banks of the Plymouth Estuary are mostly very muddy sediments with percentage of fines up to 90% and dry density values in the range of 600 to 700 kg/m$^3$; the organic content is relatively high with values up to 10%;
4. the samples from Bengal Bay are silt-rich sediment with percentage of fines up to 90% and percentage of silt of about 60% and dry density values > 1200 kg/m$^3$; almost no organic materials;
5. the dry density values of the mud-sand mixtures are mostly in the range of 400 kg/m$^3$ for predominantly muddy samples to 1300 kg/m$^3$ for sandy samples with less than 20% of fines; the dry density value can be reasonably represented by the empirical relationship proposed by Van Rijn (2018) with exception of the very silty and compacted samples of Bengal Bay;
6. surface samples from the intertidal banks of the Western Scheldt Estuary consolidate from 50% to 70% of their in-situ dry density in about 1 day for sandy samples to 7 days for muddy samples; a long consolidation period (secondary consolidation phase) of months to years is required to obtain the high dry density values of the field samples;
7. the critical bed-shear stress for surface erosion of the studied mud-sand mixtures relates to the dry density, as follows: approximately 0.7 ($\pm$0.3) N/m$^2$ for samples with dry density of 400 ($\pm$50) kg/m$^3$ to about 2 ($\pm$0.7) for dry density of 1200 ($\pm$100) kg/m$^3$; the critical bed shear stress for mass erosion is 30% to 100% higher than that for surface erosion; variations involved may depend on site specific effects;
8. translating the laboratory results into the field, the critical depth-averaged current velocities for surface erosion at intertidal banks of estuaries based on the results of this study are mostly in the range of 0.6 to 1 m/s; hence, intertidal banks (e.g. on the Western Scheldt) are mostly sedimentary areas requiring relatively high velocities/shear stress to erode (combination of currents and waves);
9. the critical bed-shear stresses for surface erosion measured in the EROMES-device are less reliable as a quantitative result. The critical shear stresses derived from the EROMES show larger scatter in comparison with the flume experiments; the effect of bed roughness variations

MUSA

on the bed-shear stress cannot be represented due to its setup and physical limitations of the EROMES; the EROMES is particularly useful for qualitative and comparative in-situ determination of the erosion resistance of bed samples;

10. the effects of varying bulk densities on the critical bed-shear stress by means of diluted samples are not fully understood yet; the dilution and mixing of higher density samples to make lower density samples may disturb the internal structure of the cohesive mud particles and the internal arrangements of grains and flocs (segregation of sediment fractions, development of a fluffy top later, etc.) resulting in deviating and unreliable results when compared to natural and undisturbed samples of the same density; especially for samples with a relative high percentage of sand; BH1 (55%) and HU1 (88%).

### 3.5.2 Recommendations regarding phase 1A

It is advised to study the erosion rate by using a flume in which a relatively small sized sediment bed is lifted upward during mass erosion phase. In this way the erosion phase can be extended and erosion rate determined from a longer erosion period, reducing the scatter in the results.

Experiments have been performed using this sediment lift during Phase 1B of the MUSA project.

MUSA

# 4 Method and results of Phase 1B experiments

## 4.1 Introduction

The intrinsic characteristics of the sediment bed also affect the erosional behaviour. Therefore, apart from understanding the influence of different sand-mud mixtures, here the bed roughness, depositional process and in-situ (field) beds have been investigated to complement the findings from phase 1A. These variations are commonly observed in nature (Figure 4-1) and therefore it is important to understand how they affect the erodibility of sediments.



Figure 4-1 Example of natural sediment beds. Left: Sandy sediments covered by shells and pebbles at de Waal river, the Netherlands; Right: Fluffy mud rich in benthic fauna at Bath-Pump, the Netherlands.

The goal of the Phase1B experiments is to assess the erodibility of these beds in terms of critical shear stress for erosion and to estimate the erosion rate. For that purpose, we performed flow flume experiments with different sand-mud mixtures under various roughness, deposited beds and undisturbed beds collected from the field. The varying roughness was induced by added shell and pebbles (herein called stones) with different surface coverage. Varying the roughness ($k_s$) in this way alters the bed shear stress and therefore the erosion capacity of the flow on the sample. We also performed experiments with deposited beds consisting of freshly and undisturbed sediments including a so called fluffy top layer. Lastly, undisturbed sediment beds were collected from the field and brought directly to the flume without any mixture or pre-treatment in order to assess the erosion characteristics of natural tidal flats, here including the effects of benthic fauna and the in-situ bed densities.

## 4.2 Methods

Three key samples were chosen in terms of sand-mud percentages and dry density, namely Bath Pumping station (BA-PU; muddy), Appelzak south of Bath-NL (BA-APP; sand-mud) and sandy bank close to pumping station (BA-4; sandy). In addition, we performed experiments with the B5 and PA1 sediments from Phase1A in order to further compare the differences in bed characteristics between the Phase 1A and Phase 1B experiments. Remoulded bed results (here called base sample) from Phase 1A are also included as a reference for comparison. Figure 4-2 shows the sample locations in the Western Scheldt Estuary (near village of Bath, the Netherlands). The experiments were performed with:

Report Phase 1A-B

28 June 2022

MUSA

- Placed (remoulded) beds with varying roughness by adding the following types of shells or stones on top of the bed:
  - Low shells
  - Mid shells
  - Low stones
  - Mid stones
  - High stones (armouring)
- Deposited beds
- Field beds

A total of 21 experiments were performed in the small flume with flow velocities up to 1 m/s (increased stepwise). The experiment procedure was similar to the Phase 1A experiments (see chapter 3.3.6). The difference was mainly in the sample preparation. The specific procedures are described below.
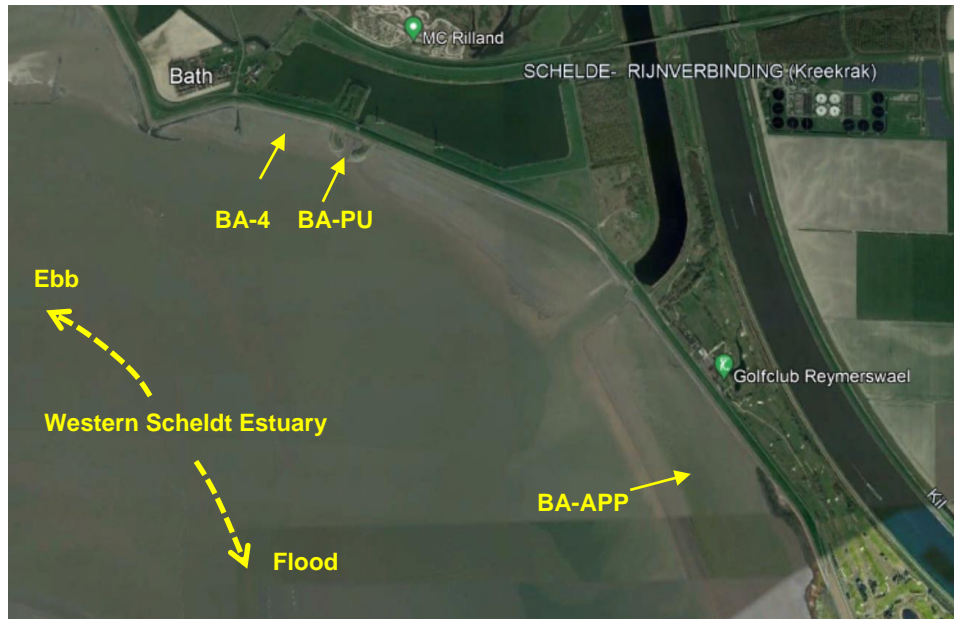


Figure 4-2 Sample locations BA-4, BA-PU and BA-APP in Western Scheldt Estuary (NL)

### 4.2.1    Roughness

For the roughness experiments, shells and stones were added on top of the remoulded bed sample with 5 variations (Figure 4-3). The "low" amount included some individual elements that should not directly affect the overall roughness but rather create turbulence near the bed. The "mid" variation was intended to change overall roughness of the sample, with still exposing the bed material underneath. The "high" variation consisted of covering almost the entire sample with pebbles to simulate high roughness but also armouring when the bed underneath is not directly exposed to the flow.



*Figure 4-3: Left: BA-PU low shells; Mid: BA-APP mid stones; Right: BA-4 high stones.*

### 4.2.2 Deposited beds

Deposited bed experiments were performed with freshly deposited sediments in the flume tray (Figure 4-4). The flume tray was filled with sediment and a 10 cm high extension was placed on top of the tray with a watertight connection (to avoid sediment spreading) and filled with water. The sample was then completely brought into suspension inside the extended sealed tray. The mixture was let to rest for about 48 hours before the experiment. Using this approach, we created and preserved the top fluffy layer to test the erosion of a recently deposited bed (with lower bulk density). The deposit beds in the results were further characterized by two elements: the top fluffy layer and the firmer sub-layers. That is because the fluffy layer of few millimetre (i.e. in the order of 1 to 3 mm) had a different behaviour than the bottom firmer sublayer.
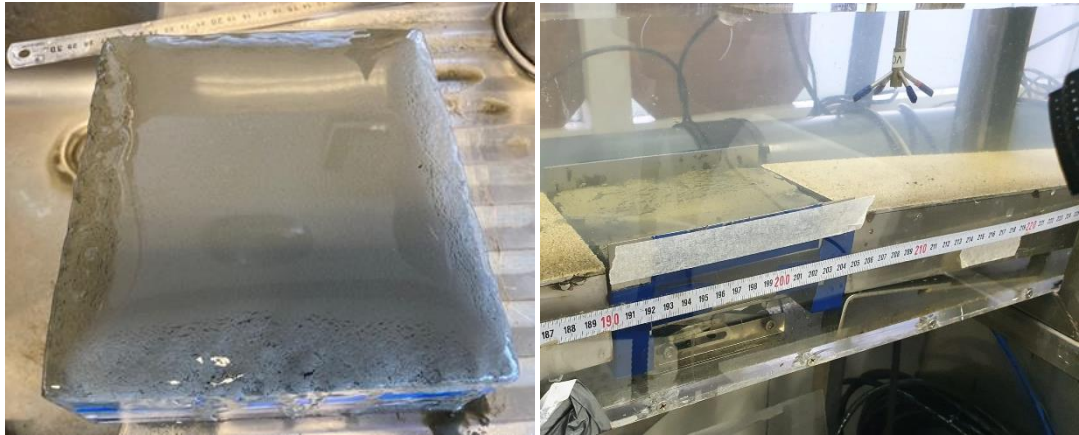


*Figure 4-4: Left: BA-APP deposited bed with the top fluffy layer. Right: Sample placed on top of the lift.*

The deposited beds experiments for PA1, B5 and APP were placed on top a sample lifter. The lift was applied to raise the sample while erosion was lowering the bed. Lifting the sample allowed to keep the sample bed level aligned with the flume bed which is particularly important to assess the erosion rates.

### 4.2.3 Field beds

The field beds were sampled directly from the tidal flats with the flume trays in order to preserve the bed characteristics in terms of composition (no artificial mixing), bulk density, benthic biota and the top bed characteristics such as roughness and sediment composition (Figure 4-5).



*Figure 4-5: Sampling the field beds at BA-4. See sample location in Figure 4-2.*

Report Phase 1A-B

28 June 2022

## 4.3 Results

In this section we present the test results showing the effects of varying roughness and bed type (i.e. placed, deposited or field) on the critical bed-shear stress for surface erosion. All results are summarized in Table 4-1.

### 4.3.1 Bed roughness variability

Determining the bed-shear stress in our experiments is not straightforward as the bed surface consists of a smooth sediment part and a rough part (composite bed roughness). We estimate the overall effective bed roughness height ($k_s$) of the beds with varying percentages of pebbles and/or shells (from low to high) to be in the range of 2 to 5 mm. This is based on the size and level of exposition of the elements above the bed.

Similarly to Equation 4 from Phase 1A, the critical bed-shear stress for erosion is defined as:

$$\tau_{cr,s} = \rho_w \, g \, (u_{cr,s}/C)^2$$

where,
$\tau_{cr,s}$    critical bed-shear stress for erosion
$\rho_w$    the water density, here 1000 kg/m³
$g$    gravity, here 9.81 m/s²
$u_{cr,s}$    critical depth-averaged flow velocity in flume, here 0.4*h
$C$    Chézy roughness = $5.75 \, g^{0.5} \log(12h/k_s)$
$H$    water depth=0.13 m
$k_s$    weighted value between smooth mud bed surface and rough stone bed surfaces.

We firstly present the results for the pebble beds, followed by the shell beds.

#### 4.3.1.1 Pebble induced roughness

The effect of pebbles resting on the bed surface on critical depth-averaged flow velocity and the associated critical bed-shear stress for surface erosion vary between the sandy and muddy samples. The critical flow velocity for erosion of the sample with pebbles is slightly lower than the reference (remoulded) sample without pebbles, but the bed shear stress for erosion is similar or higher because of the added effect of roughness ($k_s$) on the shear stress value. The effect of roughness is less pronounced for the sandy sample while the differences are larger for the higher mud percentage samples (Figure 4-12). The results of the three samples are described in more detail below.

Sandy sample **Western Scheldt BA-4** ($p_{fines<63um}$ =3%), (Figure 4-6)
- No stones (reference): $u_{cr,s}$=0.25-0.35 m/s ($k_s$=1 mm; $\tau_{cr,s}$ =0.3±0.1 N/m²); incipient erosion;
- Mid stones; $u_{cr,s}$=0.2-0.3 m/s ($k_s$=3 mm; $\tau_{cr,s}$ =0.3 ± 0.1 N/m²); incipient erosion of sand starting in front of stones/pebbles; deeper scour marks in front of 80% of stones;
- High stones; $u_{cr,s}$=0.4-0.5 m/s ($k_s$=5 mm; $\tau_{cr,s}$ = 1.0 ± 0.2 N/m²); surface is protected by layer of pebbles; erosion starts behind stones, ongoing pickup of sand into suspension.

Mud-sand sample **Western Scheldt BA-APP** ($p_{fines<63um}$ =25%), (Figure 4-7):
- No stones (reference); $u_{cr,s}$= 0.7-0.9 m/s ($k_s$=0.2 mm; $\tau_{cr,s}$ =1.3 ± 0.3 N/m²); start of erosion
- Low stones; $u_{cr,s}$=0.45-0.65 m/s ($k_s$=2 mm; $\tau_{cr,s}$ =1.1 ± 0.3 N/m²): erosion starting behind relatively high stone/pebble in centre; ongoing crater/groove erosion after displacement of stones/pebbles;

Report Phase 1A-B
28 June 2022

MUSA

- Mid stones; $u_{cr,s}$=0.45-0.65 m/s ($k_s$=3 mm; $\tau_{cr,s}$ =1.25 $\pm$ 0.3 N/m$^2$): erosion starting around stone clusters; when stones are displaced leading to ongoing crater/groove erosion;
- High stones; $u_{cr,s}$=0.5-0.6 m/s ($k_s$=5 mm; $\tau_{cr,s}$ =1.5 $\pm$ 0.3 N/m$^2$): surface is protected by stones hindering erosion crater/groove erosion starts after displacement of stones.

Muddy sample **Western Scheldt BA-PU** ($p_{fines<63um}$ =73%), (Figure 4-8)
- No stones (reference); $u_{cr,s}$=0.7-0.9 m/s ($k_s$=0.2 mm; $\tau_{cr,s}$ =1.3 $\pm$ 0.3 N/m$^2$); start of erosion
- Low stones; $u_{cr,s}$=0.6-0.7 m/s ($k_s$=2 mm; $\tau_{cr,s}$ =1.5 $\pm$ 0.3 N/m$^2$); erosion starting along flank of stone/pebble; ongoing crater erosion after displacement of stones/pebbles
- Mid stones; $u_{cr,s}$=0.6-0.7 m/s ($k_s$=3 mm; $\tau_{cr,s}$ = 1.7 $\pm$ 0.3 N/m$^2$); incipient erosion starting near craters of displaced stones; ongoing erosion at craters of many displaced stones (40%)
- High stones; $u_{cr,s}$=0.55-0.7 ($k_s$=5 mm; $\tau_{cr,s}$ =1.9 $\pm$ 0.4 N/m$^2$); erosion starting at craters of displaced stones; ongoing erosion at many craters of displaced stones (30%)



Figure 4-6 Sample BA-4; mid stones (left) and high stones (right)
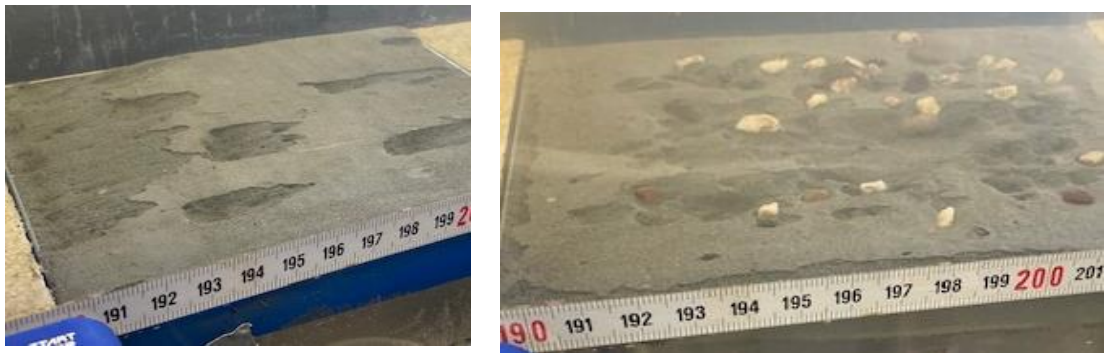


Figure 4-7 Sample BA-APP; low stones (left); mid stones (right)
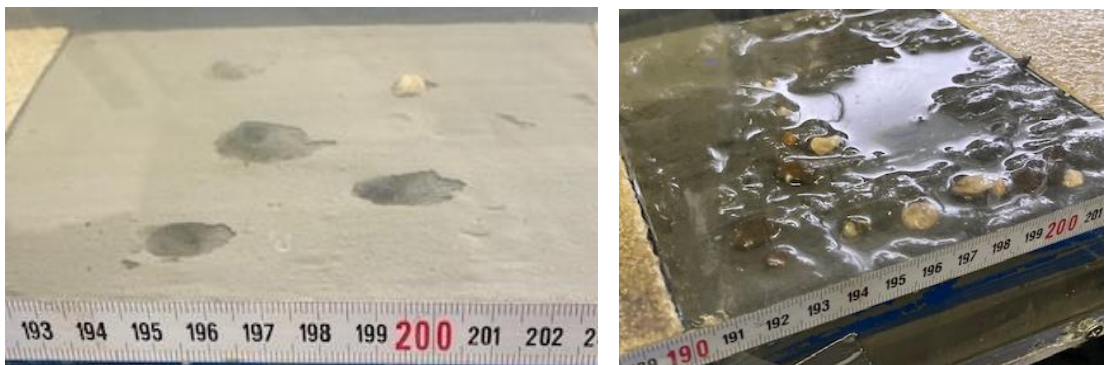


Figure 4-8 Sample BA-PU Low stones and craters (left); bed at end of test with high stones (right)

Report Phase 1A-B

28 June 2022

MUSA

### 4.3.1.2 Shell induced roughness

The effect of small shells (effective diameter 20 to 30 mm; height 5 mm) resting on the mud surface on critical depth-averaged flow velocity and the associated critical bed-shear stress for surface erosion are similar to the effect of pebbles described above. We estimate the overall effective bed roughness height ($k_s$) of a bed with a varying percentage of shells (from low to mid) to be in the range between 1 and 3 mm, as the shells have a very streamlined shape. This streamlined body also results in shells that, despite their light weight, can withstand strong flow rates. The results of the three samples are described in more detail below.

Sandy sample **Western Scheldt sample BA-4** ($p_{fines<63um}$ =3%), (Figure 4-9)
- No shells (reference): $u_{cr,s}$=0.25-0.35 m/s ($k_s$=1 mm; $\tau_{cr,s}$=0.3 $\pm$ 0.1 N/m$^2$); incipient erosion;
- Mid shells; $u_{cr,s}$=0.2-0.3 m/s ($k_s$=3 mm; $\tau_{cr,s}$=0.3 $\pm$ 0.1 N/m$^2$); erosion starting behind/in front of shells; ongoing scour with clear scour marks.

Mud-sand sample **Western Scheldt BA-APP** ($p_{fines<63um}$ =25%), (Figure 4-10):
- No shells (reference); $u_{cr,s}$=0.7-0.9 m/s ($k_s$=0.2 mm; $\tau_{cr,s}$=1.3 N/m$^2$); start of erosion
- Low shells; $u_{cr,s}$=0.6-0.7 m/s ($k_s$=1 mm; $\tau_{cr,s}$=1.3 $\pm$ 0.3 N/m$^2$): erosion starting around shells; ongoing erosion at craters of displaced shells;
- Mid shells; $u_{cr,s}$=0.5-0.65 m/s ($k_s$=3 mm; $\tau_{cr,s}$=1.35 $\pm$ 0.4 N/m$^2$); erosion starting behind 3 shells; growing erosion between shells connecting shells; flat bed undisturbed;

Muddy sample **Western Scheldt BA-PU** ($p_{fines<63um}$ =73%), (Figure 4-11)
- No shells (reference); $u_{cr,s}$=0.7-0.9 m/s ($k_s$=0.2 mm; $\tau_{cr,s}$=1.3 N/m$^2$); start of erosion
- Low shells; $u_{cr,s}$=0.6-0.75 m/s ($k_s$=1 mm; $\tau_{cr,s}$=1.4 $\pm$ 0.3 N/m$^2$); erosion starting at craters of displaced shells; growing and expanding craters;
- Mid shells; $u_{cr,s}$=0.55-0.7 m/s ($k_s$=3 mm; $\tau_{cr,s}$=1.6 $\pm$ 0.3 N/m$^2$); incipient erosion near 2 shells; slowly growing erosion; later crater erosion at displaced shells


Figure 4-9 Sample BA-4; mid shells
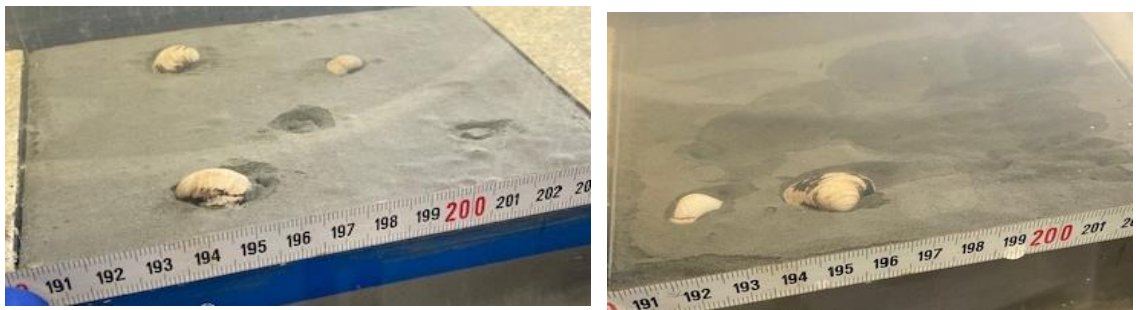

Figure 4-10 Sample BA-APP; low shells (left); mid shells (right)

Report Phase 1A-B

28 June 2022
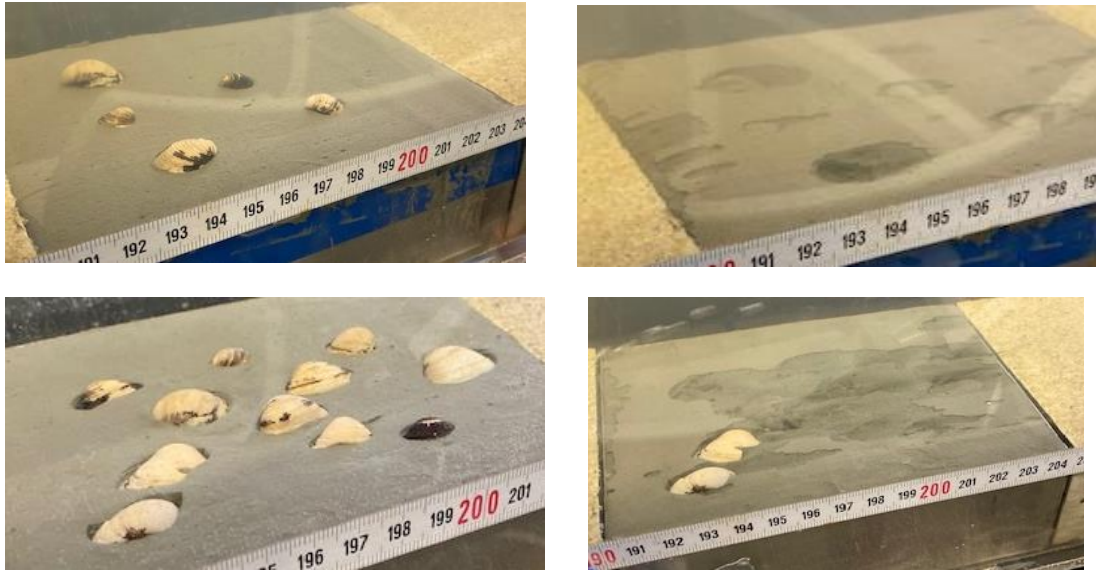
Figure 4-11 Sample BA-PU; low shells (upper); mid shells (lower)

#### 4.3.1.3 Summary of roughness induced erosion

The presence of shells and stones leads to somewhat lower critical flow velocities due to additional turbulence around the elements. In most cases the erosion is initiated around the individual parts or at the craters of displaced elements. Small shells and the pebbles are displaced at flow velocities of about 0.6 m/s and therefore the effects of the leftover craters are observed at higher flow velocities. The beds with a high percentage of shells or stones are armoured against erosion as long as the elements remain stable (i.e. around 0.6 m/s of flow velocity) and do not become dislodged. In terms of bed-shear stress values (Figure 4-12), the added roughness through shells or stones can lead to similar values (within 10% to 15%) of the critical bed-shear stress for the reference base samples from Phase 1A. Despite the lower critical flow velocity for erosion, the increase in roughness ($k_s$) leads to higher bed shear stress values that compensates for the lower critical flow velocity. Larger differences between the rougher and reference samples are observed for higher coverage (high stones representing armouring) and for mid/low shells in the mud-rich samples (see BA-PU sample).
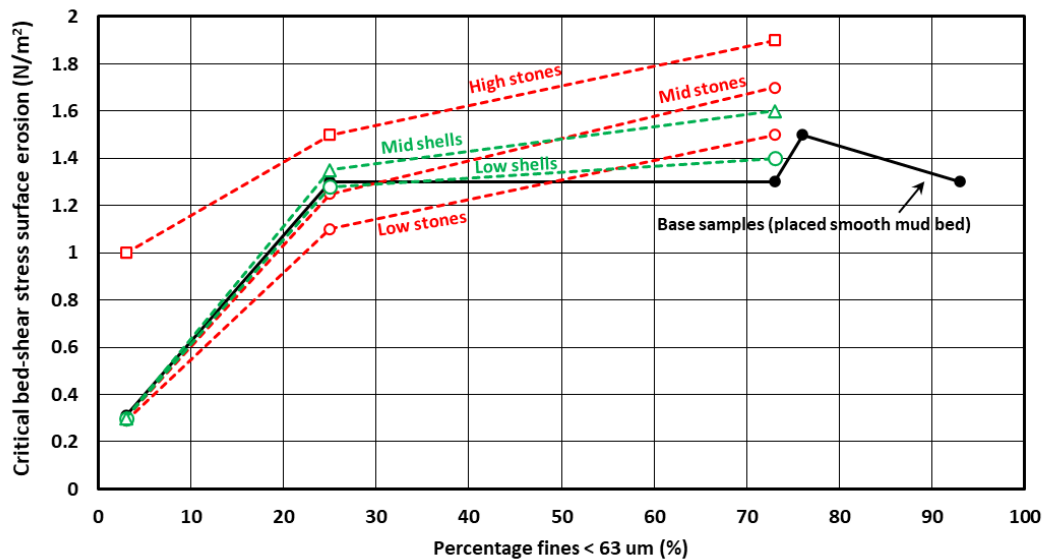


Figure 4-12.   Effect of stones and shells on critical bed-shear stress for surface erosion for five sandy and muddy samples from Western Scheldt (WS) and Noordpolderzijl (NPZ)

### 4.3.2 Type of sediment bed and depositional process

There is a clear effect of bed type (remoulded, deposited or field) on the critical depth-averaged flow velocity and the associated critical bed-shear stress for surface erosion. The freshly deposited beds result in layered beds with relatively lower bed densities in comparison with the remoulded and field beds. The top fluffy layer, in the order of 1-3 mm thick, is composed of low density mud (O-200 to 300 kg/m³ of dry density) and showed a clear interface contact with the firmer sublayer. The fluffy top eroded simultaneous as the loose layer was progressively pealed from the sample. In general, the deposited beds resulted in lower critical erosion values in comparison with the reference remoulded (placed) beds while the field samples show higher critical values for erosion (Figure 4-13). The dry density values, including the top fluffy layer, are also provided (see Table 4-1). Generally, the dry density of remoulded and field beds are in the range of 600 to 1400 kg/m$^3$, whereas the dry density of deposited beds is much lower, i.e. < 300 kg/m$^3$ for the mud-rich samples. Due to this layered behaviour of the deposits beds, the results here were further divided for the fluffy top layer and firmer sublayers. The large variation in density and compaction level helps to explain the clear differences in critical erosion values.

Sandy sample **Western Scheldt sample BA-4** ($p_{fines<63um}$ =3%)
- Remoulded (reference) bed (overall dry density 1370 kg/m$^3$); : $u_{cr,s}$=0.25-0.35 m/s ($k_s$=1 mm; $\tau_{cr,s}$=0.3 $\pm$ 0.1 N/m$^2$); incipient erosion;
- field bed (overall 1250 kg/m$^3$); $u_{cr,s}$=0.25-0.35 m/s ($k_s$=1 mm; $\tau_{cr,s}$=0.3 $\pm$ 0.1 N/m$^2$); first grain rolling to 40% of surface with rolling grains.

Mud-sand sample **Western Scheldt BA-APP** ($p_{fines<63um}$ =25%),(Figure 4-14 and Figure 4-15):
- Remoulded (reference) bed (overall dry density 1240 kg/m$^3$); $u_{cr,s}$=0.7-0.9 m/s ($k_s$=0.2 mm; $\tau_{cr,s}$=1.3 N/m$^2$; start of erosion
- deposited bed (fluffy top 580 kg/m$^3$; overall 990 kg/m$^3$);
  - fluffy top layer (0-3 mm) $u_{cr,s}$=0.2-0.3 m/s ($k_s$=0.5 mm; $\tau_{cr,s}$ =0.15 $\pm$ 0.05 N/m$^2$); 20% to 95% of top layer is eroded;
  - firmer sublayer (depth >3 mm): $u_{cr,s}$=0.45-0.65 m/s ($\tau_{cr,s}$ =0.75 $\pm$ 0.25 N/m$^2$);
- deposited bed on lift (fluffy top 270 kg/m$^3$; overall 1020 kg/m$^3$); $u_{cr,s}$=0.2-0.3 m/s ($k_s$=0.5 mm; $\tau_{cr,s}$=0.15 $\pm$ 0.05 N/m$^2$); after the top fluffy layer was eroded by the flow.
- field bed (overall dry density 1000 kg/m$^3$);
  - $u_{cr,s}$=0.3-0.4 m/s ($k_s$=1 mm; $\tau_{cr,s}$=0.4 $\pm$ 0.1 N/m$^2$) top layer removed;
  - $u_{cr,s}$=0.8-0.9 m/s ($k_s$=1 mm; $\tau_{cr,s}$=2 $\pm$ 0.3 N/m$^2$) starting groove erosion;

Muddy sample **Western Scheldt BA-PU** ($p_{fines<63um}$ =73%), (Figure 4-16 and Figure 4-17)
- Remoulded (reference) bed (overall dry density 650 kg/m$^3$); $u_{cr,s}$=0.7-0.9 m/s ($k_s$=0.2 mm; $\tau_{cr,s}$=1.3 $\pm$ 0.3 N/m$^2$); start of erosion
- deposited bed (fluffy top 250 kg/m$^3$; overall 550 kg/m$^3$);
  - fluffy top layer (0-3 mm) $u_{cr,s}$=0.2-0.3 m/s ($k_s$=0.5 mm; $\tau_{cr,s}$=0.15 $\pm$ 0.05 N/m$^2$); top layer is eroded;
  - firmer sublayer (depth >3 mm): $u_{cr,s}$=0.45-0.65 m/s ($\tau_{cr,s}$ =0.75 $\pm$ 0.25 N/m$^2$);
- field bed (>700 kg/m$^3$);
  - $u_{cr,s}$=0.3-0.5 m/s ($k$=1 mm; $\tau_{cr,s}$=0.5 $\pm$ 0.1 N/m$^2$) loose mud removed;
  - $u_{cr,s}$=0.6-0.85 m/s ($k$=1 mm; $\tau_{cr,s}$=1.5 $\pm$ 0.3 N/m$^2$) groove erosion;

Muddy sample **Noordpolderzijl B5** ($p_{fines<63um}$ =76%), (Figure 4-18)
- Remoulded (reference) bed (overall dry density 620 kg/m$^3$); $u_{cr,s}$=0.8-1 m/s ($k_s$=0.2 mm; $\tau_{cr,s}$=1.5 $\pm$ 0.3 N/m$^2$ start of erosion;
- deposited bed on lift (fluffy top < 300 kg/m$^3$; overall 455 kg/m$^3$);
  - fluffy top layer (0-3 mm) $u_{cr,s}$=0.2-0.35 m/s ($k_s$=0.5 mm; $\tau_{cr,s}$=0.2 $\pm$ 0.1 N/m$^2$); top layer is eroded;
  - firmer sublayer (depth >3 mm): $u_{cr,s}$=0.45-0.65 m/s ($\tau_{cr,s}$ =0.75 $\pm$ 0.25 N/m$^2$);

MUSA

Muddy sample **Western Scheldt PA1** ($p_{fines<63um}$ =96%), (Figure 4-19)

- Remoulded (reference) bed (overall dry density 560 kg/m$^3$); $u_{cr,s}$=0.7-0.9 m/s ($k_s$=0.2 mm; $\tau_{cr,s}$=1.3 $\pm$ 0.3 N/m$^2$; start of erosion
- deposited bed on lift (fluffy top 300 kg/m$^3$ overall 330 kg/m$^3$);
  - fluffy top layer (0-3 mm) $u_{cr,s}$=0.2-0.3 m/s ($k_s$=0.5 mm; 0.15 $\pm$ 0.05 N/m$^2$); start of erosion to erosion everywhere;
  - firmer sublayer (depth >3 mm): $u_{cr,s}$=0.45-0.65 m/s ($\tau_{cr,s}$ =0.75 $\pm$ 0.25 N/m$^2$).
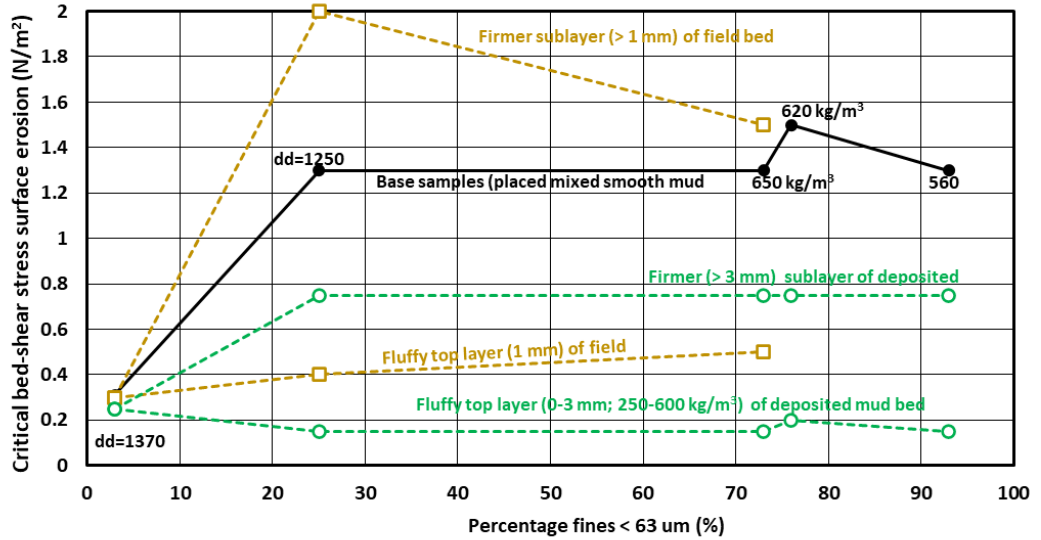


Figure 4-13. Effect of type of bed on critical bed-shear stress for surface erosion for five sandy and muddy samples from Western Scheldt (WS) and Noordpolderzijl (NPZ).
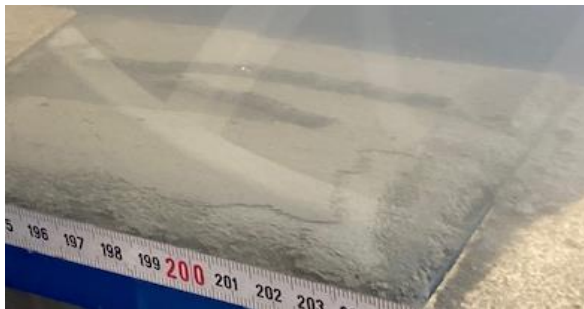


Figure 4-14 Sample BA-APP; deposited bed (left); deposited bed on lift (right)



Figure 4-15 Sample BA-APP; field bed
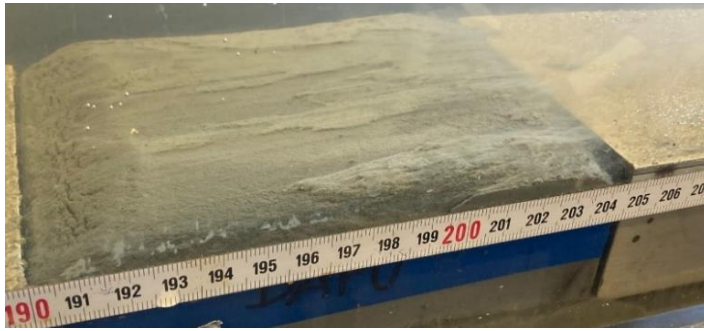
Figure 4-16 Sample BA-PU deposited bed
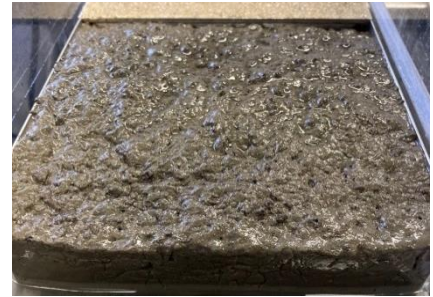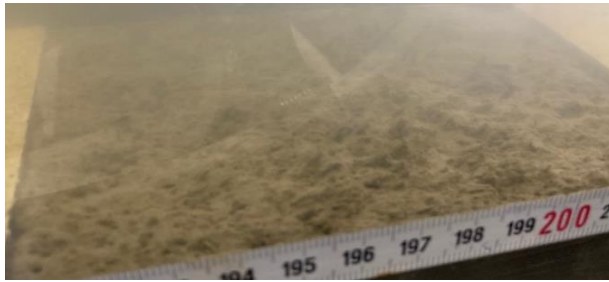


Figure 4-17 Sample BA-PU Field bed



Figure 4-18 Sample B5; Deposited bed on lift



Figure 4-19 Sample PA1; Deposited bed on lift

Report Phase 1A-B

01 March 2022

## 4.4 Conclusions

### 4.4.1 Critical bed-shear stress for surface erosion

The presence of the rough elements (i.e. shells and pebbles) generally led to lower critical flow velocities ($u_{crit}$) due to additional turbulence created around the elements. In most cases, the erosion initiated around the individual pebbles or shells or at the craters after their displacement. The pebbles and shells were displaced at flow velocities of about 0.5 to 0.6 m/s. The beds with a high percentage of coverage were armoured against erosion as long as the elements remained stable (i.e. flow < 0.5 m/s) and were not dislodged.

In terms of bed-shear stress values, the effect of rougher elements was negligibly small or slightly increased the critical bed shear stress for erosion. This is because the bed shear stress is also influenced by the roughness ($k_s$). Therefore, the reduction in the critical flow velocity is somehow compensated by the increase in roughness.

Low coverage of pebbles or shells showed a minor effect on the critical bed shear stress for erosion (mostly within 15%, i.e. near the experimental error range). Mid coverage, when the elements affect the overall sample roughness, showed minor effects for the sandy mud samples (BA-APP) but the effect was larger for the muddy BA-PU sample with a 20-25% increase in critical bed shear stress. For high pebble coverage, the armoured bed showed a higher critical shear stress for erosion compared to the reference samples. Here the stones are responsible for protecting (hiding) the sediment bed from the flow on top of the stones in a process called hiding and exposure.

There is a clear effect of bed type (remoulded, deposited or field) on the critical depth-averaged flow velocity and the associated critical bed-shear stress for surface erosion. The deposited beds including the fluffy layer eroded under lower critical shear stress than the reference remoulded samples, while the field beds required higher values to erode. The critical bed-shear stress of the fluffy top layer of a deposited bed is relatively low (0.15 to 0.2 $N/m^2$). The critical bed-shear stress of firmer sublayer just below the fluffy top (depth > 3 mm) is higher (0.75 $N/m^2$) but still lower than that of the remoulded bed. The critical bed-shear stress for erosion of the thin top layer of fields beds with loose particles and flocs is also lower (0.4 to 0.5 $N/m^2$). However, once this top layer is removed, the erosion of the firm sublayer requires a relatively high critical bed-shear stress, which is found to be higher (15% to 50%) than that of a remoulded bed. The variation in erodibility of the field bed samples probably stems from the level of consolidation and the effects of biota. The biota showed contrasting effects during the flume experiments. The biofilms and secretions act to stabilize and hold the bed (and sediment grains/flocs). On the other hand, tubes and structures helped to increase roughness and turbulence once part of the top layer started to erode. Therefore, the benthic biota acted both to stabilize and destabilize the bed in our experiments.

### 4.4.2 Erosion rates

Mass erosion rates of mud-sand samples from the phase 1B experiments are given in Table 4-1. The values are time-averaged values over short periods (100 to 200 s) in the case of a sudden mass erosion event, and over longer periods (> 1000 s) in the case of more gradual erosion.

The erosion values are in the range of 0.1 to 7 $g/m^2/s$ and give an indication of the mean erosion rate during conditions with surface erosion gradually increasing to mass erosion. The bed-shear stresses are mostly in the range of 1 to 3 $N/m^2$ ($2\pm1$ $N/m^2$). In nature, these values are representative for a period of 3 hours around peak flow of 1 m/s in a tidal channel. Assuming a smooth bed with Chézy-coefficient =70 $m^{0.5}/s$, the bed-shear stress is about 2 $N/m^2$. The total amount of eroded sediment mass during 3 hours of peak tidal flow is 3x3600x5=50,000 $gram/m^2$= 50 $kg/m^2$. Assuming a dry bulk density of 500 $kg/m^3$ at the top layer of the channel bed, the erosion layer thickness is of the order of 50/500=0.1 m. Based on this, we conclude that mass erosion rates in the range of 0.1 to 7 $g/m^2/s$ (as given in Table 4-1) are realistic values.

MUSA

Table 4-1: Critical bed-shear stress for surface and mass erosion of mud-sand samples from phase 1B (WS=Western Scheldt; NPZ= Noordpolderzijl).
1= dry density calculated from wet density; 2=fluffy top layer and sublayer; 3= results from phase 1A; 4= density of top fluffy layer and lower sublayer.

| Name | Bed type | Dry density (kg/m$^3$) | Roughness $K_s$ (mm) | $P_{fines}$ <63 | $P_{clay}$ <8 | silt/clay ratio (-) | $Vel_{crit}$ (cm/s) | $\tau_{cr,se}$ Flume (Pa) | $\tau_{cr,me}$ Flume (Pa) | Erosion rate (g/m²/s) and time (s) |
|---|---|---|---|---|---|---|---|---|---|---|
| WS PA1 | base sample[3] | 560 | 0.2 | 96 | 56 | 1.0 | 70-90 | 1.3 | 2.2 | - |
| | deposited + elevator | 325/300[4] | 0.5 | 96 | 56 | 1.0 | 25/60[2] | 0.15/0.75[2] | 1.1 | 2.1 (1620 s) |
| NPZ B5 | base sample | 620 | 0.2 | 76 | 35 | 1.4 | 80-100 | 1.5 | >3 | - |
| | deposited + elevator | 455 | 0.5 | 76 | 35 | 1.4 | 25/60[2] | 0.2/0.75[2] | 0.9 | 3.2 (1800 s) |
| WS BA4 | base sample[3] | 1370 | 1 | 3 | 0 | - | 25-35 | 0.3 | 1.4 | - |
| | mid stones | 1370 | 3 | 3 | 0 | - | 20-30 | 0.3 | 1.2 | 4 (1200 s) |
| | high stones | 1370 | 5 | 3 | 0 | - | 40-50 | 1.0 | 3.3 | 2.8 (60 s) |
| | mid shells | 1370 | 3 | 3 | 0 | - | 20-30 | 0.3 | 1.3 | 5.5 (900 s) |
| | field bed | 1250 | 1 | 3 | 0 | - | 25-35 | 0.3 | 0.8 | 2 (900 s) |
| WS BA-APP | base sample[3] | 1240 | 0.2 | 25 | 10 | 1.7 | 70-90 | 1.3 | 2.2 | 2.5 |
| | low stones | 1240 | 2 | 25 | 10 | 1.7 | 45-65 | 1.1 | 3.0 | 3 (205 s) |
| | mid stones | 1240 | 3 | 25 | 10 | 1.7 | 45-65 | 1.25 | 3.3 | 5.2 (320 s) |
| | high stones | 1240 | 5 | 25 | 10 | 1.7 | 50-60 | 1.5 | 3.3 | 4.6 (293 s) |
| | low shells | 1240 | 1 | 25 | 10 | 1.7 | 60-70 | 1.3 | 3.3 | 4.9 (165 s) |
| | mid shells | 1240 | 3 | 25 | 10 | 1.7 | 50-65 | 1.35 | 3.5 | 6.7 (184 s) |
| | deposited bed | 990/580[4] | 0.5 | 25 | 10 | 1.7 | 25/55[2] | 0.15/0.75[2] | 2.7 | - |
| | field bed | 1000* | 1 | 25 | 10 | 1.7 | 35/85[2] | 0.4/2.4[2] | - | - |
| | deposited + elevator | 1025/300[4] | 0.5 | 25 | 10 | 1.7 | 20-30 | 0.15 | 0.8 | 6.4 (2820 s) |
| WS BA-PU | base sample[3] | 650 | 0.2 | 73 | 37 | 1.2 | 70-90 | 1.3 | 2.0 | 0.7 |
| | low stones | 650 | 2 | 73 | 37 | 1.2 | 60-70 | 1.5 | - | 0.1 (900 s) |
| | mid stones | 650 | 3 | 73 | 37 | 1.2 | 60-70 | 1.7 | 3.5 | 5 (120 s) |
| | high stones | 650 | 5 | 73 | 37 | 1.2 | 55-70 | 1.9 | 3.8 | 2.7 (375 s) |
| | low shells | 650 | 1 | 73 | 37 | 1.2 | 60-75 | 1.4 | - | 0.2 (1080 s) |
| | mid shells | 650 | 3 | 73 | 37 | 1.2 | 55-70 | 1.6 | 4.0 | 3.6 (90 s) |
| | deposited bed | 550/240[4] | 0.5 | 73 | 37 | 1.2 | 25/60[2] | 0.15/0.75[2] | 0.6 | 3.6 (1500 s) |
| | field bed | 650 | 1 | 73 | 37 | 1.2 | 40/75[2] | 0.5/1.5[2] | 2.5 | - |

MUSA

# 5    References

Bosch, B. (2016). The effect of initial concentration on the consolidation behaviour of mud: A study on lake Markermeer sediment. MSc Thesis, TU Delft: Delft, the Netherlands

Deltares, 1991. Erosion of natural sediments. Report Z161-35/37. Delft, The Netherlands (see Table 11.2 in: Van Rijn, 1993)

Gyamera, E. A., Kuma, J. S. and Okae-Anti, D., 2014. Classification of Soils and Their Plasticity Index of the University of Cape Coast Research Station at Twifo Wamaso. International Journal of Soil and Crop Sciences, Vol. 2(1),25-32

Manning, A.J., Whitehouse, R.J.S. and Uncles, R.J. (2017). Suspended particulate matter: the measurements of flocs. In: R.J. Uncles and S. Mitchell (Eds), ECSA practical handbooks on survey and analysis methods: Estuarine and coastal hydrography and sedimentology, Chapter 8, pp. 211-260, Pub. Cambridge University Press, DOI: 10.1017/9781139644426, ISBN 978-1-107-04098-4

McAnally, W.H. et al., 2007. Management of fluid mud in estuaries, bays and lakes. I: Present state of understanding on character and behaviour. Journal of Hydraulic Engineering 133, 9-22

Perk, L. and Van Rijn, L.C., 2020. Measurement plan. TKI MUSA project. Report 11204950_TKI-MUSA_R2r1.

Seifert, A. and Kopf., A., 2010. Rheological characteristic of natural mud and the influence of different parameter. Marum - Center for Marine Environmental Sciences, University of Bremen, Germany

Skempton, A.W., 1953. The colloidal activity of clays. Proc. Int. Conf on Soil Mechanics and Foundation Engineering (ICOSOMEF), Zurich, Switzerland, 57-61

Soulsby, R. & Clarke, S. (2005). Bed Shear-stresses Under Combined Waves and Currents on Smooth and Rough Beds. HR Wallingford Ltd.

Van Ledden, M. 2003 Sand-mud segregation in estuaries and tidal basins. PhD Thesis, TU Delft: Delft, the Netherlands.

Van Rijn, L., Walstra, D. R., Ormondt, M. 2007 Unified view of sediment transport by currents and waves: IV Application of morphodynamic model. Journal of Hydraulic Engineering, ASCE. 133(7) DOI: 10.1061/(ASCE)0733-9429(2007)133:7(776).

Van Rijn, L.C. and Barth, R., 2018. Settling and consolidation of soft mud-sand layers. Journal of Waterway, Port, Coastal and Ocean Engineering, ASCE. Doi: 10.1061/(ASCE)WWW.1943-5460.0000483

Van Rijn, L.C., 2018. Erodibility of mud-sand mixtures. Report www.leovanrijn-sediment.com

Van Rijn, L.C. 2020. Erodibility of mud-sand bed mixtures. Journal of Hydraulic Engineering, Vol. 146, No. 1, ASCE. Doi: 10.1061/(ASCE)HY.1943-7900.0001677

Van Rijn, L.C., Colina Alonso, A. and Manning, A. J., 2020. Literature review on sand and mud. TKI MUSA project. Report 11204950-001-ZKS-0002

Van Rijn, L.C. and Koudstaal, K.R., 2021. Literature review; Measuring and interpretation of settling velocity and particle size. TKI-MUSA report, Deltares, Delft, The Netherlands

Waterproof, 2019a. Metingen Holwerd-Ameland; meetresultaten en laboratoriumanalyse januari-maart 2019. Rapport WP2019.1155 (in Dutch).

Waterproof, 2019b. Metingen Holwerd-Ameland; meetresultaten en laboratoriumanalyse september-oktober 2019. Rapport WP2019.1176 (in Dutch).

Wentworth, C. K. (1922). "A Scale of Grade and Class Terms for Clastic Sediments". The Journal of Geology. 30 (5): 377–392. DOI:10.1086/622910

Wurpts, R., 2005. 15 Years experience with fluid mud definition of the nautical bottom with rheological parameters. Terra et Aqua, No. 99.

Wurpts, R and Greiser, N., 2005. Monitoring and dredging technology in muddy layers. Chinese-German joint symposium on hydraulic and ocean engineering, Darmstadt, Germany

# 6 Appendix A: Sampling locations & impression

## 6.1 Noordpolderzijl



*Figure 6-1: Sampling location Noordpolderzijl*
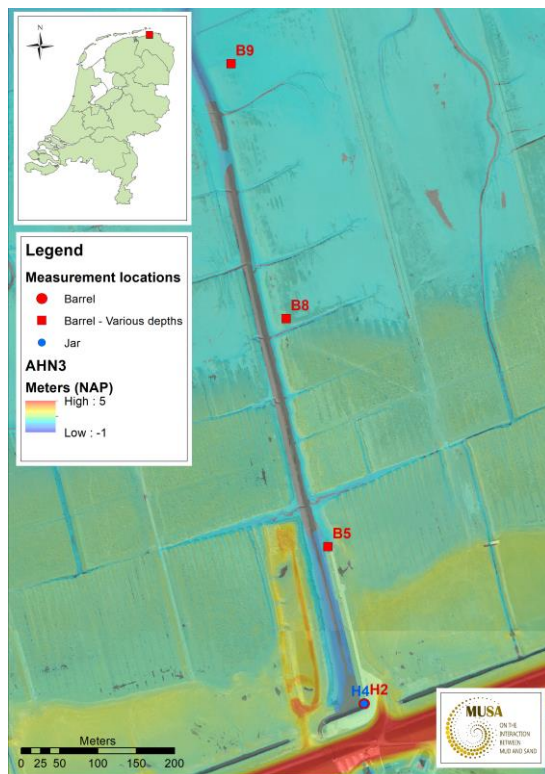


*Figure 6-2: Sampling location Noordpolderzijl (detail)*

*Figure 6-3: Impression of sampling / situation at Noordpolderzijl*

Report Phase 1A-B

01 March 2022

## 6.2 Western Scheldt; Hulst
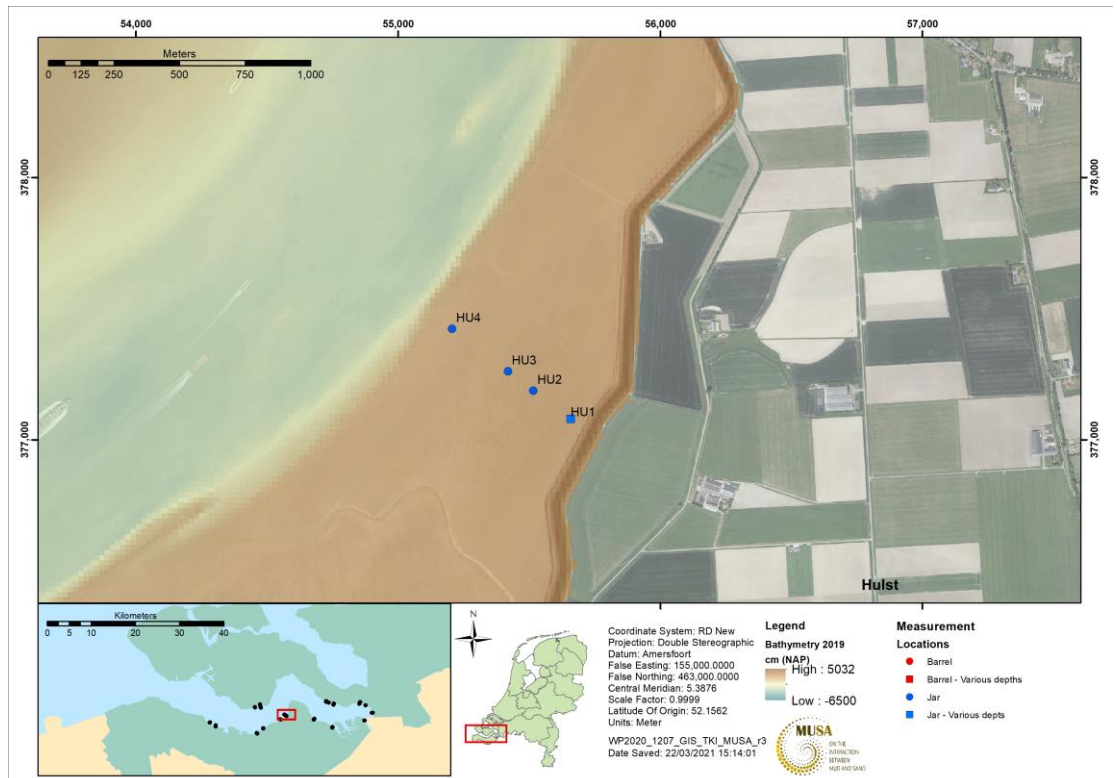


Figure 6-4: Sampling locations Hulst, Western Scheldt



Figure 6-5: Impression of sampling location HU1



Figure 6-6: Impression of sampling location HU2, HU3 and HU4

Report Phase 1A-B

01 March 2022

## 6.3    Western Scheldt; Baalhoek
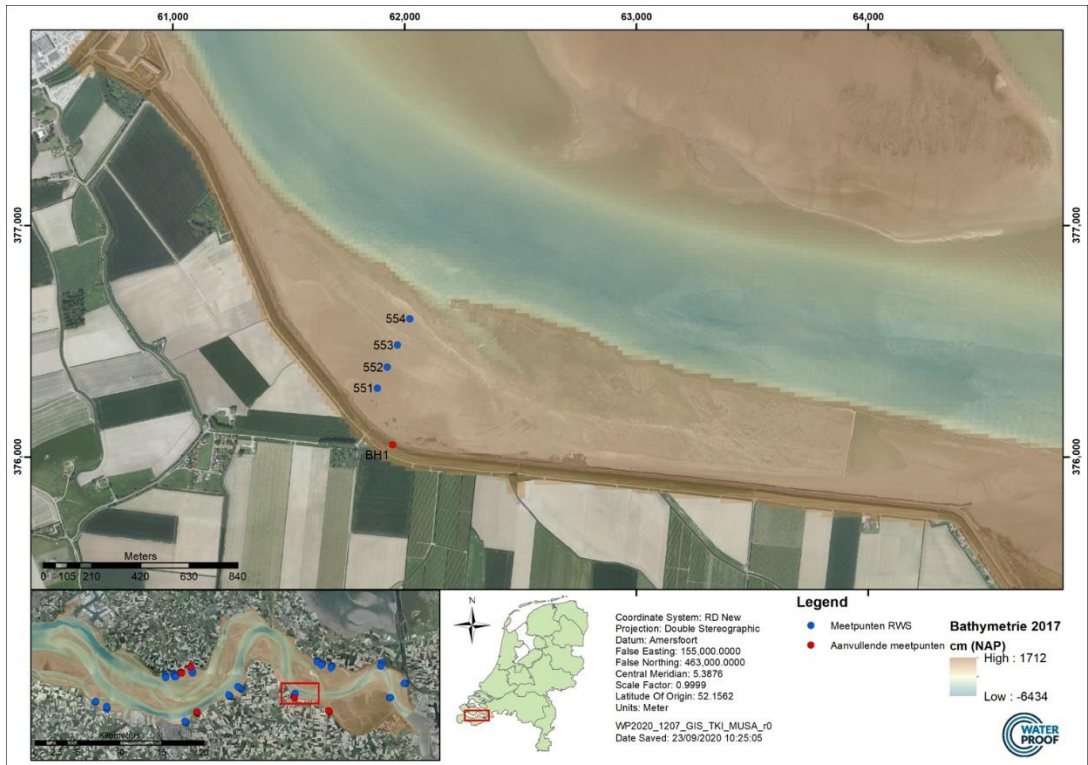


*Figure 6-7: Sample locations at Baalhoek*



*Figure 6-8: Mud sampling at location BH1*

Report Phase 1A-B

01 March 2022

## 6.4 Western Scheldt; Saeftinghe
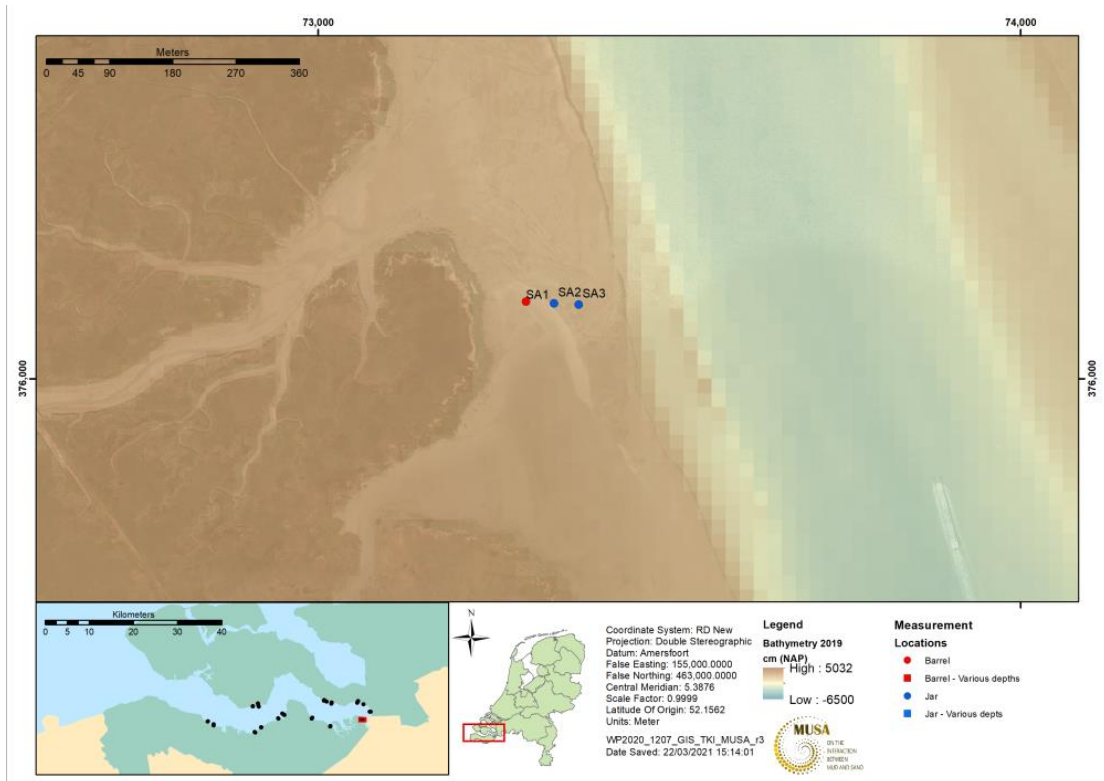


*Figure 6-9: Sample locations at Saeftinghe*
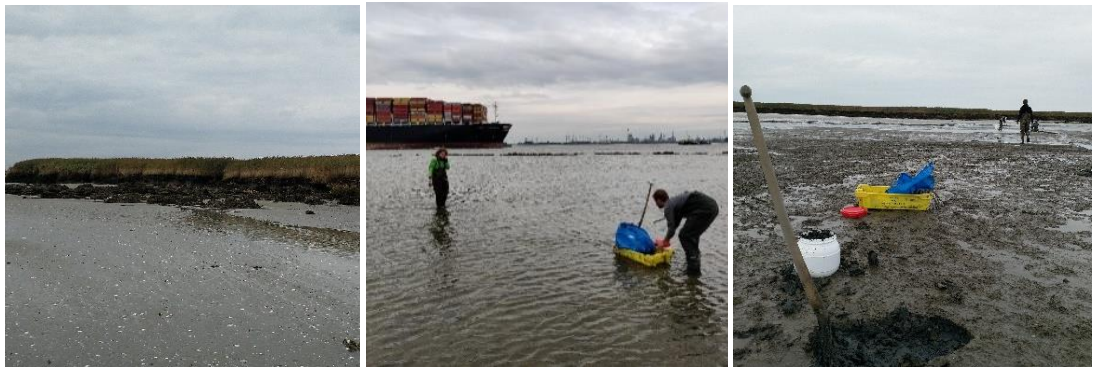


*Figure 6-10: Sampling at Saeftinghe*

Report Phase 1A-B

01 March 2022

## 6.5 Western Scheldt; Harbour De Paal
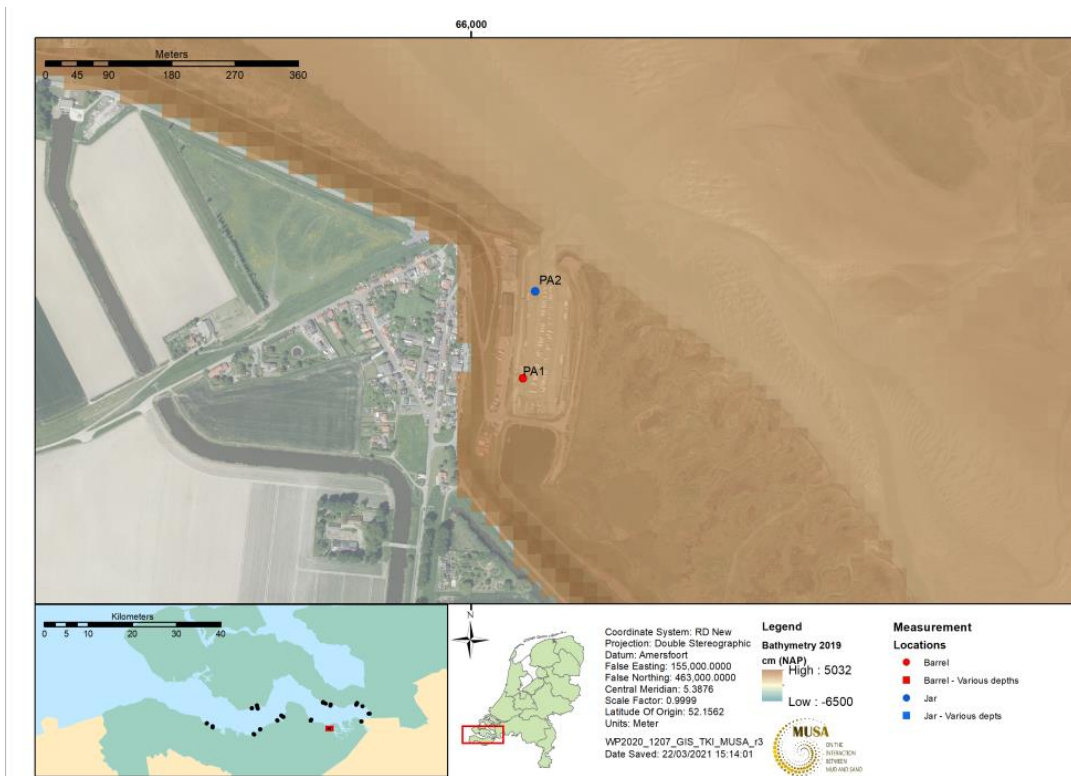


*Figure 6-11: Sample locations at Harbour De Paal*



*Figure 6-12: Sampling at harbour De Paal, sample PA1*

Report Phase 1A-B

01 March 2022

## 6.6     Western Scheldt; Zwemersdam & Baarland
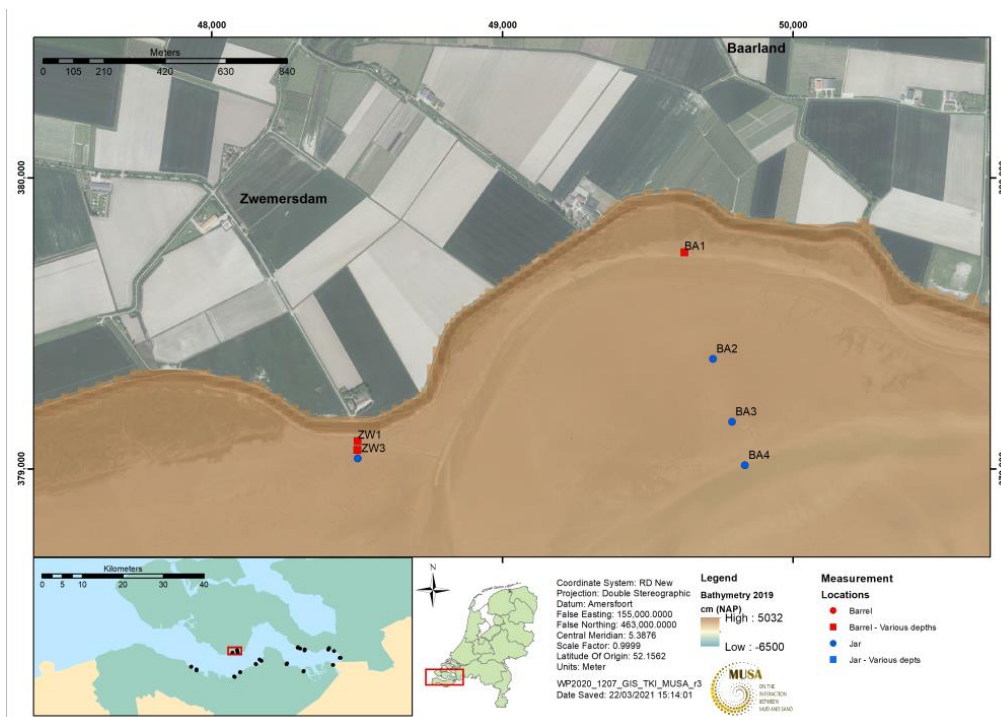


Figure 6-13: Sample locations at Zwemersdam & Baarland



Figure 6-14: Sampling at Baarland (BA1)



Figure 6-15: Sampling at Zweemerdam (ZW3)

## 6.7 Western Scheldt; Paulina Polder
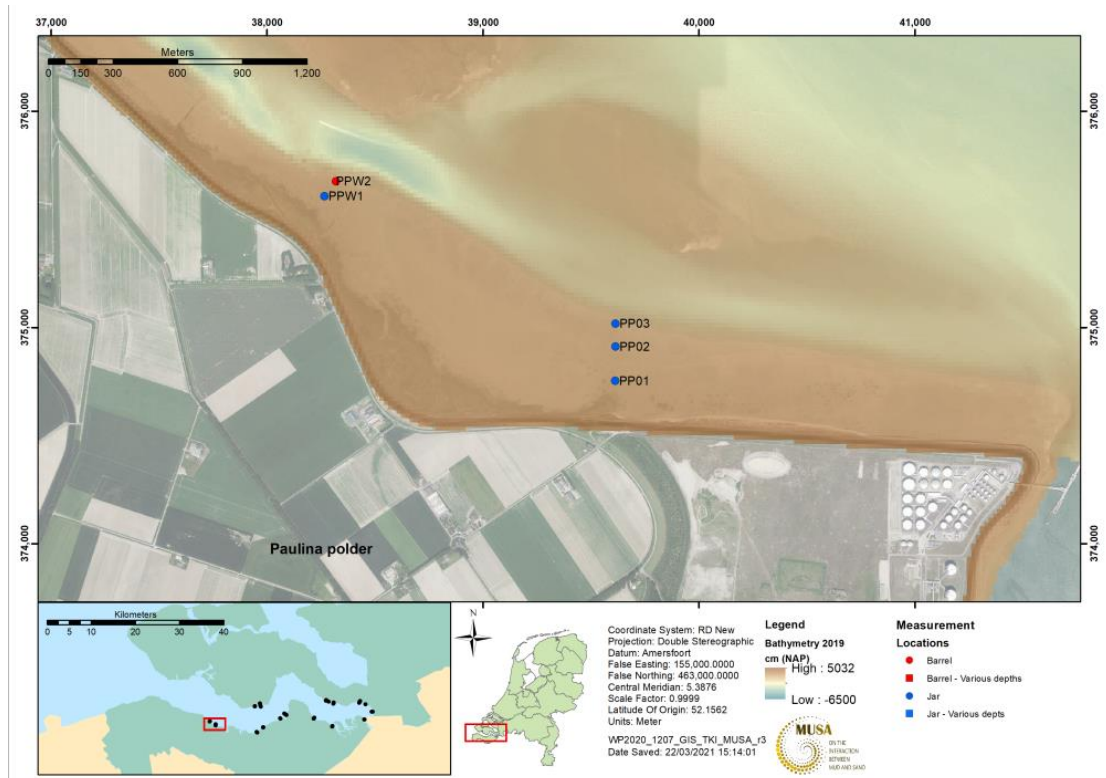


*Figure 6-16: Sample locations at Paulina Polder*



*Figure 6-17: Sampling at Paulina Polder PPO1 (left) and PPW2 (right)*

## 6.8    Western Scheldt; Terneuzen
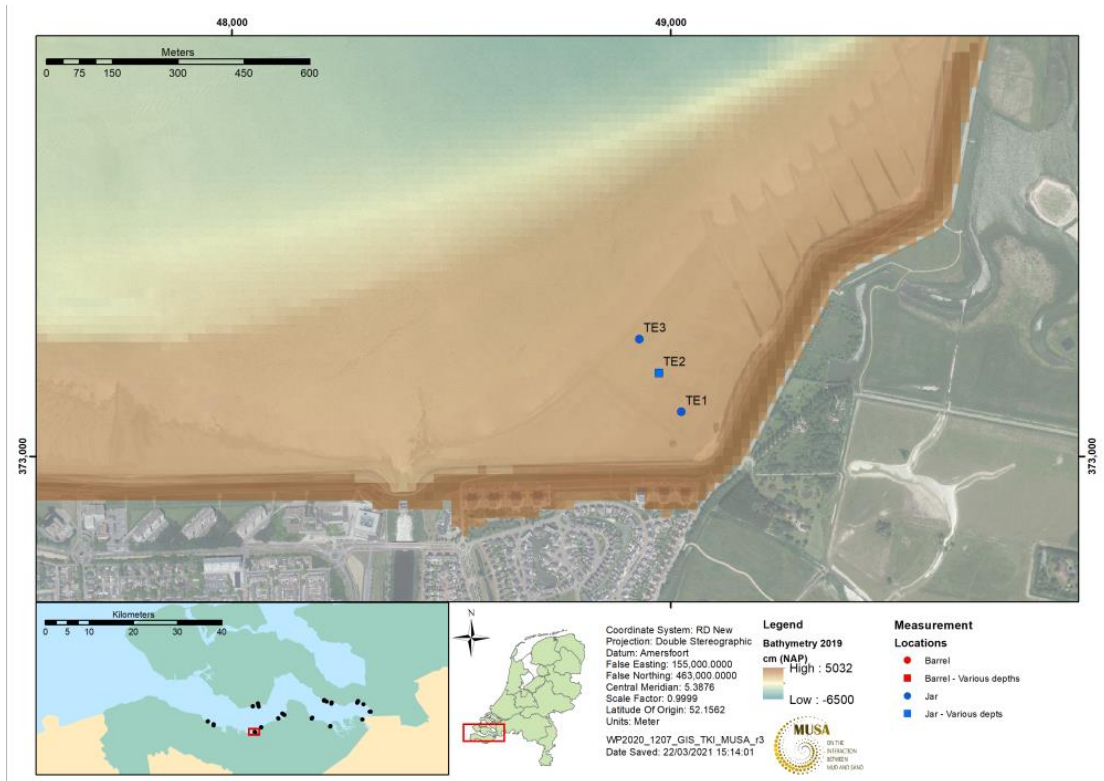


*Figure 6-18: Sample locations at Terneuzen*



*Figure 6-19: Sampling at Terneuzen, location TE2*

## 6.9 Western Scheldt; Hulst-west
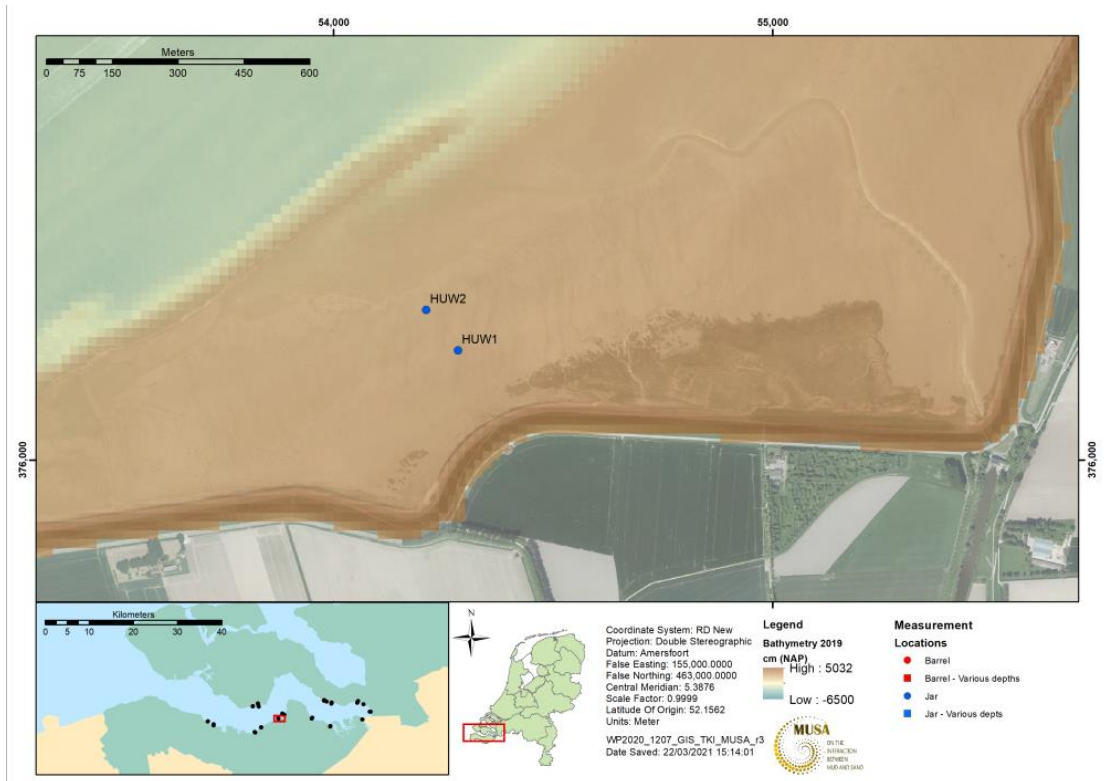


Figure 6-20: Sample locations at Hulst-west



Figure 6-21: Sampling at Hulst West, location HUW2

Report Phase 1A-B

01 March 2022

## 6.10    Western Scheldt; Harbour Griete
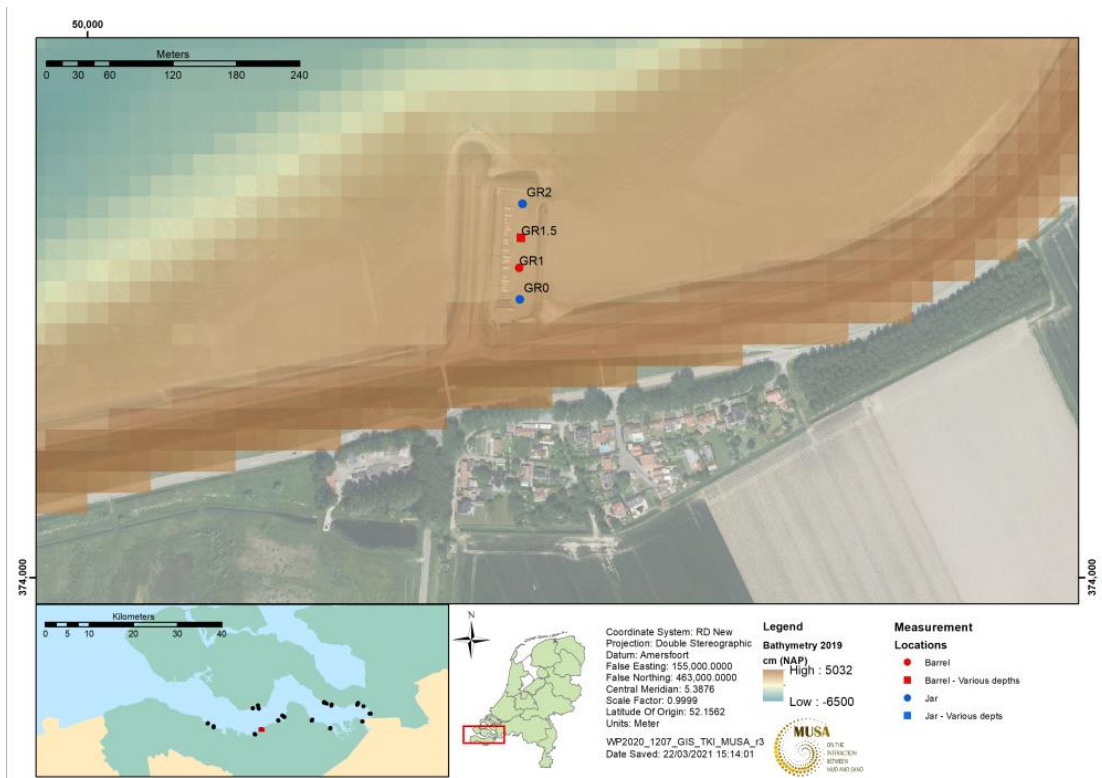


*Figure 6-22: Sample locations at harbour Griete*
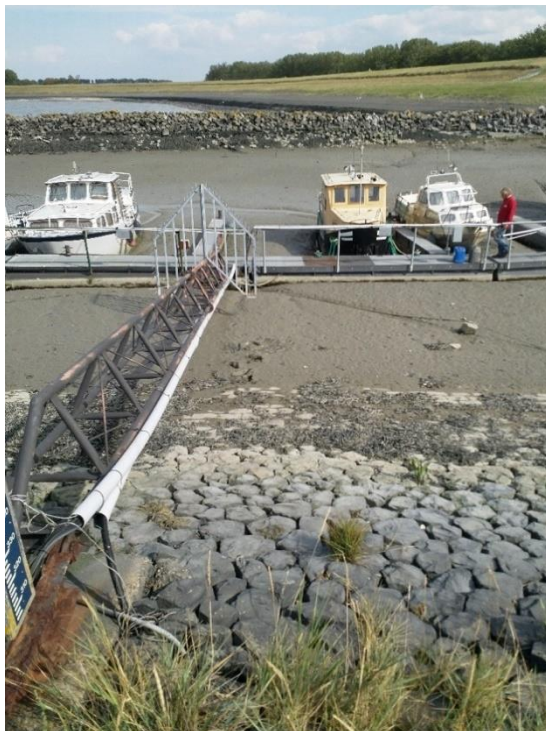


*Figure 6-23: Sampling at harbour Griete (GR 1.5)*

Report Phase 1A-B

01 March 2022

## 6.11 Western Scheldt; Waarde
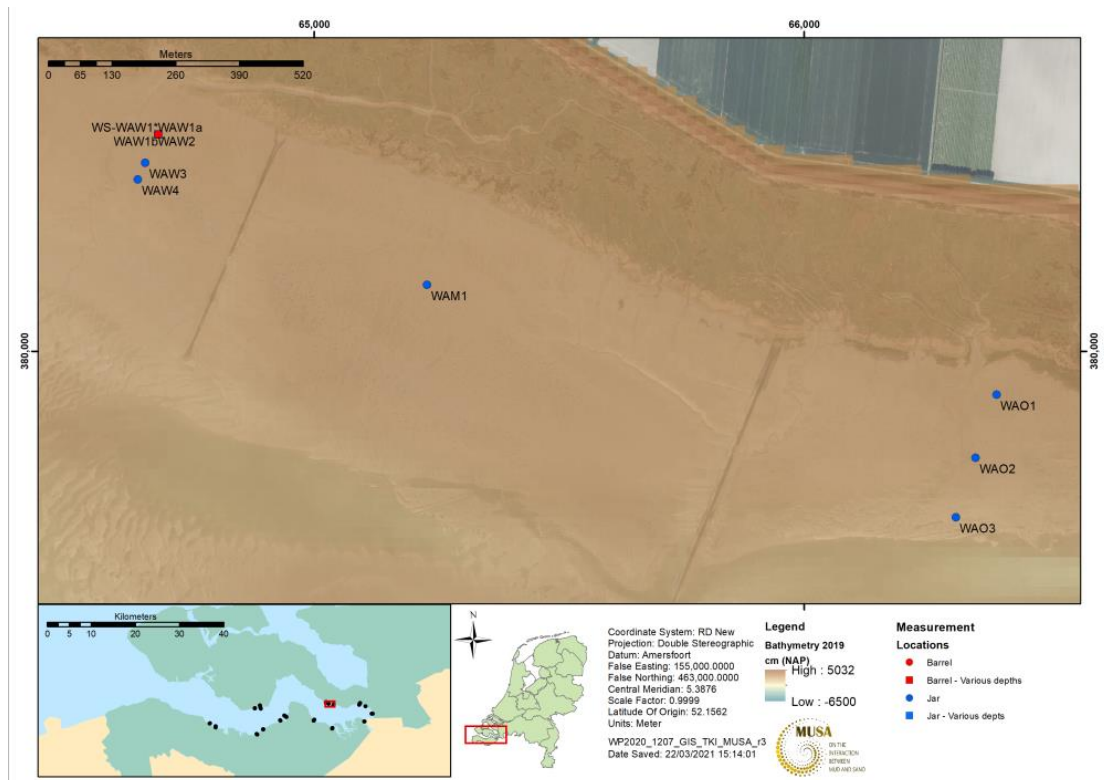


Figure 6-24: Sample locations at Waarde



Figure 6-25: Overview of landscape at Waarde-west



Figure 6-26: Mud bank between tidal flat and higher overgrown land at Waarde-Oost

Report Phase 1A-B

01 March 2022

## 6.12    Western Scheldt; Bath
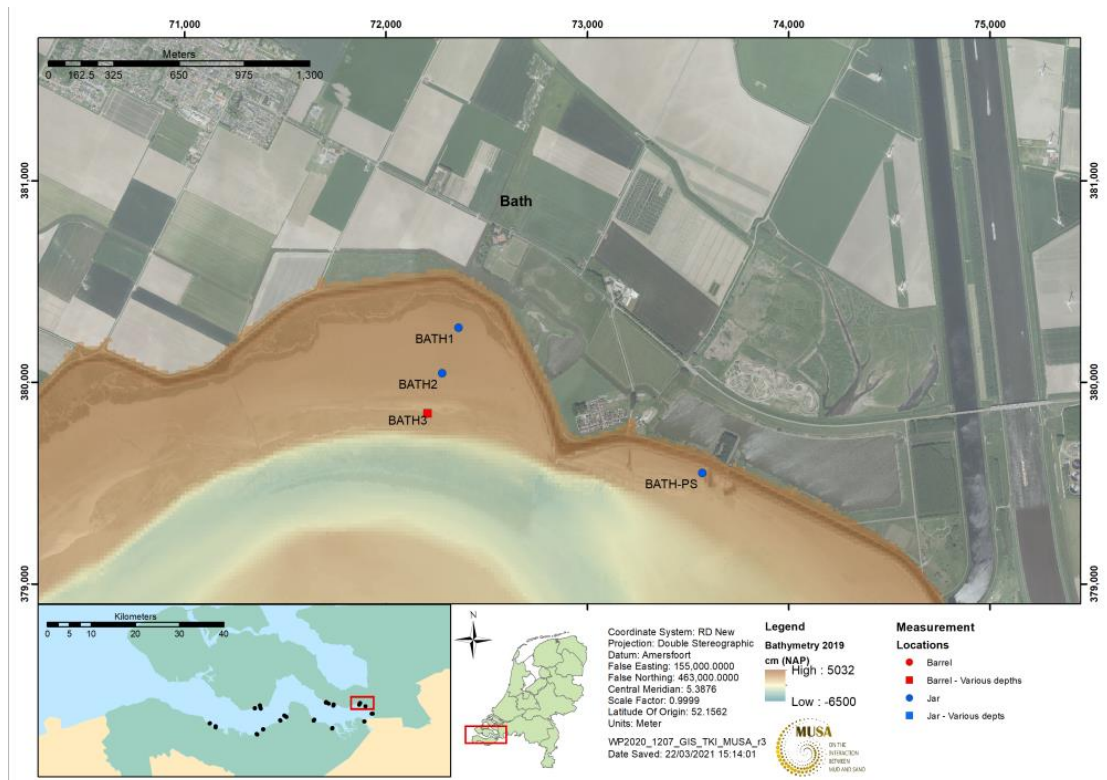


*Figure 6-27: Sample locations at Bath*



*Figure 6-28: Pit made at location BATH3, where soft grey mud with a brown top layer overlays a peat layer, located at 0.20 m below the surface*

Figure 6-29: Sampling at pumping station BATH-PS. Very sandy intertidal flat near outlet pumping station (upper panel) and surface of firm muddy sand with soft upper layer of 10 to 20 mm (lower panel).

Report Phase 1A-B

01 March 2022

## 6.13    Western Scheldt; Appelzak
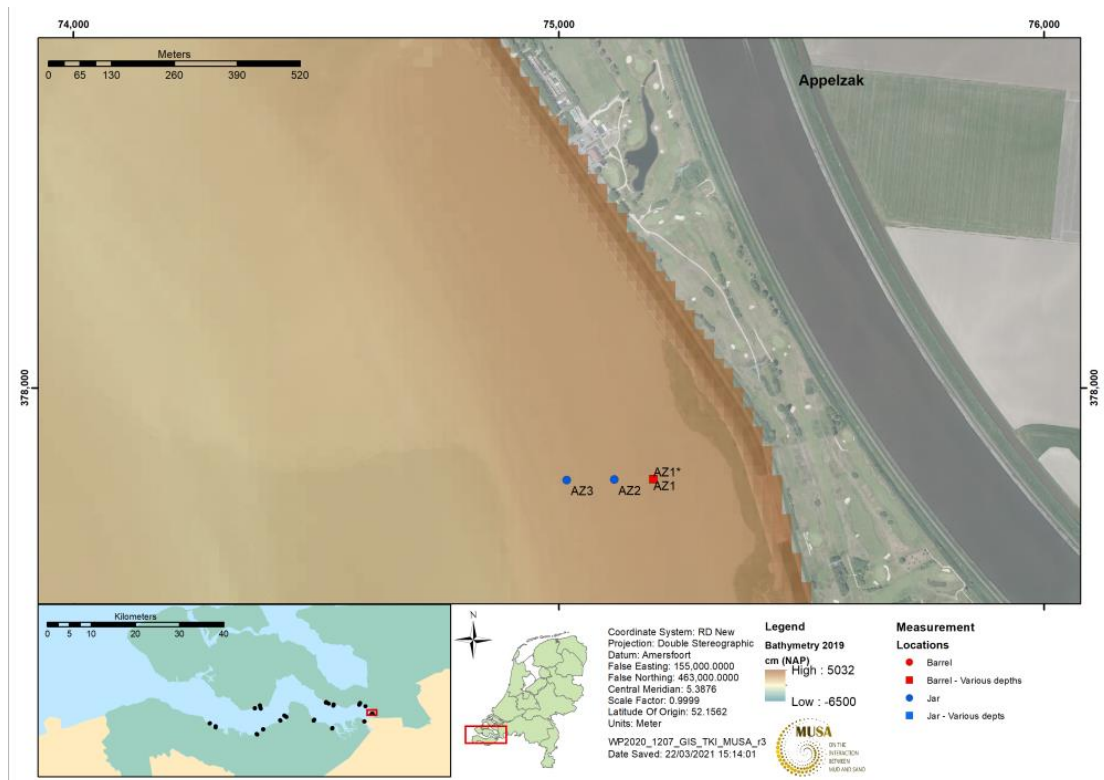


Figure 6-30: Sample locations at Appelzak



Figure 6-31: Mud sampling location AZ1, reed on the edge of the mudflat

## 6.14    Scheldt estuary
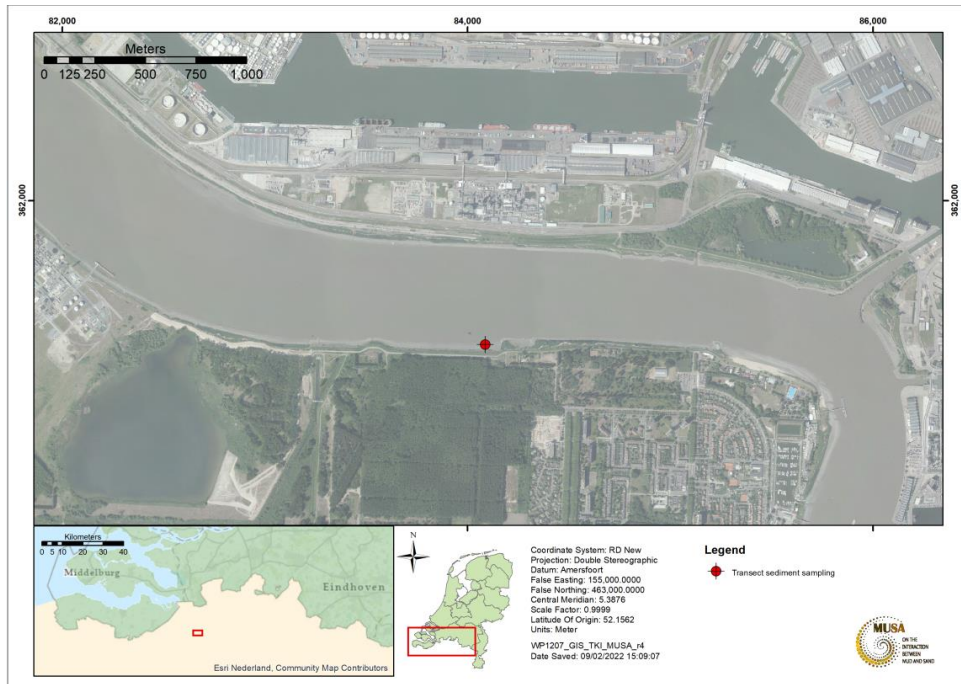


*Figure 6-32: Sampling location Oosterweel near Antwerp. Loc 1: At the low water level line; Loc 2: Low water level line +8 m towards the shore; Loc 3: Low water level line +24 m towards the shore*

Report Phase 1A-B

01 March 2022

## 6.15    Plym (UK)
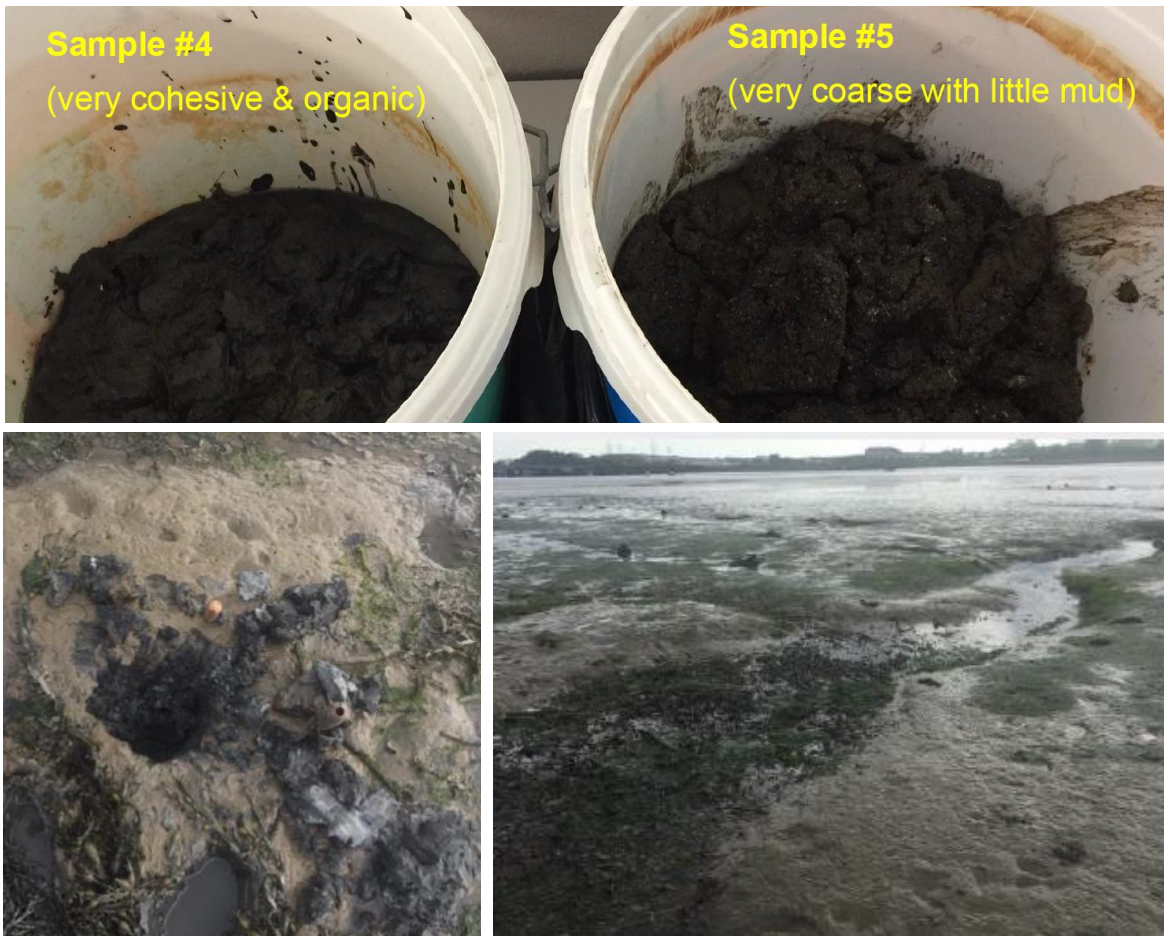


*Figure 6-33: Sampling location at Plymouth (UK). Courtesy from Prof. Manning.*

# 7 Appendix B: Consolidation experiment results

## 7.1 Consolidation experiment on base mud H2
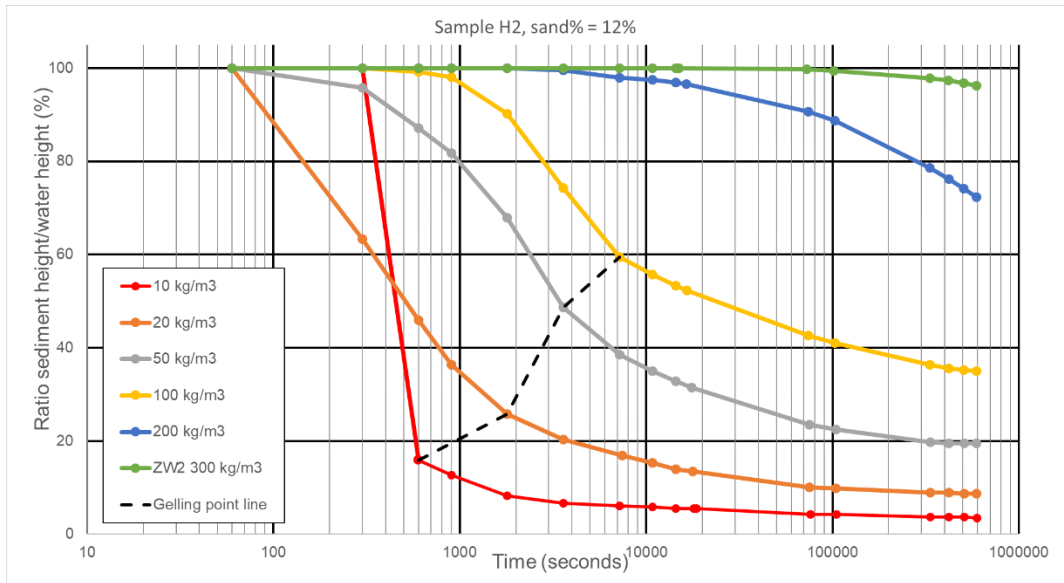


*Figure 7-1: Settling height as function of time based on consolidation test for H2; initial dry density of 10 to 300 kg/m3; dashed line as contraction points*
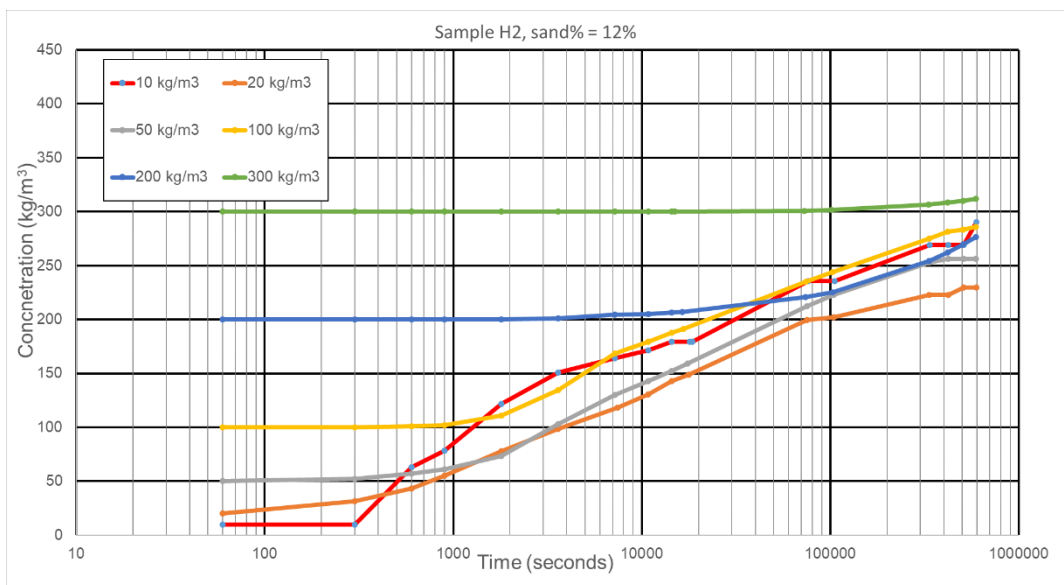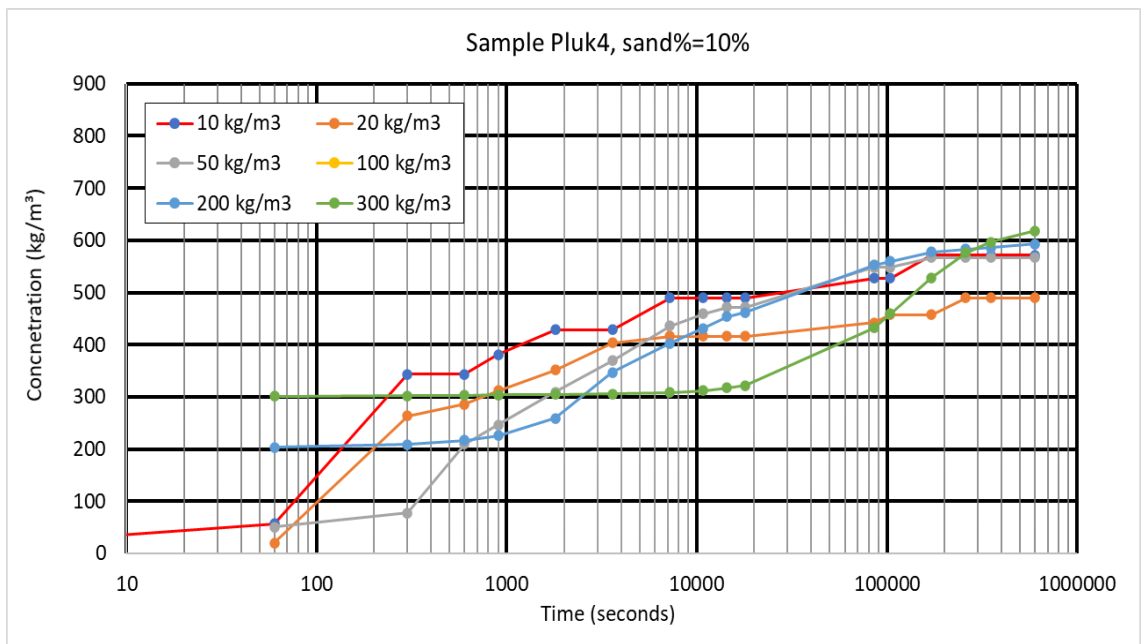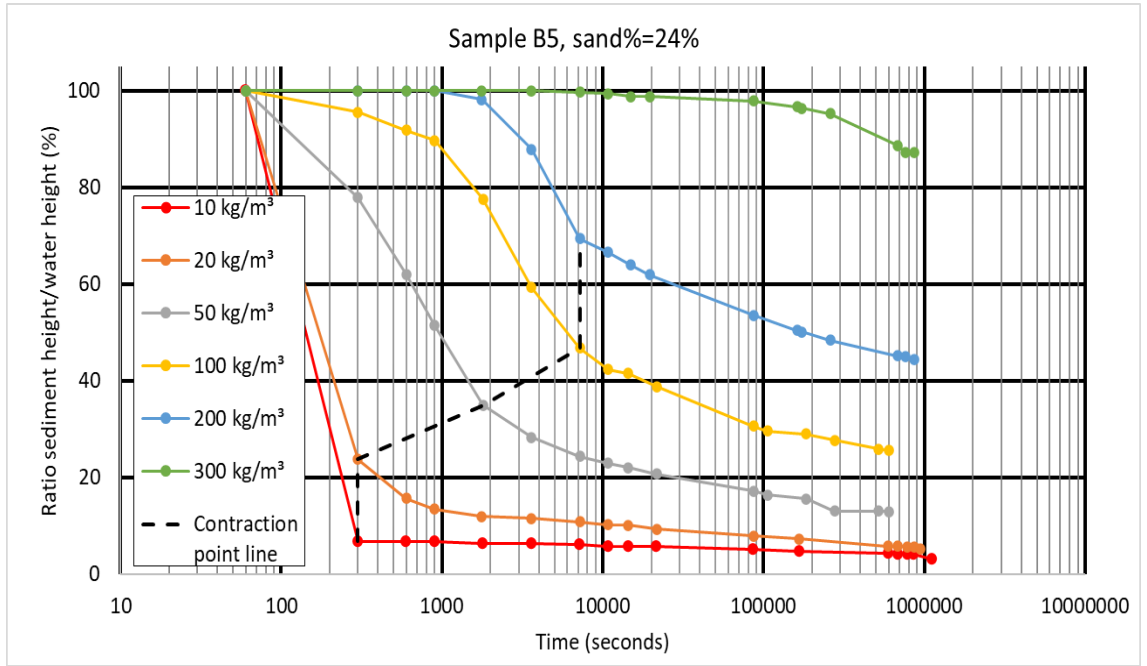


*Figure 7-2: Dry mud density as function of time based on consolidation test for H2; initial dry density of 10 to 300 kg/m3*

## 7.2 Consolidation experiment on base mud GR1
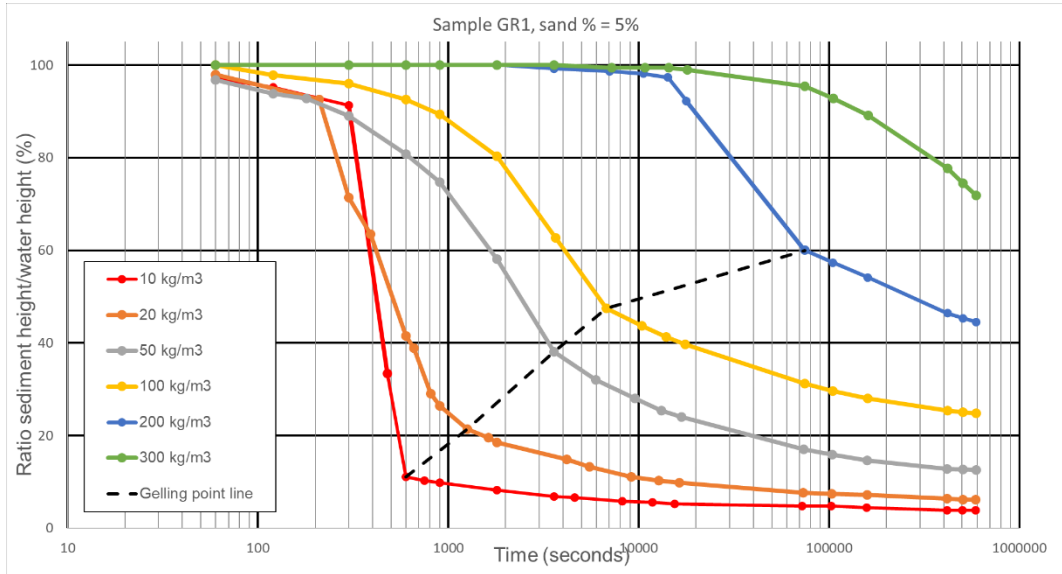


*Figure 7-3: Settling height as function of time based on consolidation test for GR1; initial dry density of 10 to 300 kg/m3; dashed line as contraction points*
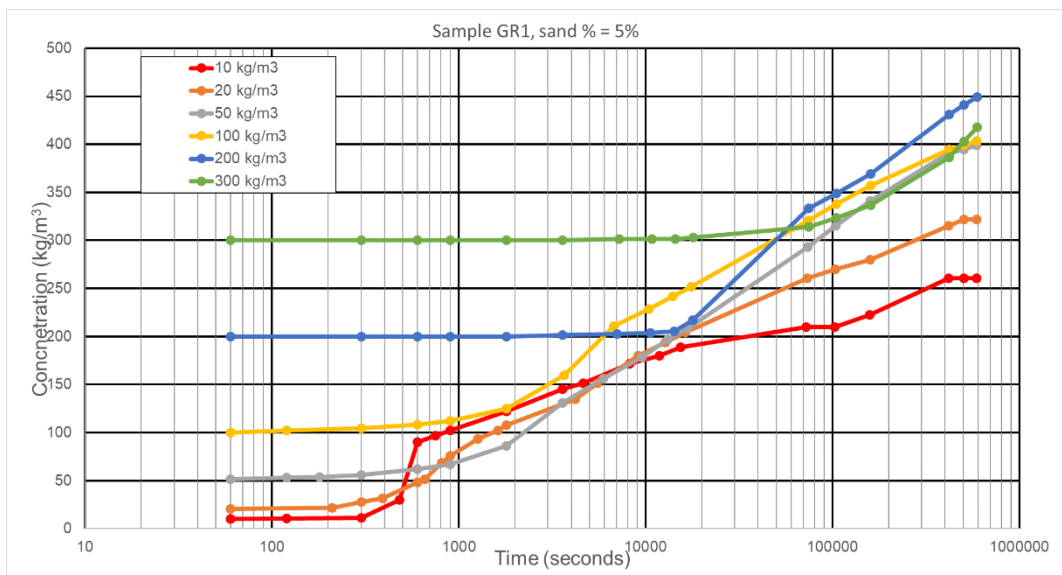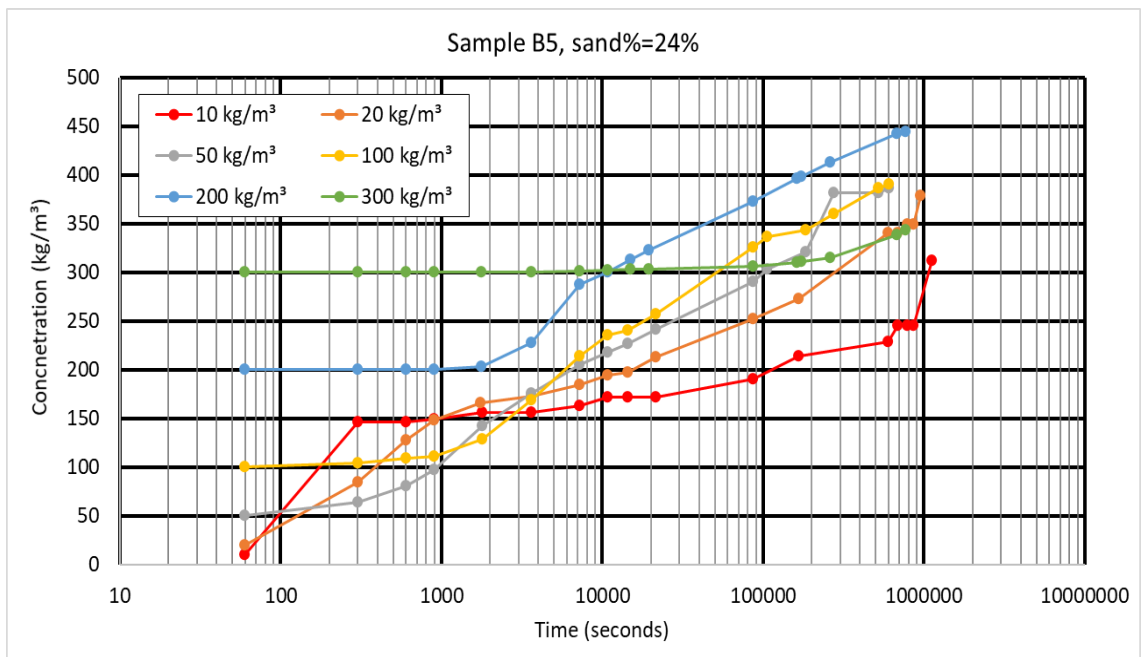


*Figure 7-4: Dry mud density as function of time based on consolidation test for GR1; initial dry density of 10 to 300 kg/m3*
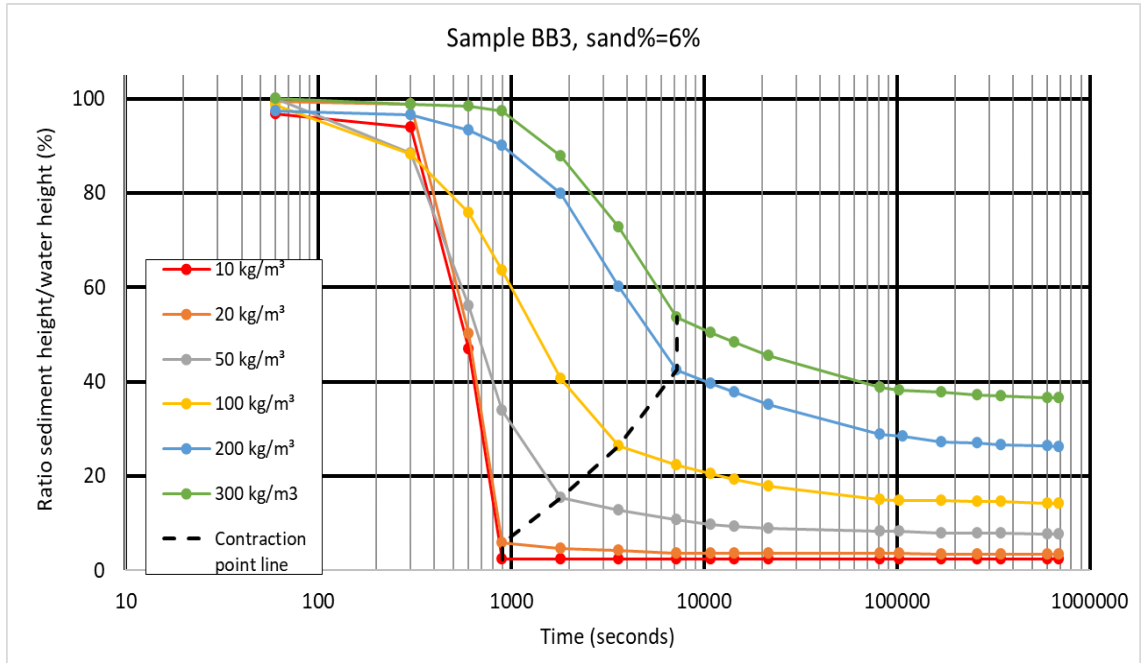
## 7.3  Consolidation experiment on base mud ZW2
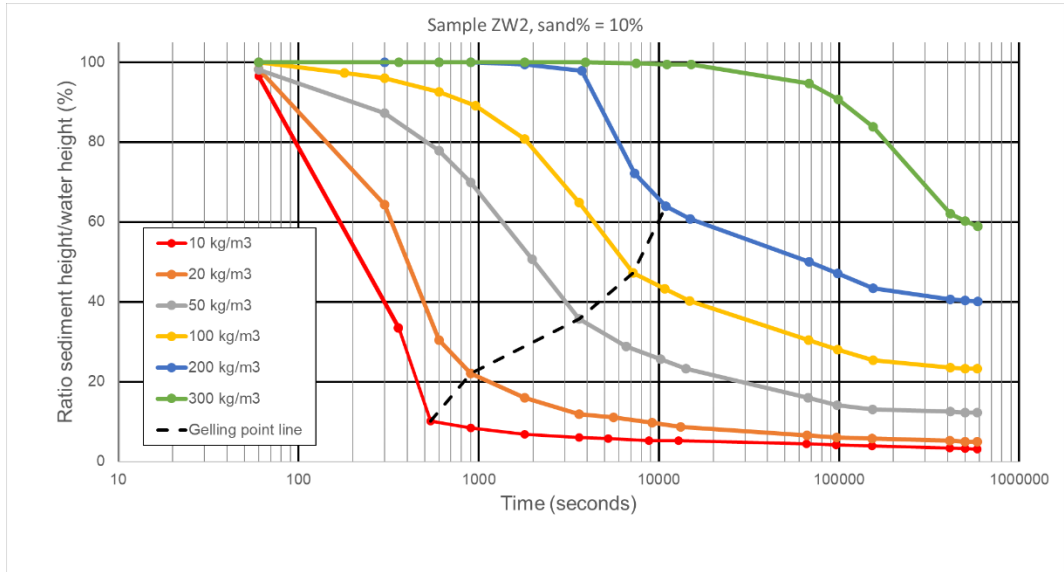


*Figure 7-5: Settling height as function of time based on consolidation test for ZW2; initial dry density of 10 to 300 kg/m3; dashed line as contraction points*
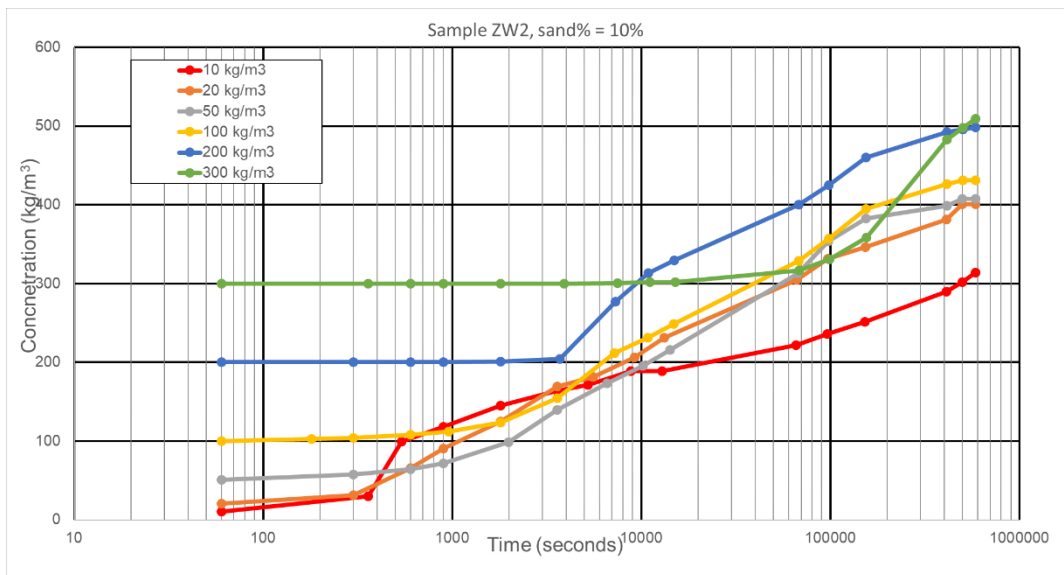


*Figure 7-6: Dry mud density as function of time based on consolidation test for ZW2; initial dry density of 10 to 300 kg/m3*

## 7.4    Consolidation experiment on base mud WAW1
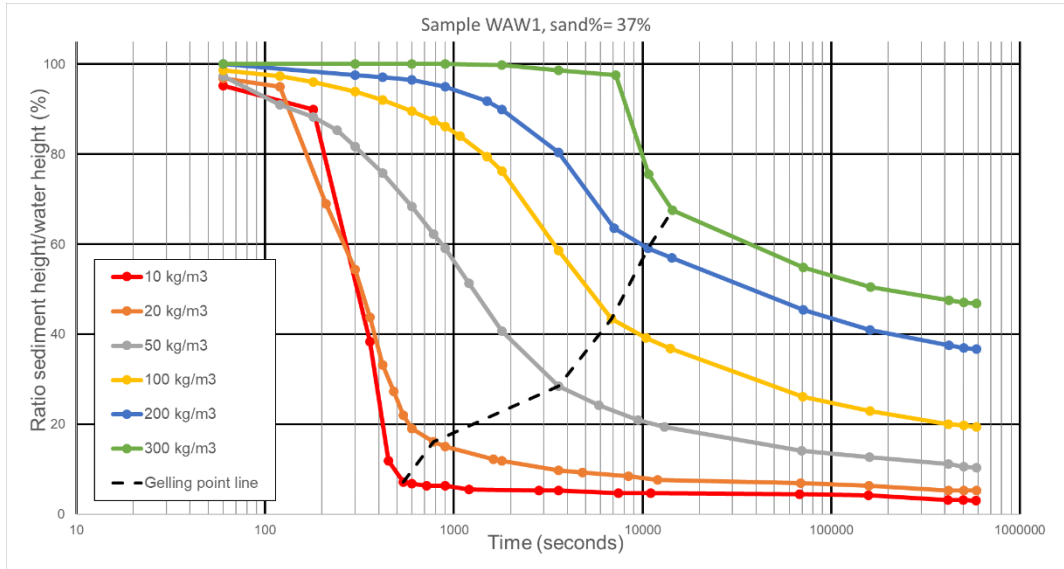


*Figure 7-7: Settling height as function of time based on consolidation test for WAW1; initial dry density of 10 to 300 kg/m3; dashed line as contraction points*
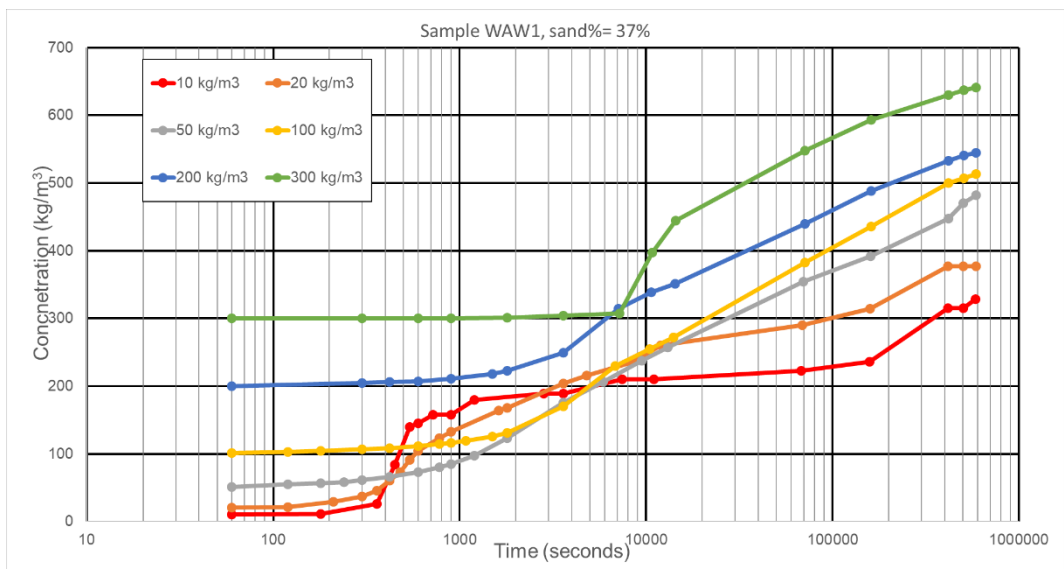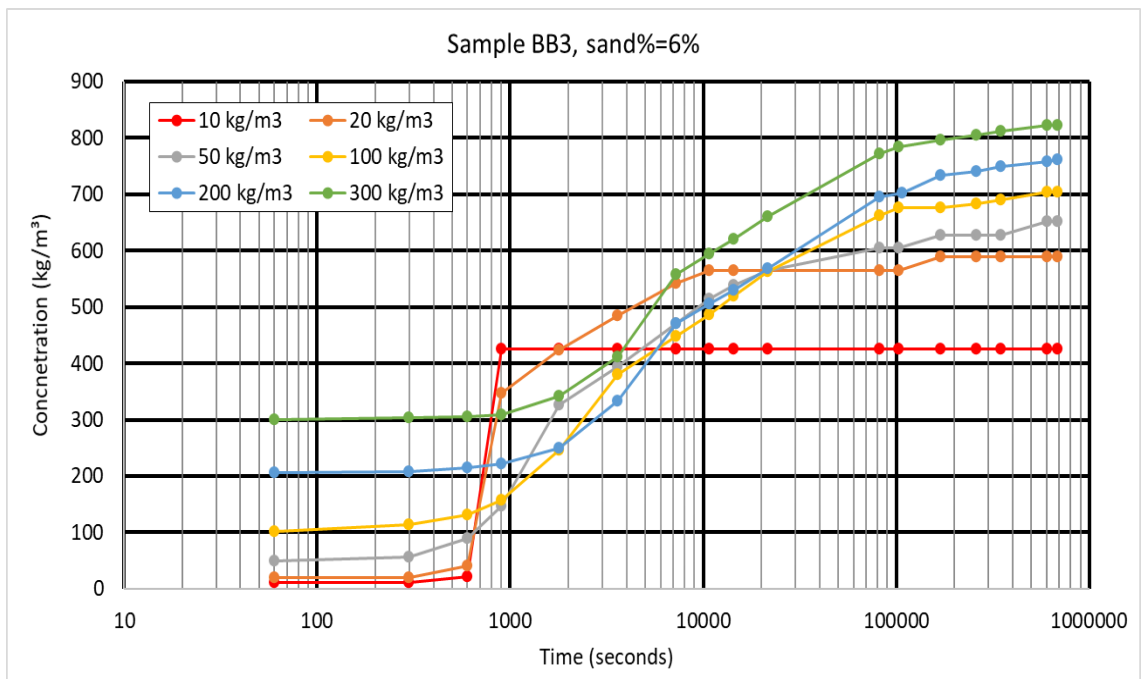


*Figure 7-8: Dry mud density as function of time based on consolidation test for WAW1; initial dry density of 10 to 300 kg/m3*

Report Phase 1A-B

01 March 2022

## 7.5      Consolidation experiment on base mud BH1
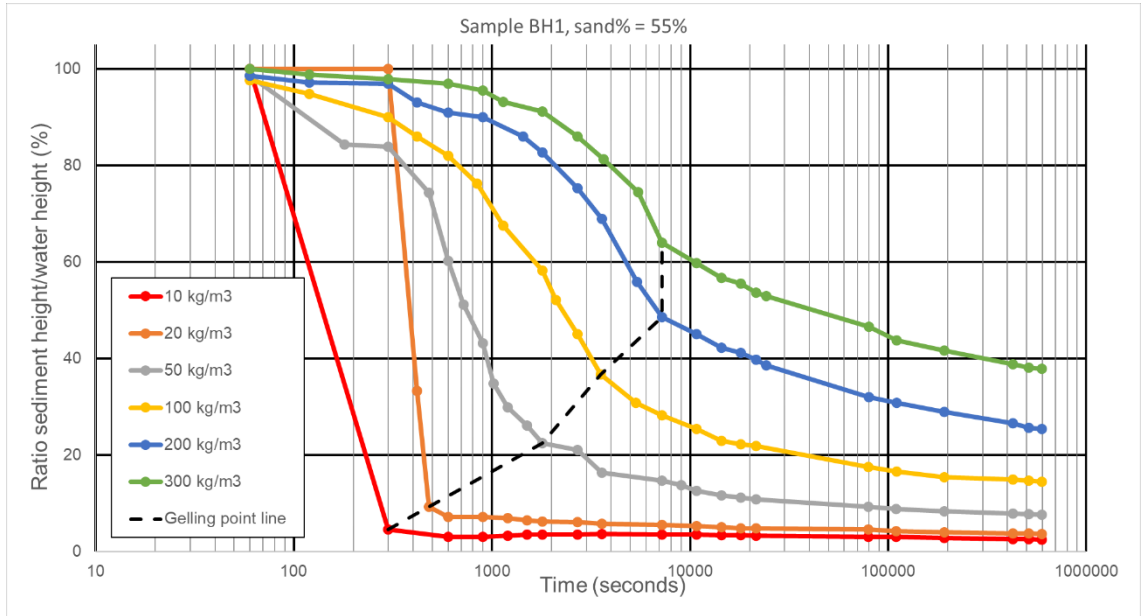


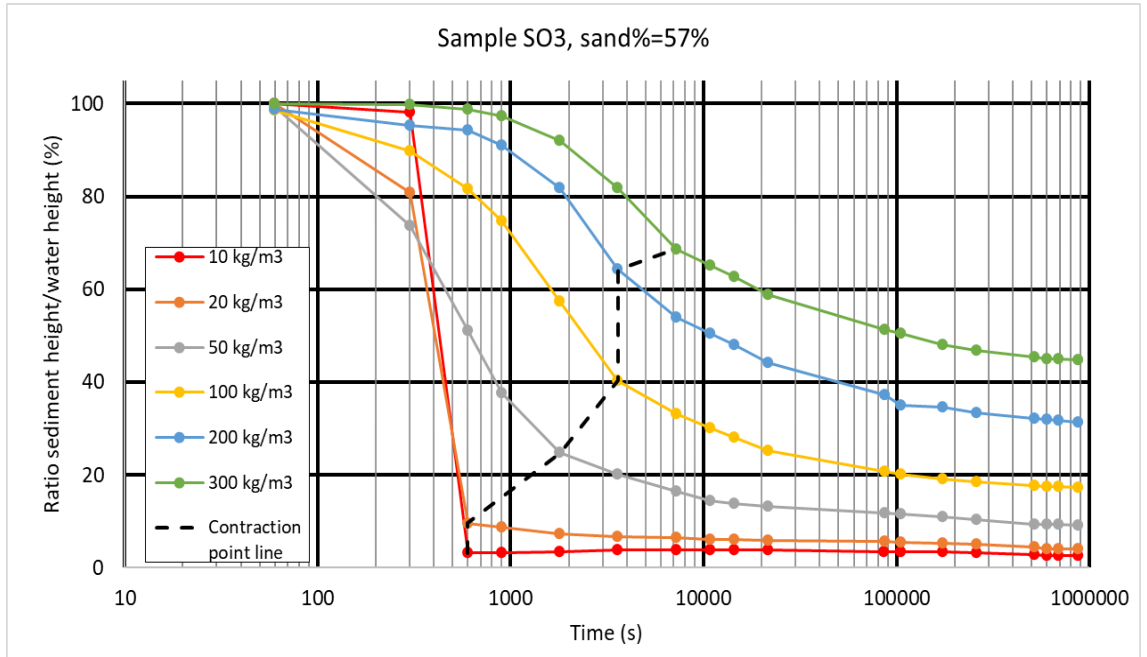*Figure 7-9: Settling height as function of time based on consolidation test for BH1; initial dry density of 10 to 300 kg/m3; dashed line as contraction points*
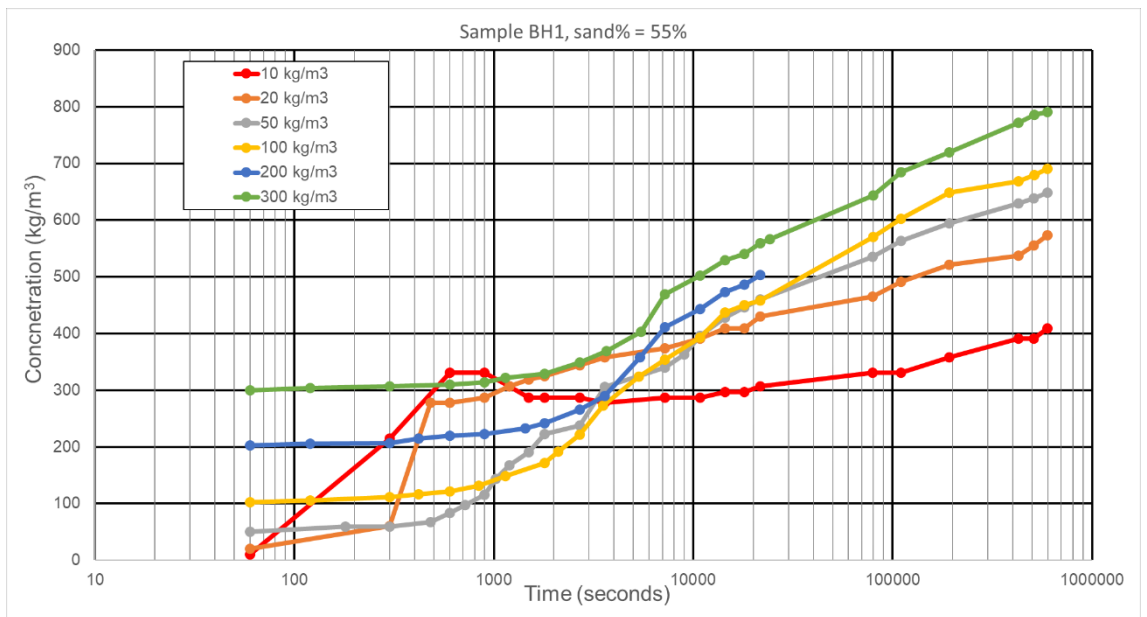


*Figure 7-10: Dry mud density as function of time based on consolidation test for BH1; initial dry density of 10 to 300 kg/m3*

Report Phase 1A-B

01 March 2022

## 7.6 Consolidation experiment on base mud HU1
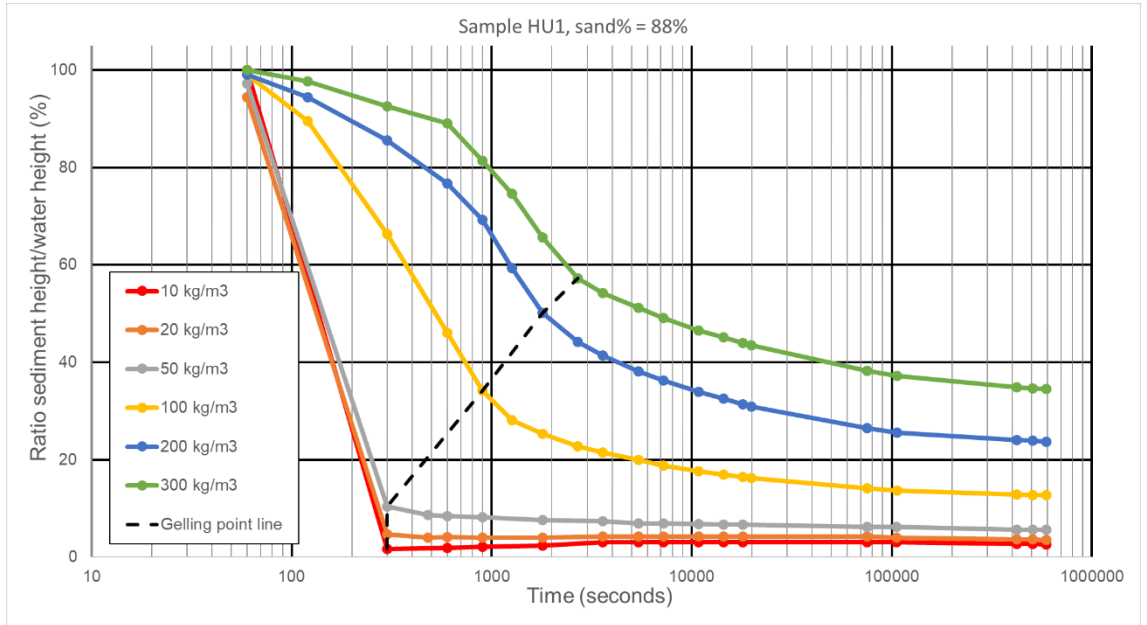


*Figure 7-11: Settling height as function of time based on consolidation test for HU1; initial dry density of 10 to 300 kg/m3; dashed line as contraction points*
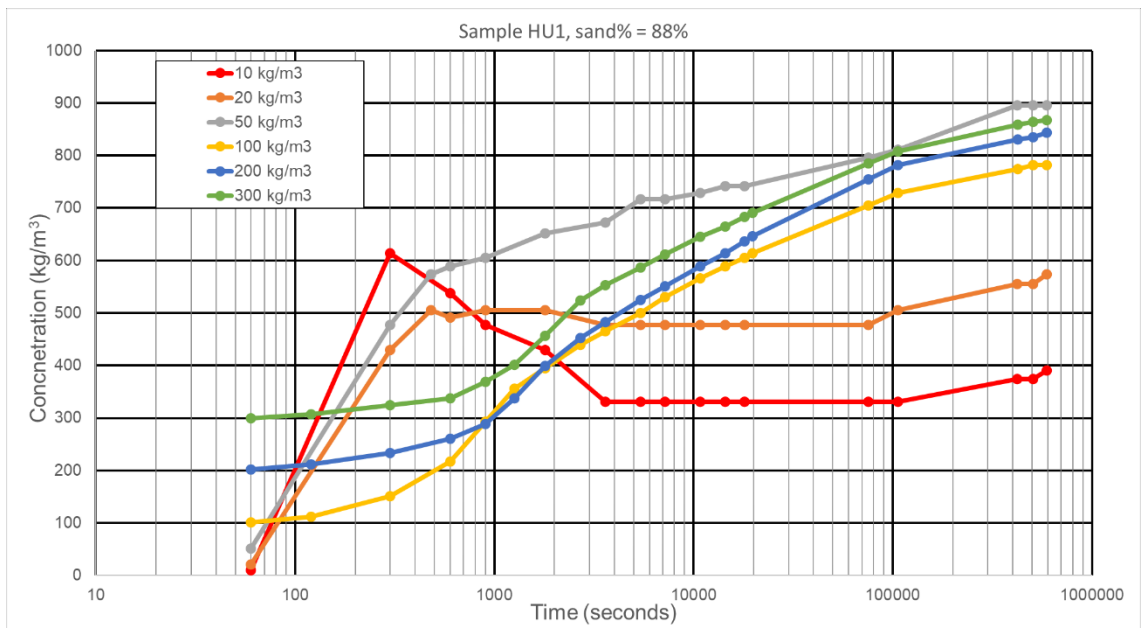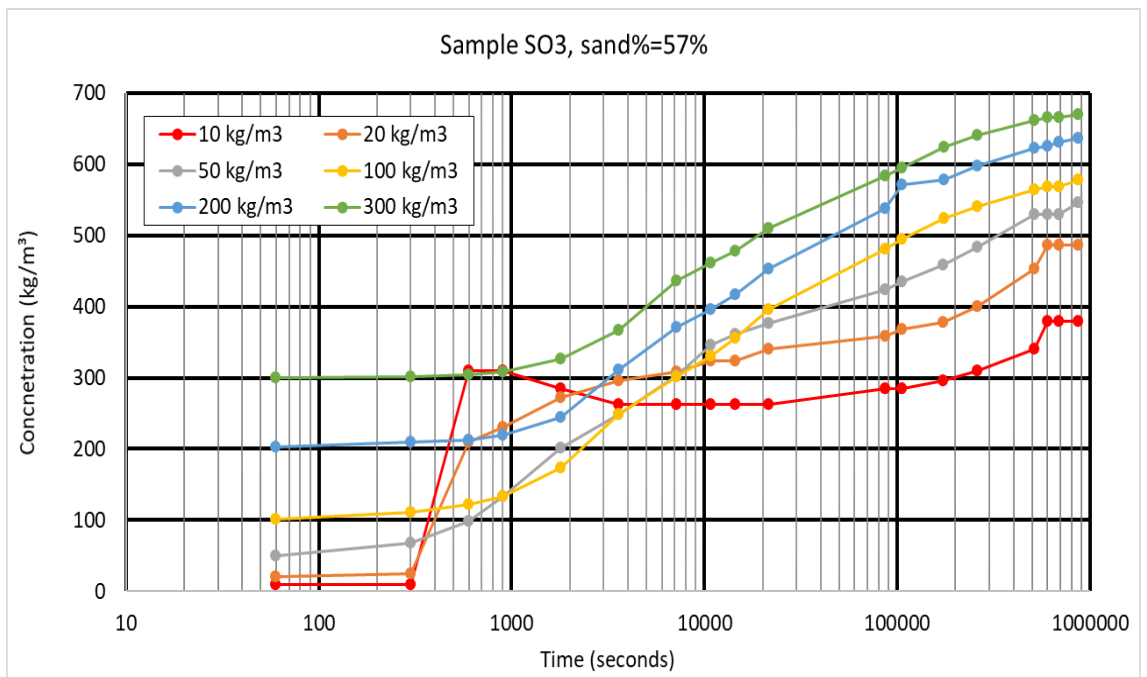


*Figure 7-12: Dry mud density as function of time based on consolidation test for HU1; initial dry density of 10 to 300 kg/m3*
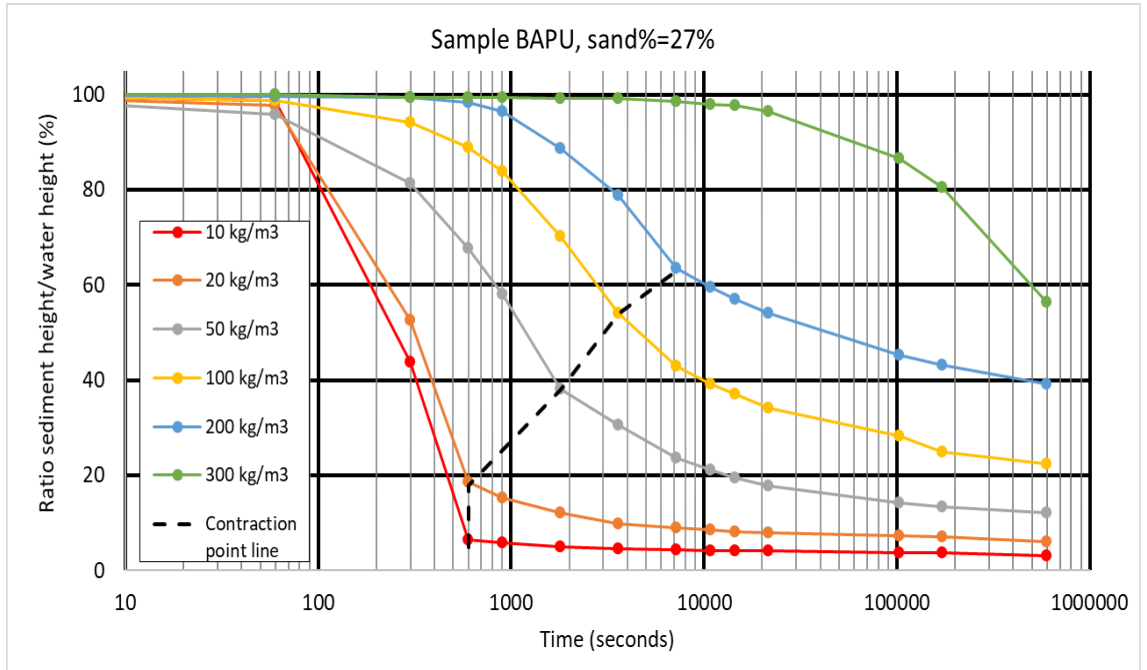
## 7.7 Consolidation experiment on base mud PA1
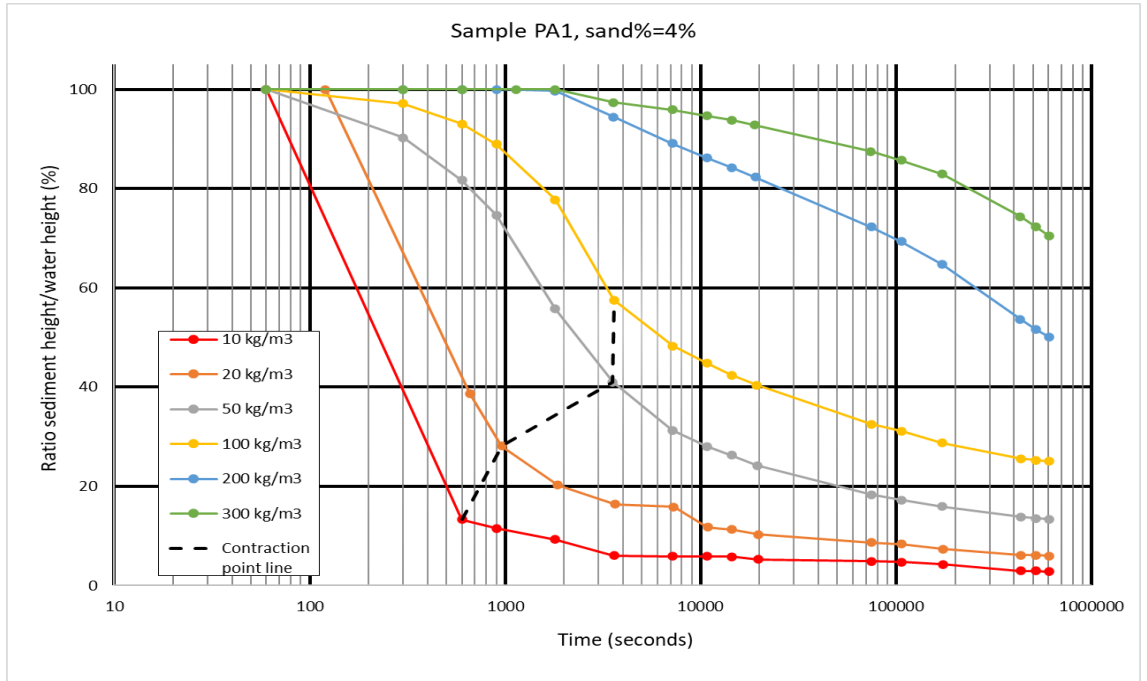


*Figure 7-13: Settling height as function of time based on consolidation test for PA1; initial dry density of 10 to 300 kg/m3; dashed line as contraction points*
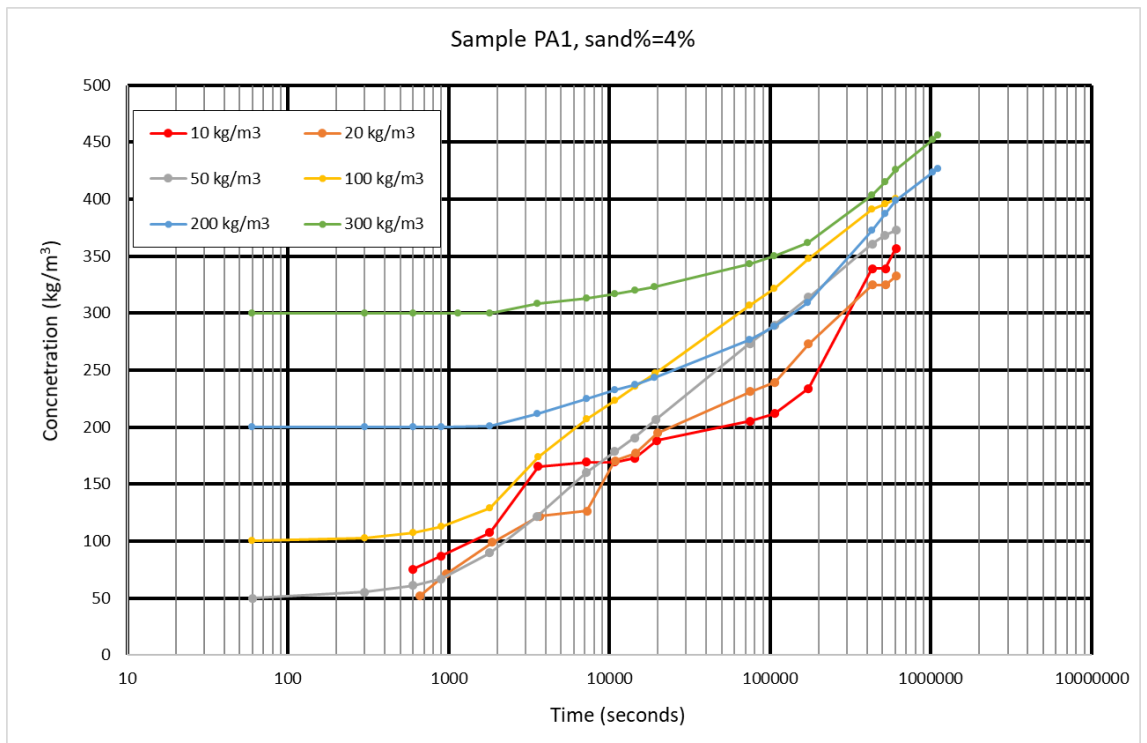


*Figure 7-14: Dry mud density as function of time based on consolidation test for PA1; initial dry density of 10 to 300 kg/m3*

## 7.8 Consolidation experiment on base mud PLUK1
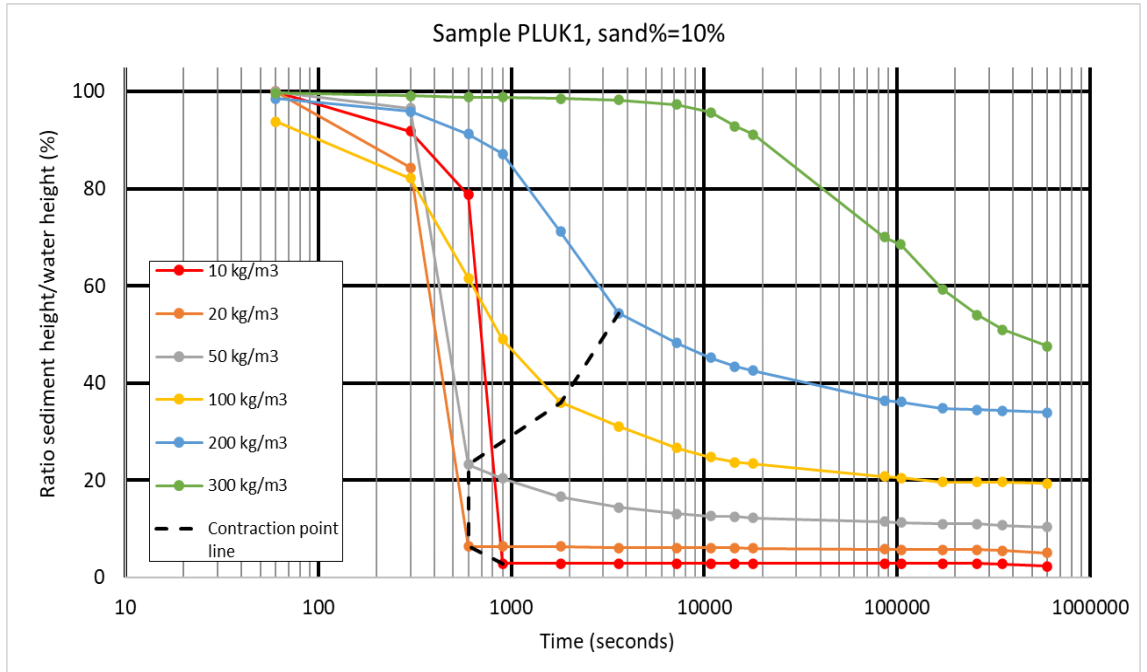


*Figure 7-15: Settling height as function of time based on consolidation test for PLUK1; initial dry density of 10 to 300 kg/m3; dashed line as contraction points*
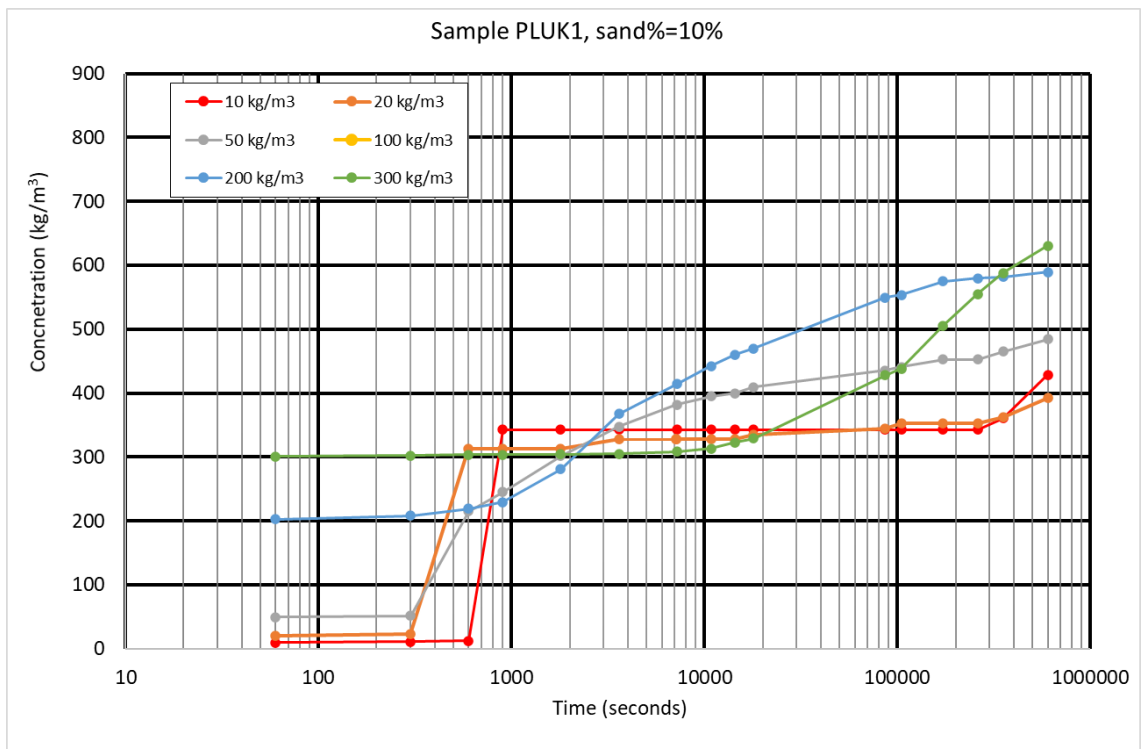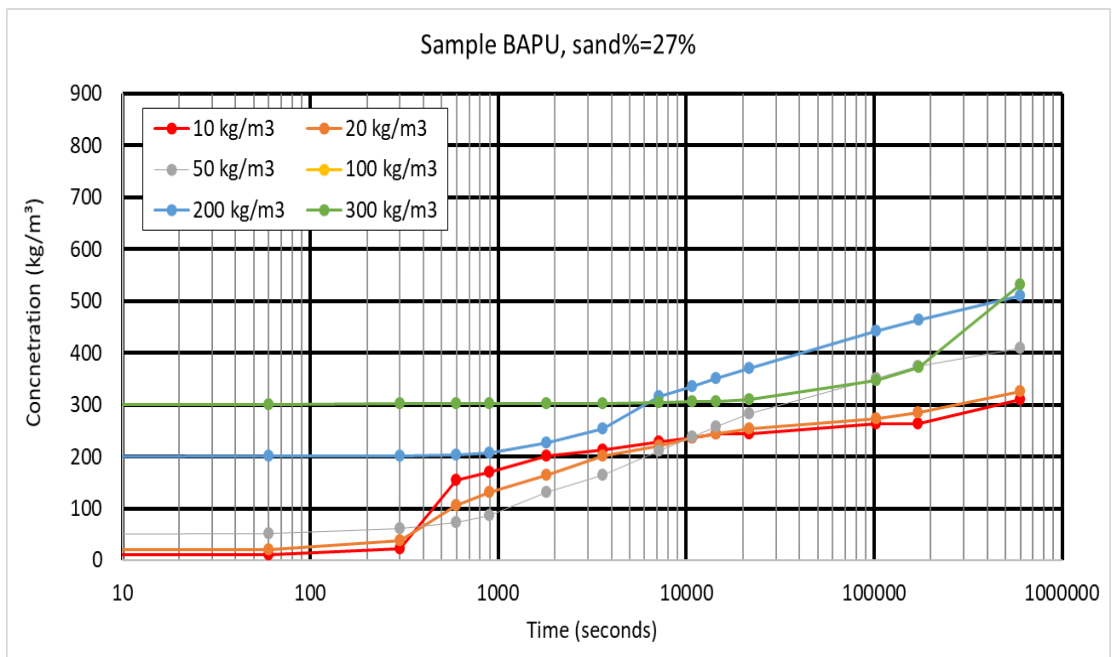


*Figure 7-16: Dry mud density as function of time based on consolidation test for PLUK1; initial dry density of 10 to 300 kg/m3*

Report Phase 1A-B

01 March 2022
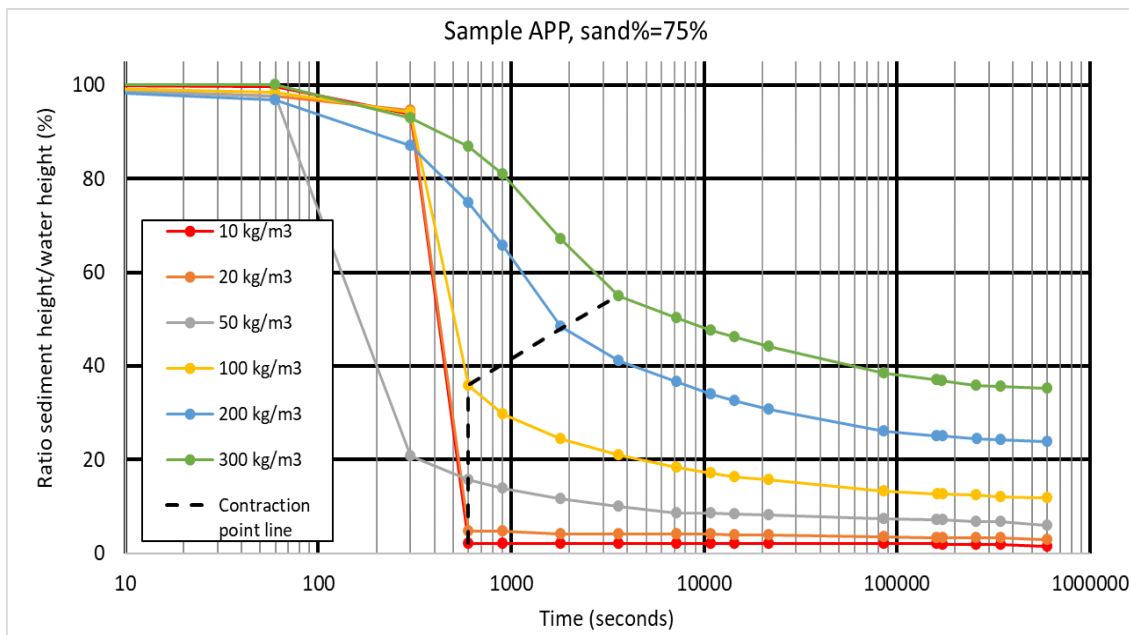
## 7.9 Consolidation experiment on base mud PLUK4
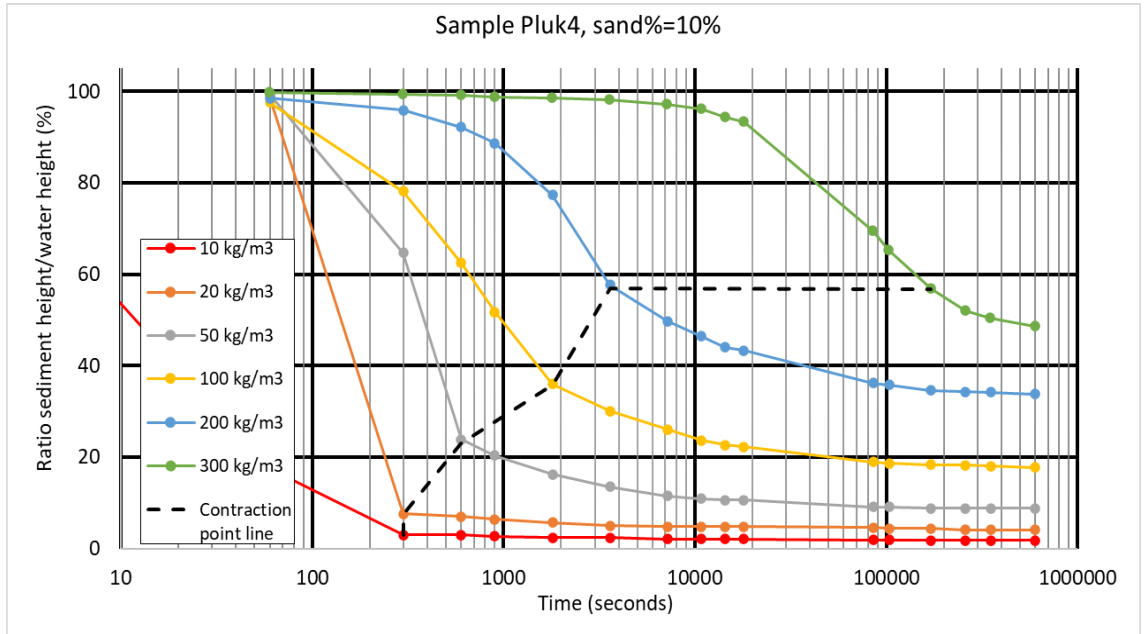


Figure 7-17: Settling height as function of time based on consolidation test for PLUK4; initial dry density of 10 to 300 kg/m3; dashed line as contraction points



Figure 7-18: Dry mud density as function of time based on consolidation test for PLUK4; initial dry density of 10 to 300 kg/m3

Figure 7-19:Settling height as function of time based on consolidation test for B5; initial dry density of 10 to 300 kg/m3; dashed line as contraction points
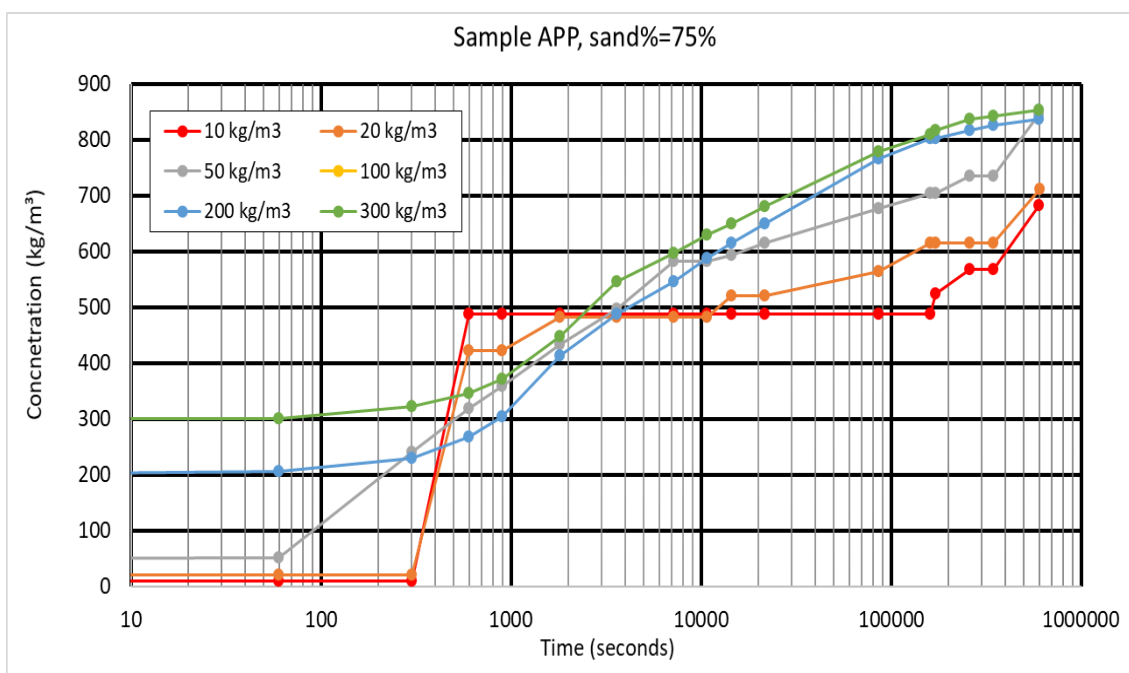


Figure 7-20: Dry mud density as function of time based on consolidation test for B5; initial dry density of 10 to 300 kg/m3

Report Phase 1A-B

01 March 2022
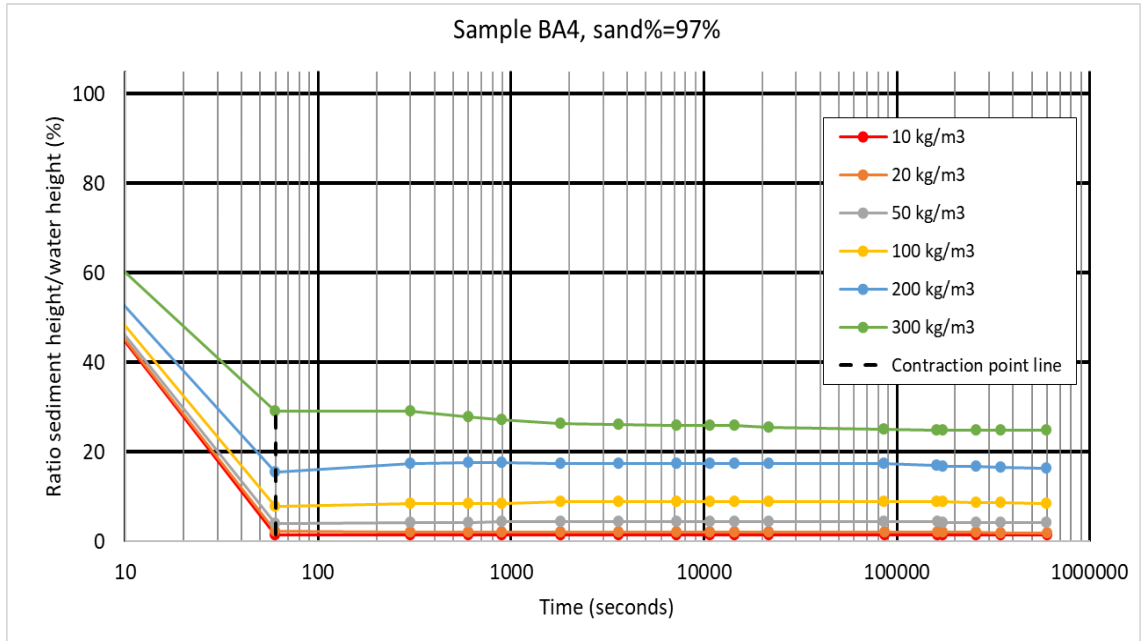
## 7.11    Consolidation experiment on base mud BB3



*Figure 7-21: Settling height as function of time based on consolidation test for BB3; initial dry density of 10 to 300 kg/m3; dashed line as contraction points*
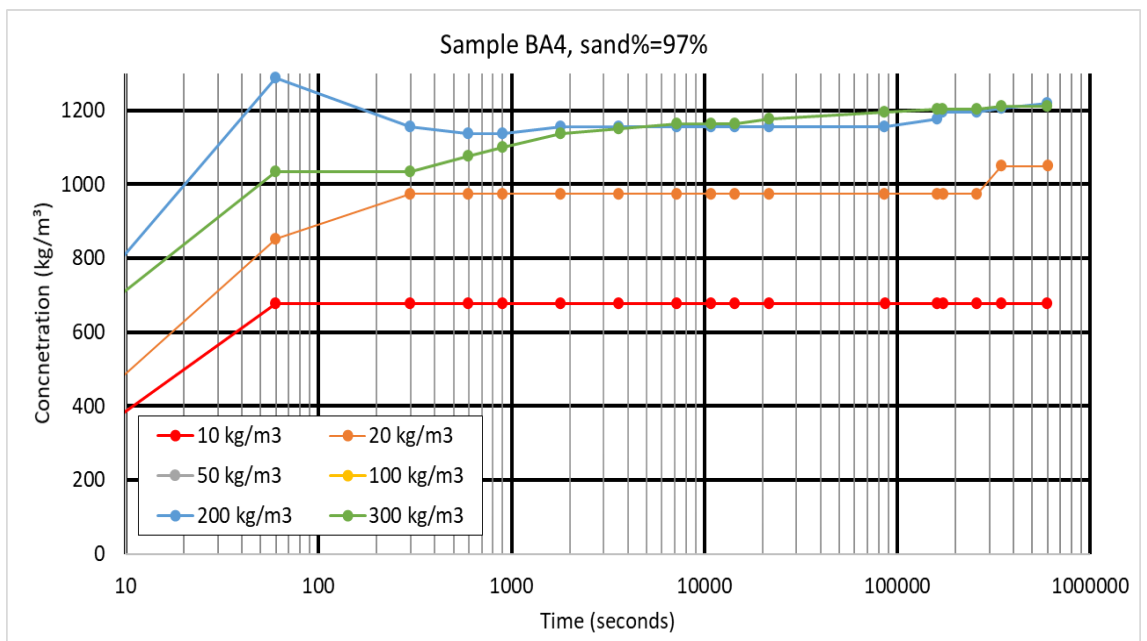


*Figure 7-22: Dry mud density as function of time based on consolidation test for BB3; initial dry density of 10 to 300 kg/m3*

Report Phase 1A-B

01 March 2022

## 7.12    Consolidation experiment on base mud SO3



*Figure 7-23: Settling height as function of time based on consolidation test for SO3; initial dry density of 10 to 300 kg/m3; dashed line as contraction points*



*Figure 7-24: Dry mud density as function of time based on consolidation test for SO3; initial dry density of 10 to 300 kg/m3*

MUSA

## 7.13    Consolidation experiment on base mud BAPU



*Figure 7-25: Settling height as function of time based on consolidation test for BAPU; initial dry density of 10 to 300 kg/m3; dashed line as contraction points*



*Figure 7-26: Dry mud density as function of time based on consolidation test for BAPU; initial dry density of 10 to 300 kg/m3*

## 7.14 Consolidation experiment on base mud APP



*Figure 7-27: Settling height as function of time based on consolidation test for APP; initial dry density of 10 to 300 kg/m3; dashed line as contraction points*



*Figure 7-28: Dry mud density as function of time based on consolidation test for APP; initial dry density of 10 to 300 kg/m3*

## 7.15 Consolidation experiment on base mud BA4



*Figure 7-29: Settling height as function of time based on consolidation test for BA4; initial dry density of 10 to 300 kg/m3; dashed line as contraction points*



*Figure 7-30: Dry mud density as function of time based on consolidation test for BA4; initial dry density of 10 to 300 kg/m3*

Report Phase 1A-B

01 March 2022

# 8 Appendix C: Screenshots of videos performed during flow-flume experiments

## 8.1 Flow flume experiment on base mud H2
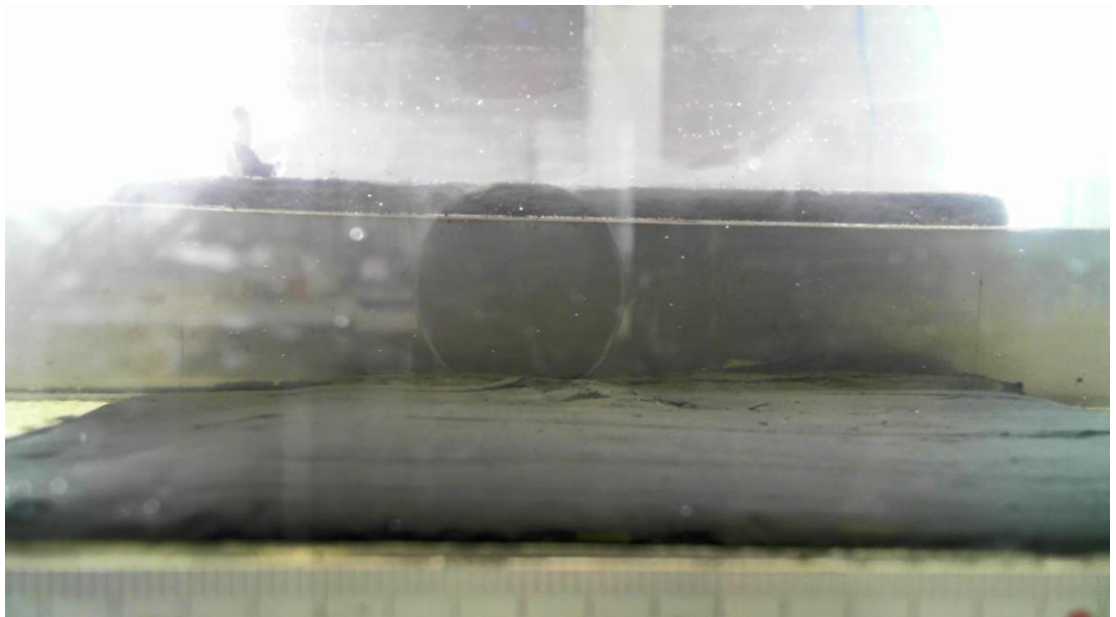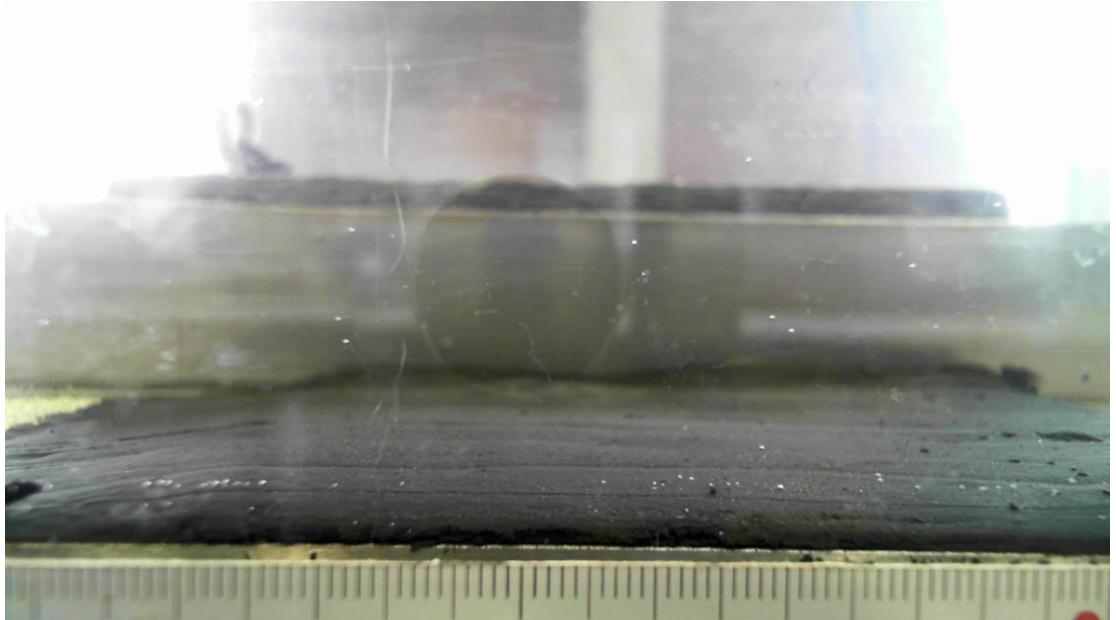




*Figure 8-1: Screenshot of video performed on flow-flume experiment H2. Upper panel: at start of experiment, lower panel: at end of experiment*
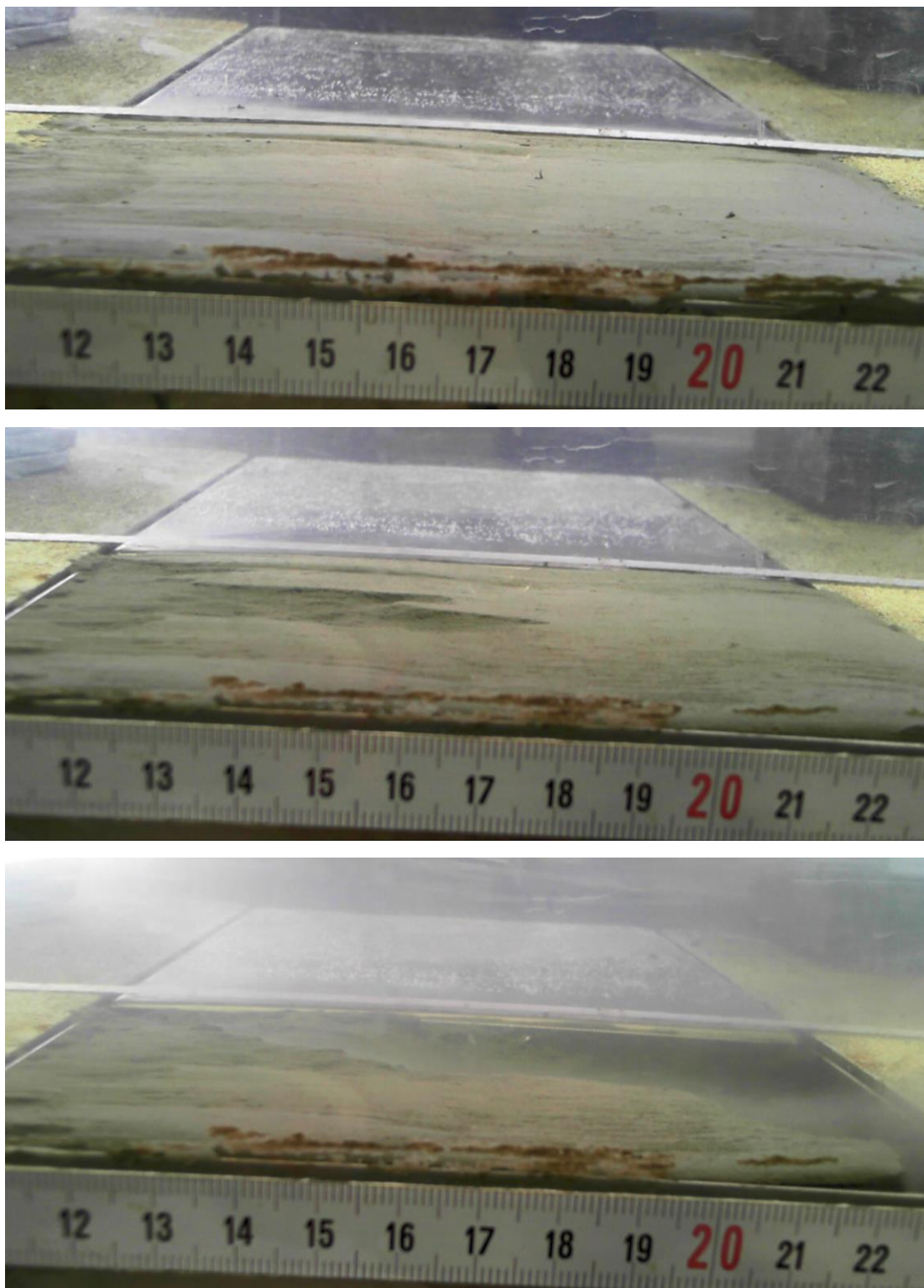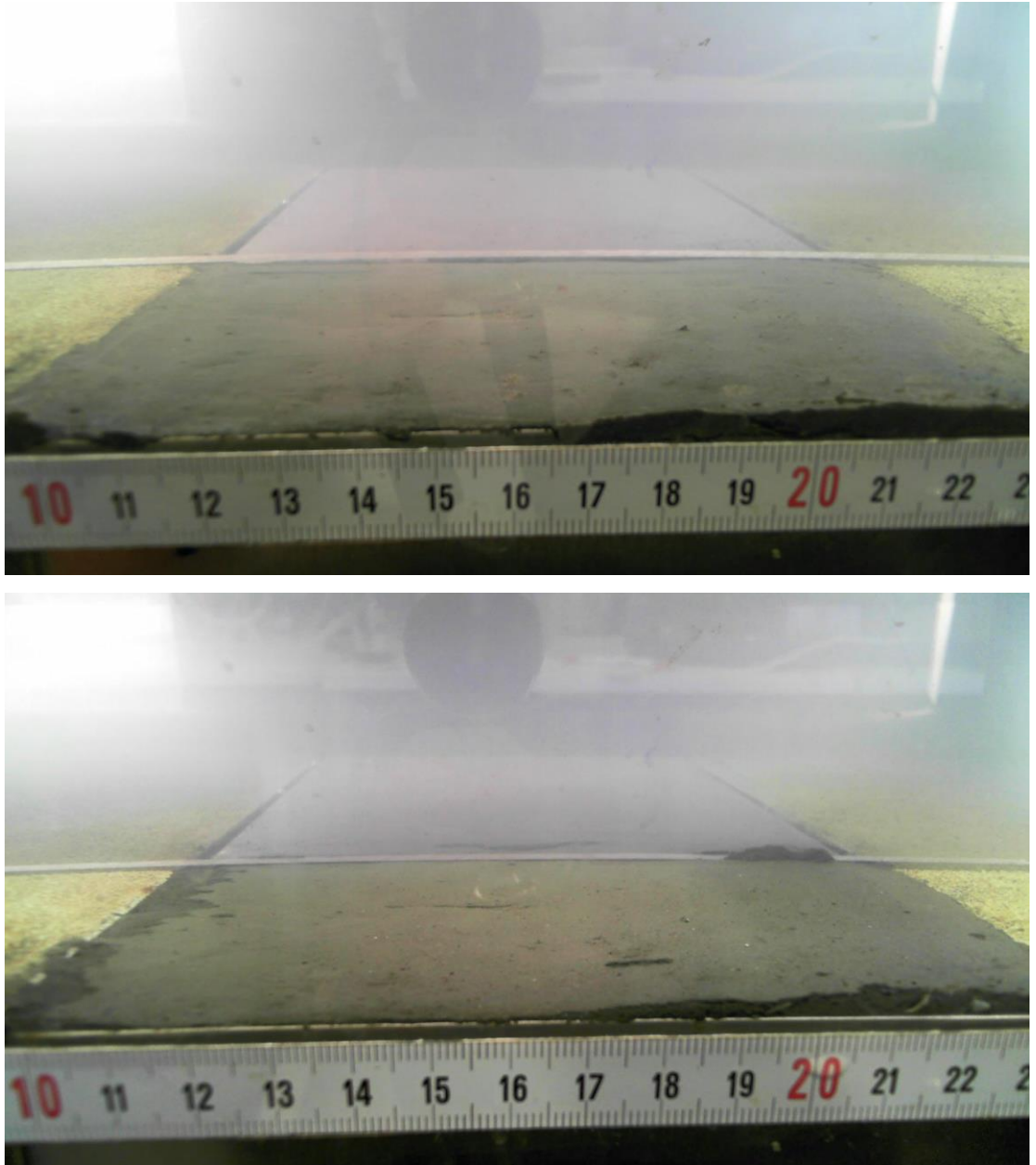
## 8.2    Flow flume experiment on base mud GR1
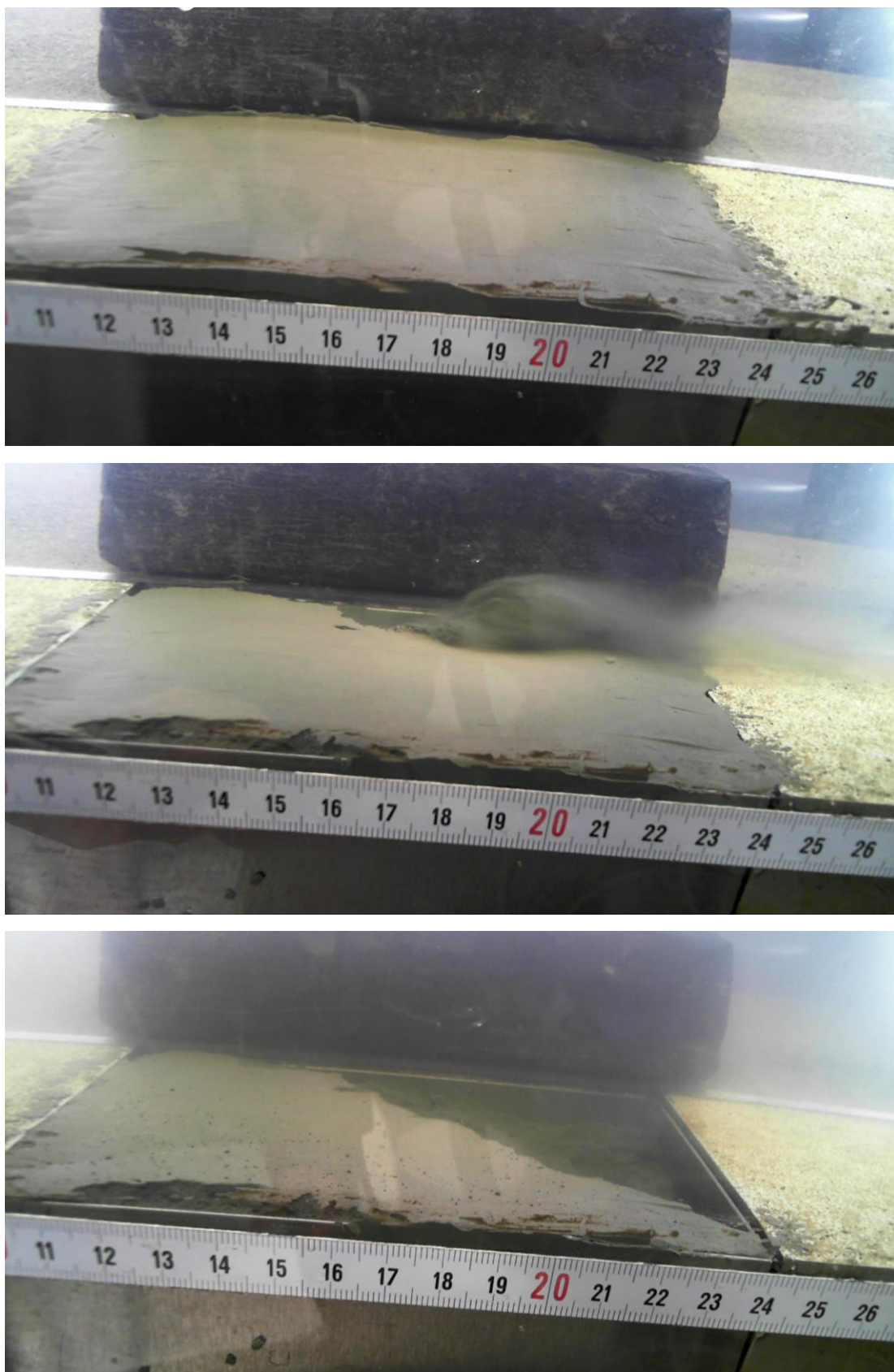


*Figure 8-2: Screenshot of video performed on flow-flume experiment GR1. Upper panel: at start of experiment, middle panel during experiment, lower panel: at end of experiment*

Report Phase 1A-B

01 March 2022

## 8.3 Flow flume experiment on base mud ZW2
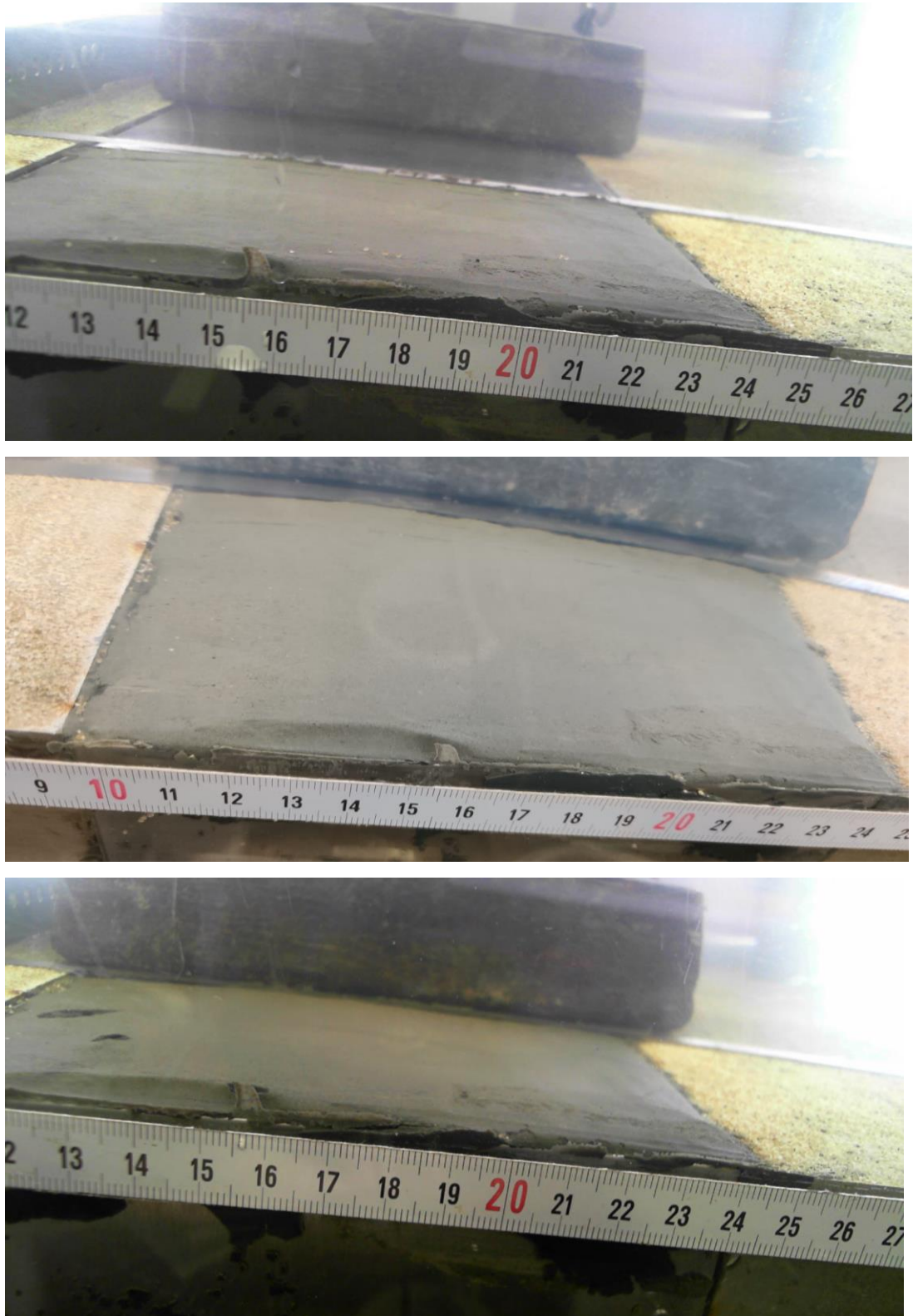


*Figure 8-3: Screenshot of video performed on flow-flume experiment ZW2. Upper panel: at start of experiment, middle panel during experiment, lower panel: at end of experiment*

Report Phase 1A-B

01 March 2022

## 8.4 Flow flume experiment on base mud WAW1



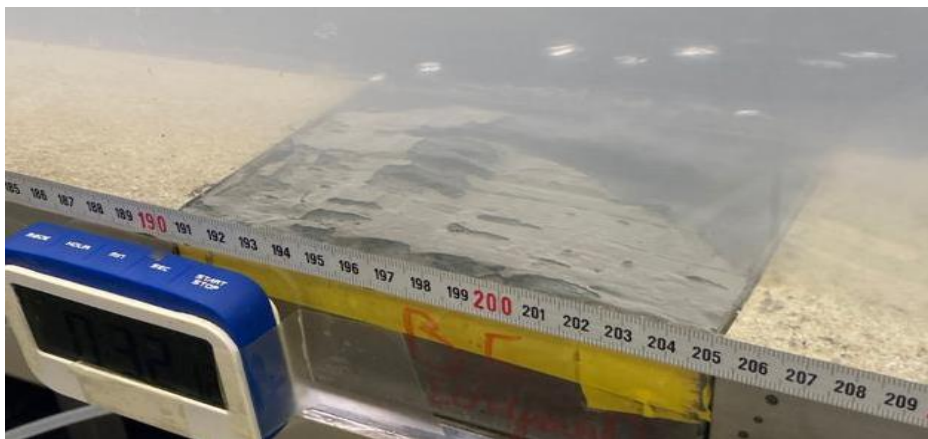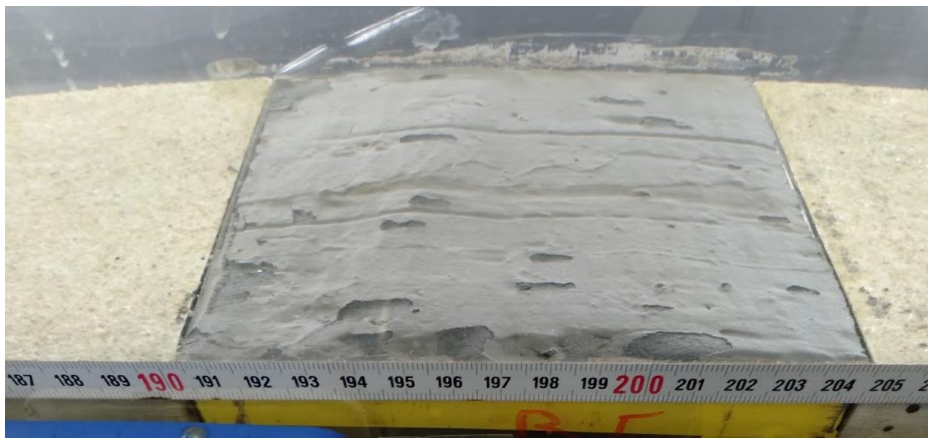*Figure 8-4: Screenshot of video performed on flow-flume experiment WAW1. Upper panel: at start of experiment, middle panel during experiment, lower panel: at end of experiment*

Report Phase 1A-B

01 March 2022

## 8.5    Flow flume experiment on base mud BH1



*Figure 8-5: Screenshot of video performed on flow-flume experiment BH1. Upper panel: at start of experiment, lower panel: at end of experiment*

## 8.6    Flow flume experiment on base mud HU1



*Figure 8-6: Screenshot of video performed on flow-flume experiment HU1. Upper panel: at start of experiment, middle panel during experiment, lower panel: at end of experiment*

MUSA

## 8.7    Flow flume experiment on base mud PA1



*Figure 8-7: Pictures of flow-flume experiment PA1. Upper panel: at start of experiment, middle panel during experiment, lower panel: at end of experiment*
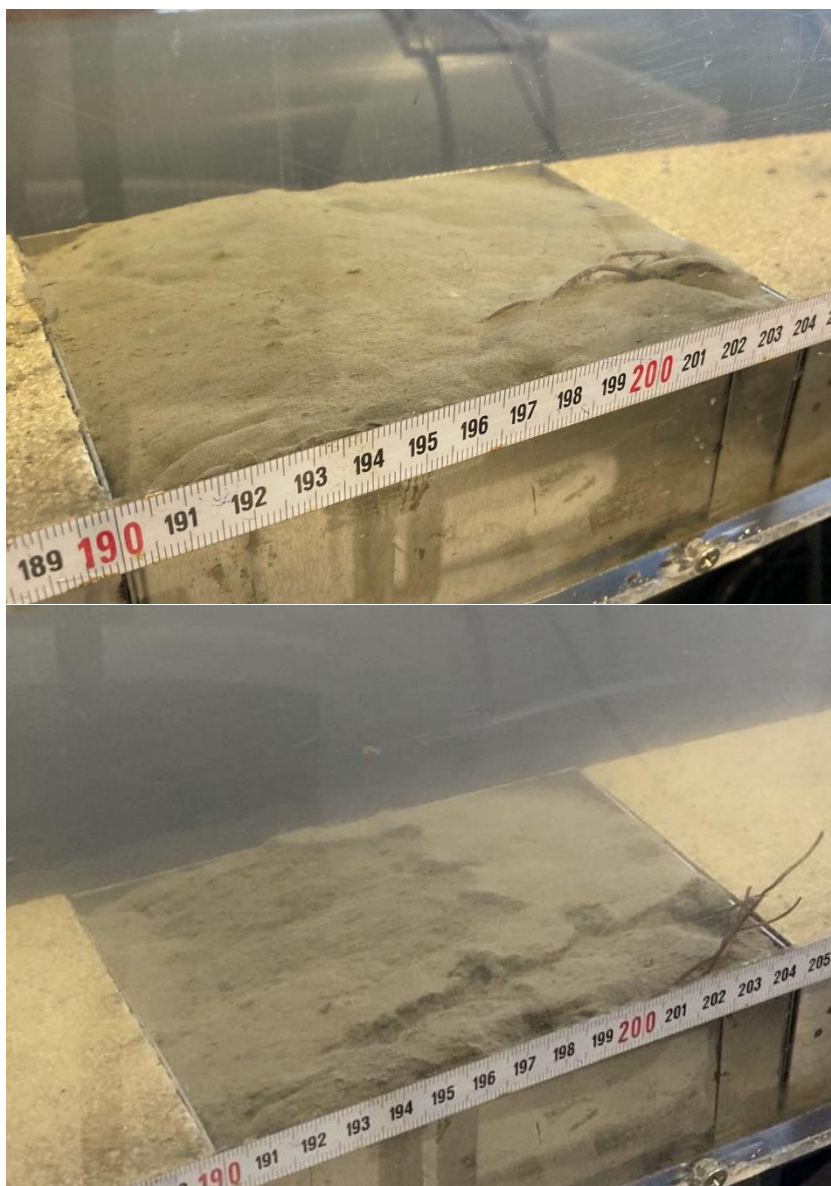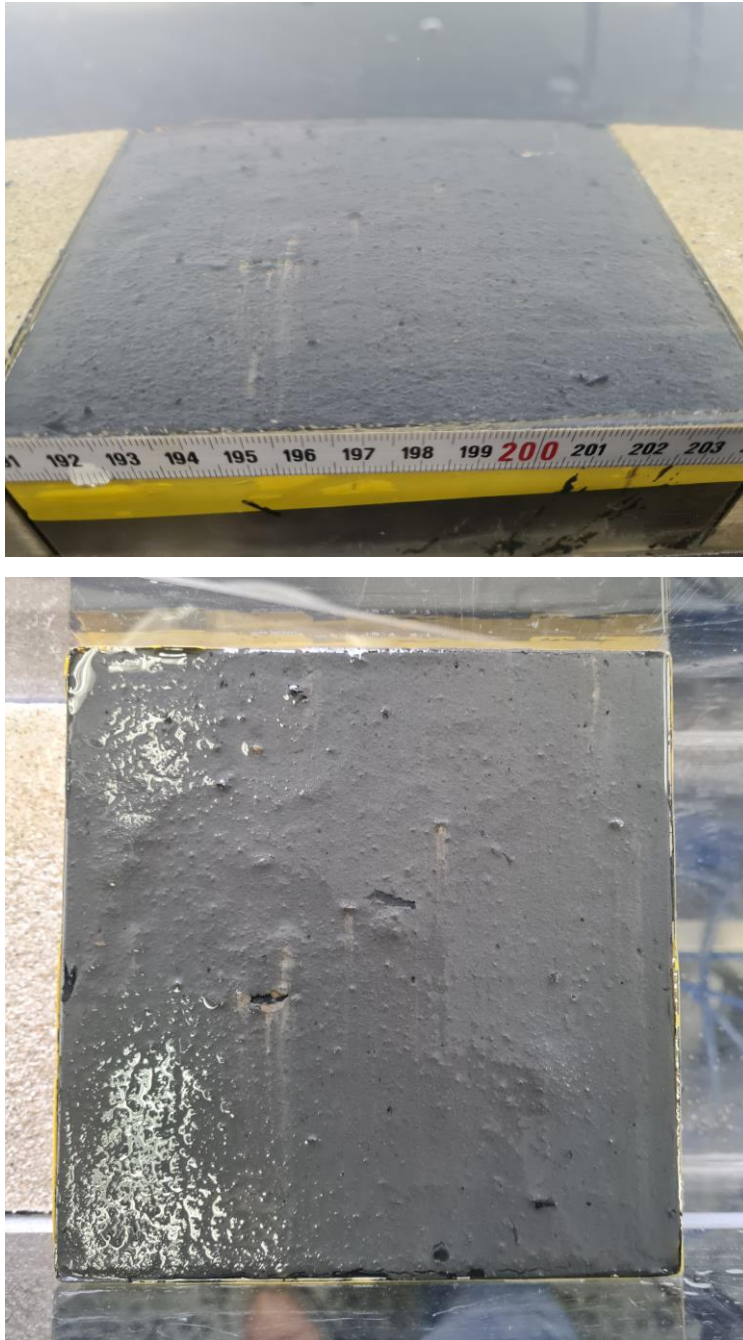
## 8.8    Flow flume experiment on base mud PLUK1



*Figure 8-8: Pictures of flow-flume experiment PLUK1. Upper panel: at start of experiment, middle panel during experiment, lower panel: at end of experiment*

Report Phase 1A-B

01 March 2022

MUSA

## 8.9  Flow flume experiment on base mud PLUK4



*Figure 8-9: Pictures of flow-flume experiment PLUK4. Upper panel: at start of experiment, lower panel: at end of experiment*

Report Phase 1A-B

01 March 2022

MUSA

## 8.10 Flow flume experiment on base mud B5



*Figure 8-10: Pictures of flow-flume experiment B5. Upper panel: at start of experiment, lower panel: at end of experiment*

Report Phase 1A-B

01 March 2022

MUSA

## 8.11 Flow flume experiment on base mud BB3



*Figure 8-11: Pictures of flow-flume experiment BB3. Upper panel: at start of experiment, middle panel: during experiment, lower panel: at end of experiment*
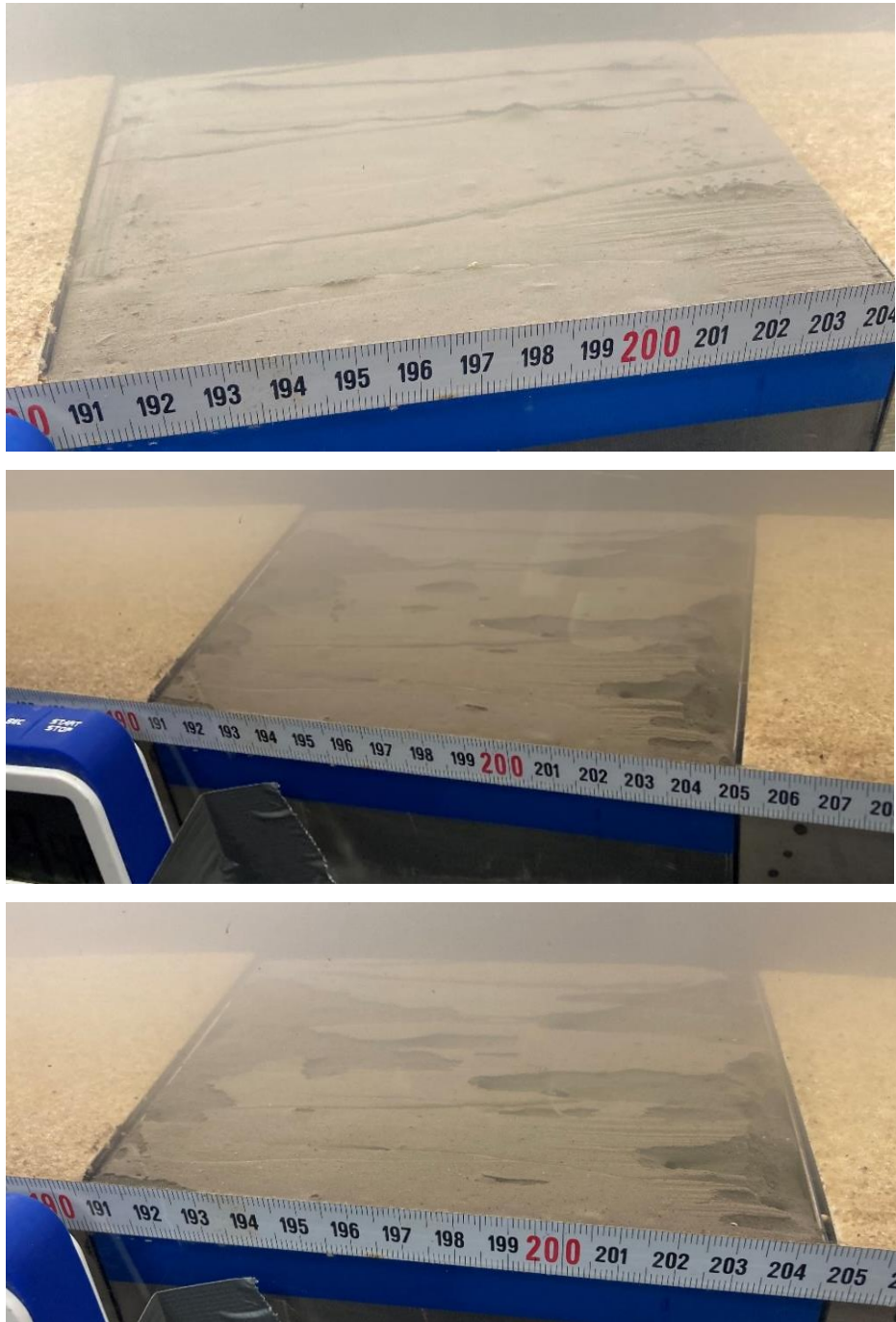
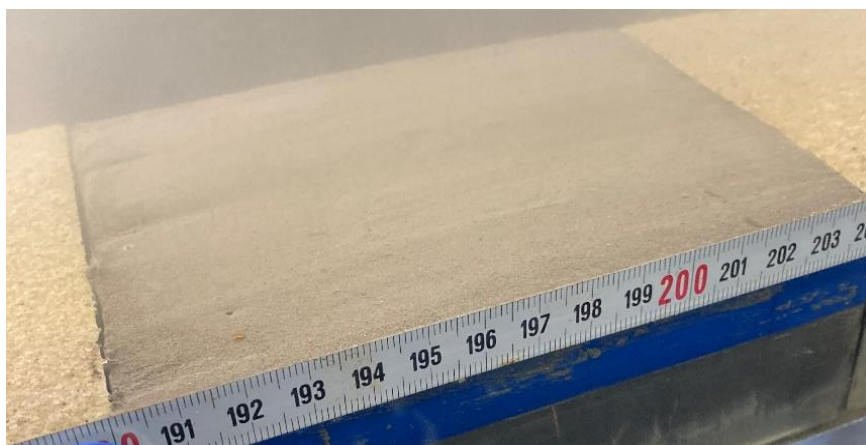## 8.12    Flow flume experiment on base mud SO3



*Figure 8-12: Pictures of flow-flume experiment SO3. Upper panel: at start of experiment, middle panel: during experiment, lower panel: at end of experiment*

Report Phase 1A-B

01 March 2022

MUSA

## 8.13    Flow flume experiment on base mud BAPU



*Figure 8-13: Pictures of flow-flume experiment BAPU. Upper panel: at start of experiment, middle panel: during experiment, lower panel: at end of experiment*

Report Phase 1A-B

01 March 2022

MUSA

## 8.14    Flow flume experiment on base mud APP



*Figure 8-14: Pictures of flow-flume experiment APP. Upper panel: at start of experiment, two middle panels: during experiment, lower panel: at end of experiment*

MUSA

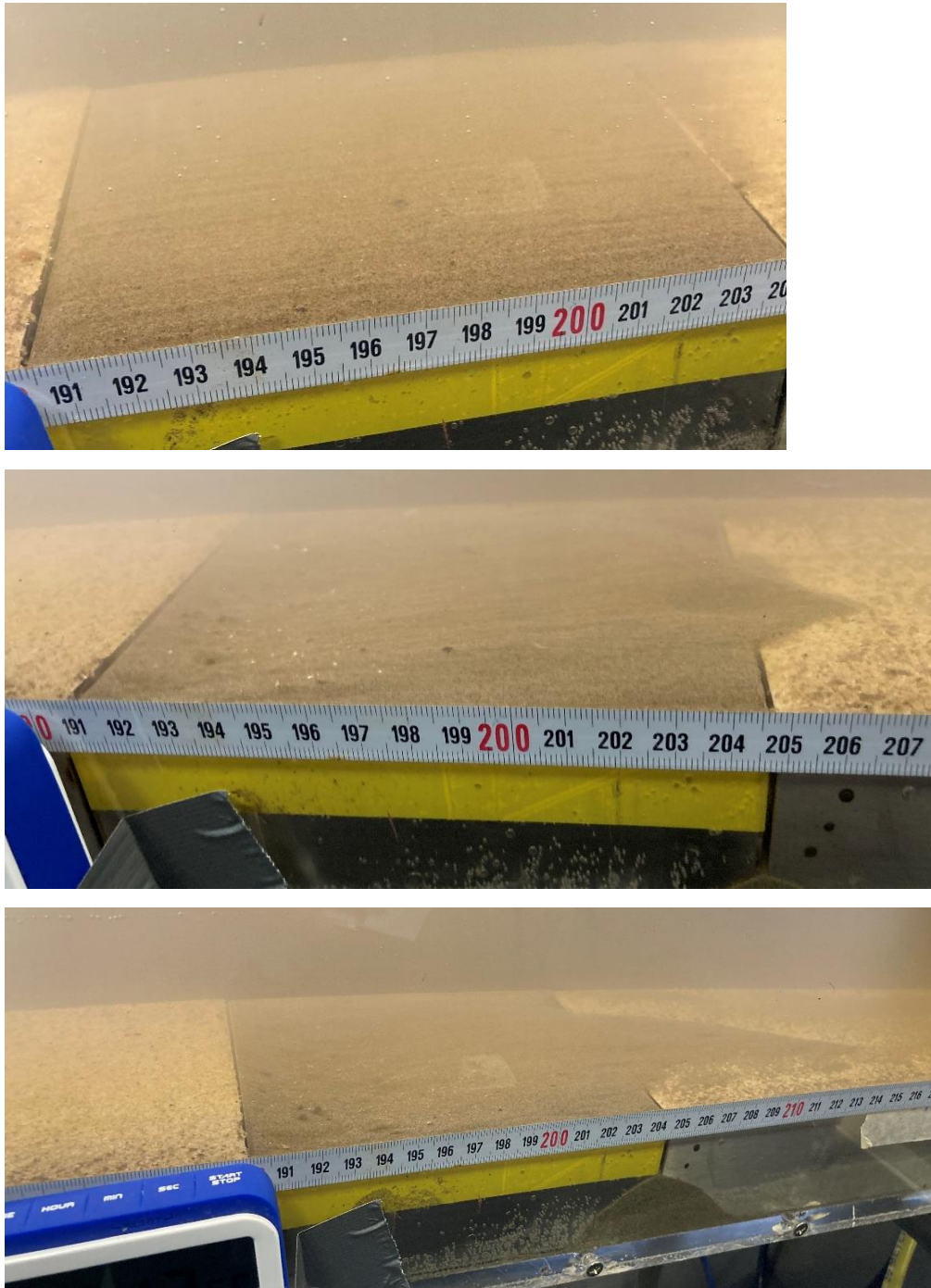## 8.15    Flow flume experiment on base mud BA4



*Figure 8-15: Pictures of flow-flume experiment BA4. Upper panel: at start of experiment, middle panel: during experiment, lower panel: at end of experiment*

Report Phase 1A-B

01 March 2022

MUSA